Dynamics and statistics of systems with long range interactions: application to 1-dimensional toy-models

Alessio Turchi

UNIVERSITÀ DEGLI STUDI DI FIRENZE
Dipartimento di Sistemi e Informatica
Dottorato in "Dinamica non Lineare e Sistemi Complessi", ciclo XXIV, FIS03

UNIVERSITÉ D'AIX-MARSEILLE
Centre de Physique Théorique, UMR 7332
Ecole doctorale "Physique et Sciences de la Matiere", ED 352

Dynamics and statistics of systems with long range interactions: application to 1-dimensional toy-models

Candidate: Alessio Turchi

Supervisors: Duccio Fanelli, Xavier Leoncini

Referees: Julien Barré, Giovanni De Ninno

Jury members: Armando Bazzani, Rita Casadio, Duccio Fanelli, Xavier Leoncini, Alberto Verga, Julien Barré

Firenze, 2012

Contents

Italian abstract

Titolo della tesi:
Dinamica e statistica di sistemi con interazione a lungo raggio: applicazioni a modelli giocattolo 1-dimensionali.

Questo lavoro di tesi è focalizzato sullo studio e la caratterizzazione dei sistemi dinamici con interazione a lungo raggio (LR). Questi ultimi vengono definiti tali sulla base della legge che governa l'interazione tra elementi costitutivi. Per tali sistemi infatti il potenziale V scala con la distanza r come $V \sim \frac{1}{r^\alpha}$, con α minore della dimensione spaziale d. La difficoltà nello studio di questi sistemi cresce all'aumentare del numero di gradi di libertà, dal momento che è necessario considerare la configurazione di ogni elemento per calcolare il potenziale che agisce su una singola particella.
Negli ultimi decenni questo campo di studi ha visto nascere un crescente interesse, dovuto principalmente alle caratteristiche dinamiche e termodinamiche peculiari che è possibile osservare nei sistemi LR. Nello specifico, la natura complessa della loro dinamica fa emergere proprietà contro-intuitive e inaspettate, come la presenza di stati stazionari di fuori-equilibrio (QSS), il cui tempo di vita diverge con l'aumentare del numero N di gradi di libertà.
Nel limite $N \to \infty$ il sistema resta indefinitamente intrappolato nei QSS, senza mai raggiungere la soluzione asintotica prevista sulla base della termodinamica convenzionale. I QSS possono essere pertanto considerati veri e propri stati di equilibrio nel limite di taglia infinita, risultando gli unici accessibili e misurabili.
I QSS sono tipicamente associati a funzioni di distribuzione fortemente non-maxwelliane ed impongono di fatto una attenta rivisitazione di concetti termodinamici chiave sviluppati nel contesto di gas perfetti interagenti tramite collisioni a corto raggio. Nello specifico è possibile osservare proprietà particolari come la presenza di calore specifico e suscettività magnetica negativi (in sistemi isolati), inequivalenza degli insiemi statistici, bande di valori proibiti nelle quantità termodinamiche (salti di temperatura) e peculiari fenomeni di auto-organizzazione spaziale.
Sebbene le interazioni LR costituiscano la base dei più noti sistemi fisici, nella pratica sperimentale è possibile osservare gli effetti dinamici o termodinamici sopracitati solo nel limite in cui i contributi a corto raggio, urti, rumore, risultino trascurabili. Nonostante questo, le teorie nate nell'ambito delle interazioni LR sono state applicate con succcesso per descrivere la dinamica di sistemi auto-gravitanti, di vortici 2-dimensionali

e di sistemi con interazioni onda-particella; presentano inoltre importanti applicazioni nel campo della fisica dei plasmi carichi.
Attualmente, la teoria che ha mostrato maggiore accuratezza nel descrivere la termodinamica dei QSS di un sistema LR è quella dovuta a Lynden-Bell, sviluppata alla fine degli anni '70 nel contesto della dinamica galattica. La teoria è stata applicata con successo alla soluzione del modello *Hamiltonian Mean Field* (HMF), che è assurto a sistema paradigmatico delle interazioni LR. Infatti, l'HMF possiede una ricca fenomenologia che risulta potenzialmente applicabile allo studio di alcuni sistemi laser (FEL e CARL). Lo studio analitico di questo modello, con la sopracitata teoria di Lynden-Bell, è stato finora limitato ad una specifica e restrittiva condizione iniziale, denominata "water-bag".

Il mio lavoro originale di tesi si è inizialmente focalizzato sull'estensione della soluzione di Lynden-Bell per l'HMF, generalizzando l'analisi a condizioni iniziali di "water-bag" a più livelli. L'intento di questo studio è quello di riuscire ad approssimare condizioni iniziali continue più realistiche.

In seguito, sempre in riferimento al modello HMF, mi sono concentrato sulla caratterizzazione della termodinamica dei QSS nell'insieme statistico canonico. Si tratta di uno studio complesso che presenta notevoli problematiche tuttora irrisolte, legate all'implementazione pratica di un bagno termico per sistemi LR. Il mio lavoro si è incentrato sulla definizione formale di tale insieme statistico: nello specifico ho mostrato come, applicando la teoria termodinamica convenzionale, sia possibile misurare un calore specifico "cinetico" negativo, in un sistema non isolato. Una prima conseguenza di tale inaspettata proprietà porta, come dimostrato nel corso di questo lavoro, alla violazione del secondo principio della termodinamica, consentendo di realizzare una macchina termica che esegue lavoro positivo prendendo calore dal termostato freddo e rilasciandolo in quello caldo. Un tale risultato ci spinge a riconsiderare l'applicabilità della attuale teoria termodinamica al caso dei sistemi LR, e alla eventuale ridefinizione della legge di Fourier per la trasmissione del calore.

L'ultima parte di questa tesi è dedicata allo studio di alcuni modelli a lungo raggio che si possono configurare come estensioni del modello HMF.
In una prima fase, mi sono concentrato sul modello 1-dimensionale noto come α-HMF, definito su un reticolo. Questo modello consente di variare la forza dell'interazione controllata dal parametro reale α. Nel limite $N \to \infty$ quest'ultimo modello è analiticamente equivalente all'HMF per $\alpha < 1$. Ho studiato inoltre la persistenza degli stati QSS nel limite in cui la dinamica passa da LR a corto raggio ($\alpha = 1$) e mi sono dedicato allo studio del regime $\alpha > 1$, evidenziando la presenza di una transizione di fase tipica del regime LR. I risultati di questo studio suggeriscono una generalizzazione della definizione dei sistemi LR che tenga conto della dipendenza da r della forza, piuttosto che del potenziale.

L'ultimo capitolo della tesi è dedicato alla caratterizzazione di un nuovo modello LR, che si configura come una naturale estensione del precedente α-HMF, dotato di un termine di distanza continuo. L'obiettivo prefissato è quello di studiare la dinamica e la termodinamica LR in modelli complessi e di potenziale interesse applicativo. In questo lavoro introduttivo, incentrato sullo studio degli stati termodinamici di equilibrio, ho mostrato come la presenza di uno spazio delle fasi più esteso consenta l'insorgenza di fenomeni di auto-organizzazione con elevata simmetria. Quest'ultima risulta in un potenziale efficace di campo medio simile ai modelli studiati in precedenza e una transizione di fase simile a quella osservata sia per l'HMF che per l'α-HMF, rendendo affine la descrizione statistica dei tre modelli.

French abstract

Titre de la thèse:
Dynamique et statistique de systèmes avec interactions à longue portée: applications à des modèles simplifiés unidimensionnels.

Ce thèse a comme objectif l'étude et la caractérisation des systèmes dynamiques avec interaction à longue portée (LR). Ces derniers sont définis tels en vertu de la loi d'interaction entre les éléments constitutifs qui les caractérise: le potentiel d'interaction V varie avec la distance r comme $V \sim \frac{1}{r^\alpha}$, avec α plus petit que la dimension spatiale d dans laquelle est immergé le système. La difficulté de l'étude de ces systèmes croît si l'on augmente le nombre de degrés de liberté, étant donné qu'il est nécessaire de considérer la configuration de chaque élément pour calculer le potentiel qui agit sur chaque particule.
Au cours des dernières décennies ce domaine d'études a vu naître un intérêt croissant, dû principalement aux caractéristiques dynamiques et thermodynamiques particulières que l'on peut observer dans les systèmes LR. Plus spécifiquement la nature complexe de leur dynamique met en évidence des propriétés contre-intuitives et inattendues, comme l'existence d'états stationnaires hors-équilibre (QSS), dont le temps de vie diverge si l'on augmente le nombre N de degrés de liberté.
Dans la limite $N \to \infty$ le système reste piégé indéfiniment dans les QSS, sans jamais parvenir à la solution asymptotique prédite sur la base de la thermodynamique classique. Les QSS peuvent donc être considérés comme des états d'équilibre réel dans la limite de taille infinie, puisqu'ils se révèlent les seuls accessibles et mesurables.
Les QSS sont décrits typiquement par une fonction de distribution fortement non-Maxwellienne, menant donc à la redéfinition des concepts thermodynamiques clé développés dans le contexte de gaz parfaits interagissant par des collisions à courte portée. Plus spécifiquement on peut observer des propriétés particulières comme présence de chaleur spécifique et susceptibilité magnétique négatives (dans des systèmes isolés), inéquivalence des ensembles statistiques, de valeurs interdites dans les quantités thermodynamiques (sauts de température) et phénomènes caractéristiques d'auto-organisation spatiale.
Même si les interactions LR constituent la base des systèmes physiques les plus connus, dans la pratique expérimentale il est possible d'observer les effets dynamiques ou thermodynamiques précités seulement si les contributions à courte portée, chocs, bruit,

sont négligeables. Malgré cela, les théories nées dans le cadre des interactions LR ont été appliquées avec succès pour décrire la dynamique des systèmes auto-gravitants,de tourbillons bidimensionnels et de systèmes avec interactions onde-particule;elles présentent en outre d'importantes applications dans le domaine de la physique des plasmas chargés.
A l'heure actuelle c'est à Lynden-Bell que nous devons la description la plus détaillée de la thermodynamique des QSS d'un système LR; sa théorie se développe à la fin des années '70 dans le contexte de la dynamique galactique. La théorie a été appliquée avec succès à la solution du modèle *Hamiltonian Mean Field* (HMF), qui est élevé à système paradigmatique des interactions LR. En effet l'HMF possède une riche phénoménologie qui s'avère potentiellement applicable à l'étude des quelques systèmes laser (FEL e CARL). L'étude analytique de ce modèle, avec la théorie susmentionnée de Lynden-Bell, a été jusqu'à présent limitée à une condition initiale spécifique et restrictive appelée "water-bag".

Mon travail original de thèse s'est tout d'abord consacré à l'extension de la solution de Lynden-Bell pour l'HMF , de façon à comprendre une généralisation de la condition initiale de water-bag à plusieurs niveaux. L'objectif de cette étude est de réussir à approcher des conditions initiales continues plus réalistes.

Par la suite, toujours en me référant au modèle HMF, je me suis intéressé à la caractérisation de la thermodynamique des QSS dans l'ensemble statistique canonique. Ce dernier est une étude complexe qui présente d'importantes problématiques qui sont toujours sans solution; elles sont liées à l'implémentation pratique d'un bain thermique pour systèmes LR. Mon travail a eu comme objectif la définition formelle de cet ensemble statistique. Plus spécifiquement j'ai montré comment, en appliquant la théorie thermodynamique standard, il est possible de mesurer une chaleur spécifique "cinétique" négative même dans un système non isolé. Une première conséquence de cette propriété inattendue amène, comme le démontre le travail de ce thése, à la violation du second principe de la thermodynamique, en consentant de réaliser une machine thermique qui exécute un travail positif en prenant de la chaleur du thermostat froid pour la relâcher dans le thermostat chaud. Un tel résultat nous pousse à reconsidérer l'applicabilité de la théorie thermodynamique actuelle dans le cas des systèmes LR et à redéfinir éventuellement la loi de Fourier pour la transmission de la chaleur.

Enfin la dernière partie de mon thèse est consacrée à l'étude de quelques modèles sur longue portée qui peuvent être considérés comme extensions du modèle HMF.
Tout d'abord je me suis concentré sur le modèle monodimensionnel connu comme α-HMF, défini sur un réseau. Ce modèle consent de varier la force de l'interaction contrôlée par le paramètre réel α. Dans la limite $N \to \infty$ ce dernier modèle est analytiquement équivalent à l'HMF pour $\alpha < 1$. Dans ce travail j'ai étudié la persistance des états QSS dans la limite où la dynamique passe de LR à courte portée

($\alpha = 1$); en outre je me suis consacré à l'étude du régime $\alpha > 1$ en relevant la présence d'une transition de phase typique du régime LR. Les résultats de cette étude suggèrent une généralisation de la définition des systèmes LR qui prenne en considération la dépendance de r de la force plutôt que du potentiel.

Le dernier chapitre de cette thèse est consacré à la caractérisation d'un nouveau modèle LR, qui est considéré comme une extension naturelle du précédent α-HMF, doté d'un terme de distance continu. L'objectif préfixé est d'étudier la dynamique et la thermodynamique LR dans des modèles complexes et d'intérêt potentiel applicatif. Dans ce travail d'introduction centré sur l'étude des états thermodynamiques d'équilibre, j'ai montré comment la présence d'un espace des phases plus étendu permet l'apparition de phénomènes d'auto-organisation avec une symétrie élevée. Cette dernière génère un potentiel efficace de champ moyen semblable aux modèles étudiés précédemment, et une transition de phase semblable à celle que l'on observe aussi bien pour l'HMF que pour l'α-HMF, ce qui rend analogue la description statistique des trois modèles.

Introduction

Among spatially extended systems, a role of paramount importance is played by those interacting with a long-range potential. In fact two of the four fundamental forces in nature, electromagnetism and gravitation, are intrinsically long-range, giving raise to couplings between every interacting element. In many practical situations long-range effects are difficult to observe due to the external noise or because of screening effects originating from different charges distribution. However, it is found that this class of systems is of key importance in many different fields of study, ranging from astrophysics [1, 2], to plasma physics [3], hydrodynamics [4, 5], atomic physics [6] and nuclear physics [7].
These physical systems have been widely studied since the very start of modern science. However, despite the abundance of theoretical and numerical results, their statistical thermodynamic description still poses many problems. A first great challenge lies in the fact that the great number of inter-particles couplings give raise to analytical and numerical difficulties. Moreover, the common assumptions at the very basis of statistical mechanics often rely on the short-range locality of the interaction, which allows one to separate the system into independent parts.
In recent years the study of long-range systems knew a great burst of activity. Thanks to seminal results developed in the context of astrophysics and cosmology, it was realized that the thermodynamics of few simplified models can be solved analytically in different statistical ensembles (e.g. microcanonical). These latter results paved the way to the developing of a generalized statistical thermodynamic theory and to the rigorous description of a broader range of phenomenology, e.g. negative specific heat or ensemble inequivalence.
A new phenomenon observed in numerical simulations and theoretically confirmed in few solvable cases consists in the striking fact that long-range systems may develop long-lasting metastable stationary states, far from the equilibrium, with a lifetime that diverges with the system size. In the thermodynamic limit these states become the solely experimentally accessible, and it was found that they are described by equilibrium distribution functions that do not generally obey to the Boltzmann-Gibbs statistics.

A great amount of theoretical effort was devoted in the last decades into developing a rigorous interpretative framework of the above out-of-equilibrium phenomena. A seminal work pioneered by Lynden-Bell [8] in the context of galactic dynamics, was based on the Vlasov equation that describes the motion of a collisionless gas in the continuous limit. This theoretical approach resulted in a modified statistics that made it possible to characterize the metastable states via a maximum entropy principle. This latter approach was found to be able to accurately predict the value of macroscopic observables in selected long-range many-particles systems, in accordance with numerical simulations.
Lynden-Bell results can be considered a first viable method to describe an isolated long-range system in the microcanonical ensemble. Despite this success there are still open questions on how to describe the interaction of such systems with an external thermal bath, or even on how to physically construct the heat reservoir. This latter problem prevents the rigorous application of the theory to many real-world physical settings, where energy exchange with external systems takes place.
Another problem that limits the general application of the above theory to a broader range of systems, is that its predictive adequacy was confirmed only with reference to simplified models, the most paradigmatic one being the Hamiltonian Mean Field (HMF). Statistical description of more complex long-range interactions, which are not rigorously mean-field, still faces numerical and theoretical problems.

The work of this thesis will concentrate on developing the general knowledge of dynamical and statistical properties of long-range systems. In the course of the thesis we will show how the general microcanonical Lynden-Bell theory can be extended to a class of generalized initial conditions. Also, we will try to apply the latter to describe the interaction with an external thermal bath. We will show how this generalized approach introduces new challenges to statistical physics, pointing out the necessity of a better understanding of the basic assumptions behind our knowledge of long-range thermodynamics.
In the last chapters we will introduce a new model for long-range interactions, which we solved analytically and which adds a layer of complexity to the previously studied systems. in particular, by working in this context, we were able to observe a rich phenomenology, including a solid to gas phase transition. Hopefully these results will make it possible to model interesting behaviours, like self-organization as observed in real systems.

The outline of this thesis is the following:

- The first chapter will be focused on a generic introduction to long-range

theory and the key properties that characterize this class of systems. We will briefly review the main results present in literature in order to provide the reader with a comprehensive picture of the topics contained within this work. For a more in-depth understanding of the subject, an extended review on long-range physics was published recently by A. Campa et. al. [9].

- In the second chapter we will introduce the Hamiltonian Mean Field model, to which we shall extensively refer all along the thesis work. We will briefly review its main features and its equilibrium statistical solution both in the microcanonical and in the canonical ensemble, revisiting the results so far obtained in literature on this paradigmatic model.

- In the third chapter we will introduce the theory of metastable Quasi-Stationary-States emergence. In the mean-field continuous limit, this out-of-equilibrium states can be described as equilibrium solutions of the Vlasov equation. We will propose an extension of the Lynden-Bell theory so far employed in the literature, in order to take into account a generalized family of initial conditions, i.e. the "multi-level water-bag". In this general setting we will validate the theory versus numerical simulations.

- In the fourth chapter we will argue for a possible description of a canonical HMF model. Our aim is to elucidate the interaction with an external thermal bath. Rather than focusing on the practical construction of the heat reservoir, we will give a formal description of the interaction with the latter and explore the statistical properties of the system at thermal equilibrium. Surprising counter-intuitive features (like negative kinetic "canonical" specific heat) are observed, which eventually lead to paradoxes when considering a thermal machine working in such setting. These latter results call for an extended thermodynamic theory of long-range systems.

- The fifth chapter is devoted to a numerical characterization of the properties of a long-range lattice model at the short range threshold. We will show how long-range features may still survive in situations where the interaction is technically short-range, according to the classical definition that relies on the decay of the potential with distance. Based on this observation we argue that a more correct definition of long-range systems would take into account the scaling of the interaction force.

- In the sixth chapter we will introduce a new Hamiltonian long-range model, which takes into account the scaling of the potential with respect to a continuous metric distance term. We were able to find an equilibrium solution for this model in the thermodynamic limit, which shows good agreement

with numerical simulations. Living in a more complex phase space, this model shows a rich phenomenology which yields to spatial self-organization and solid-to-gas phase transitions. In the thermodynamic limit we are able to reproduce the transition observed for the HMF, showing effective equivalence between the two models for a wide range of parameters.

- Finally, in the last chapter, we will sum up and conclude.

Chapter 1

Systems with long-range interactions

Systems with long-range interactions are defined through the scaling law of the governing potential. In the following we suppose that the system can be described by Hamiltonian equations and that the interaction can be decoupled in a two-body translationally invariant potential V_p. The latter acts between pairs of constituting elements, and the total potential is given by the sum over all the pairs $V = \sum_p V_p$. This is the case for the systems under study in this work.
We assume also that the potential V_p scales with a distance parameter r, defined on the appropriate metric of the space, and that this scaling can be represented by the following form:

$$V_p(r) = \frac{A}{r^\alpha} \,. \tag{1.1}$$

We consider a system to be *long-range* if $\alpha \leq d$, where d is the dimension of the space where the system is embedded. Otherwise it is considered *short-range*.
To understand the meaning of this definition we must explain in detail how the scaling properties of the potential are related to key thermodynamic properties of the system like extensivity and additivity. These aspects are discussed in section 1.2.

This introductory chapter is devoted to a short discussion of the main theoretical aspects behind long-range physics. For an extensive review see [9]. In the first part 1.1 we will show few examples of long-range systems. In the following section 1.2 we will make a short introduction to the main thermodynamic features of long-range systems, to better explain the difference with respect to short-range interactions. In section 1.3 we will elaborate on the thermodynamic description of long-range systems in the canonical and microcanonical ensemble. Finally in section 1.4 we will introduce the main dynamical out-of-equilibrium

features of long-range models, defining the metastable quasi-stationary-states (QSS) that characterize these systems.

1.1 Examples of Long-Range Systems

Two of the four fundamental interactions in nature, gravity or electromagnetism, are long-range. As we will show later, the long-range nature of a system can be associated to the presence of unusual thermodynamic and dynamic properties: as an example we can observe ensemble inequivalence, negative specific heat and temperature jumps, while dynamically the system can relax towards peculiar out-of-equilibrium states where it remains trapped for a time which diverges with the system size.
In many cases these effects are not detectable, due to the presence of stronger short-range effects (e.g. collisions or noise) that destroy the long-range nature of the underlying physics. This is especially true in the case of gravity, were the overall weakness of the interaction makes long-range effects to become important only at very large scales. Also, in the case of electromagnetism, the effective shielding provided by opposite charges may hide long-range interactions in many physical situations of interest.

This work will be focused on the study of few paradigmatic Hamiltonian models. However there are plenty of examples of genuine long-range interacting systems, to which we shall allude in the following.

Interaction	α	**d**
Gravitational potential	1	3
Coulomb potential	1	3
2D vortices	0	2
HMF	0	1
HMF extensions	$0 \leqslant \alpha < 1$	1

Figure 1.1: Classification of long-range interacting systems based on the embedding dimension d and the characteristic scaling exponent α of the interaction.

Gravitational systems

Systems interacting with a gravitational force in three dimensions are naturally long-range. The gravitational potential scales like $\frac{1}{r}$, which implies $\alpha = 1$ and $d = 3$ in the classification scheme that follows equation (1.1). To avoid short-range divergences, it is customary to introduce an hard core effective short-range cut-off in the above scaling. This prevents problems in the definition of the thermodynamic potential.
The study of these kind of systems has deep implications both in astrophysics and cosmology, but also to collisionless fluid mechanics. Historically, long-range physics was initially developed in order to answer problems coming from this field of application, like evidences of negative specific heat [10, 11, 12] as well as metastable trapping dynamical states [8] in galactic dynamics.

Coulomb-interacting systems

Charged systems with a Coulomb interaction are similar to gravitations systems, being the scaling of the potential the same, and analogous considerations apply to the short-range renormalization due to divergencies.
In mixed charge conducting systems, usually the amount of unbalanced charge is moved to the boundary, so in most cases we limit ourselves to study systems with zero total charge. Also in the Debye-Hückel approximation, were the temperature T is high enough that particles obey to Boltzmann's statistics, the effective potential is given by $V_{eff} \sim \frac{1}{r} e^{-\frac{r}{\lambda_D}}$, where

$$\lambda_D = \sqrt{\frac{k_b T}{4\pi e^2 \rho}} \tag{1.2}$$

is the characteristic Debye length, ρ is the charge density and k_b is the Boltzmann's constant. This length is the range of effectiveness of the shielding effects, and marks the threshold to plasma behaviour. Looking to the dependence of λ_D on the thermodynamic parameters we see that long-range effects are relevant only in the regime of high temperature or low densities. The first one is found in high-temperature plasmas, were observations evidence the presence of out-of-equilibrium trapping states [13, 14] and negative specific heat [15]. The low density conditions are met in the intergalactic medium, which has a Debye length $\lambda_D \sim 10^5$m.

2D hydrodynamics

The physics of two-dimensional incompressible fluids is an important field of application were long-range effects may appear [16]. Generally speaking, in the case of two-dimensional flows, we can observe the formation of interacting large-scale coherent structures (vortices).
The stream function $\Phi(\vec{r})$, where $\vec{r}$ is the position vector on the plane, is related to the modulus of the vorticity vector $\omega = \frac{\partial v_y}{\partial x} - \frac{\partial v_x}{\partial y}$, defined on the velocity field $[v_x, v_y]$, through the Poisson equation $\Delta\Phi(\vec{r}) = -\omega$.
One can find a solution to the previous equation over an infinite domain Θ in the form:

$$\Phi(\vec{r}) = \int_\Theta \omega(\vec{r}\,')G(|\vec{r} - \vec{r}\,'|)d\vec{r}\,' \,, \tag{1.3}$$

where $G = -\frac{1}{2\pi}\ln(|\vec{r} - \vec{r}\,'|)$ is the Green's function.
Energy E is given by:

$$\begin{aligned} E =& \frac{1}{2}\int_\Theta (v_x^2 + v_y^2)d\vec{r} = \frac{1}{2}\int_\Theta (\nabla\Phi)^2 d\vec{r} = \frac{1}{2}\int_\Theta \omega(\vec{r})\Phi(\vec{r})\, d\vec{r} \\ =& \frac{1}{4\pi}\int_\Theta\int_\Theta \omega(\vec{r})\omega(\vec{r}\,')\ln(|\vec{r} - \vec{r}\,'|)\, d\vec{r}d\vec{r}\,' \,. \end{aligned} \tag{1.4}$$

This is obtained on an infinite domain, where the term coming from the integration over the boundary vanishes. Equation (1.4) shows that vortices have a logarithmic interaction, that corresponds to $\alpha = 0$ and $d = 2$, according to the above classification scheme.
The long-range nature of the interaction emerges even more clearly if we approximate the vorticity field with a sum of point vortices with given circulation Γ_i located in $\vec{r}_i$: $\omega(\vec{r}) = \sum_i \Gamma_i \delta(\vec{r} - \vec{r}_i)$. If this assumption holds then the energy takes the form:

$$E = -\frac{1}{4\pi}\sum_{i,j|i\neq j} \Gamma_i\Gamma_j \ln|\vec{r}_i - \vec{r}_j| \,, \tag{1.5}$$

which is clearly logarithmic.
These kind of systems are of key importance in hydrodynamics and have been extensively studied in the past. In particular they display evidences of ensemble inequivalence and negative specific heat [17, 18, 19].

Simplified (toy) models

Physically realistic models of long-range interactions are difficult to study numerically, especially in higher dimensions, due to the large number of degrees

of freedom involved and the fact that the matrix of interaction between each element constituting the system (everything is interacting with everything) gets very large. For this reason, theoretical studies on long-range interacting systems are customarily performed by resorting to simplified toy models, which enables one to reproduce the long-range dynamical and thermodynamic properties in a phase space of reduced complexity.
This strategy is common to many fields in theoretical physics. For example the well known Ising model is widely used to mimic ferromagnetic spin systems.
In the last decades many long-range toy models were introduced in literature. Among them the HMF is certainly the most extensively studied and paradigmatic. Many of the results presented in this work are related to this model.
The HMF was shown capable of reproducing many key long-range features, with complex 1-D phase transitions, metastable stationary states [20, 21] and negative specific heat [22, 23]. A more extended description of the model is the subject of chapter 2.

Small systems

Systems which are governed by short-range forces, but whose size is comparable with the interaction range, can also manifest long-range features like ensemble inequivalence. These latter systems are briefly mentioned in this section as an exception to the generic classification (1.1). This is an important field of application, relevant to many different physical systems like atomic clusters, large nuclei or quantum fluids, where phenomena like out-of equilibrium phase transitions and negative specific heat [24, 25] could be eventually interpreted by resorting to the thermodynamic theory developed in the long-range framework.

1.2 Extensivity and Additivity

A long-range system has key distinctive features that mark the difference with respect to the physics of short-range ones. Typically one encounters several problems when defining the thermodynamic variables for systems subject to long-range interactions. The system may be non-extensive and non-additive, meaning that we may expect a counter-intuitive behaviour of the thermodynamic potentials with respect to the well known theoretical framework developed in the short-range context.

1.2.1 Extensivity and Kac rescaling

Given a system formed by N particles, in the thermodynamic limit we define *intensive* a quantity whose value does not depend on the system size, while we call *extensive* a quantity that scales proportionally to N. To make an example, density or temperature are intensive, while the energy E is usually extensive.
Extensive quantities allow the definition of intensive ones, like energy density $\epsilon = \frac{E}{N}$, that have a finite value in the thermodynamic limit, and bears key importance in thermodynamic applications.
This property is satisfied in case of short-range systems, where the number of interactions between particles is proportional to N, but we can easily understand how this condition is not obviously met in long-range ones, where the number of interactions scales with N^2.
In order to understand better this latter fact, let us consider as an example the potential energy U of a single particle, interacting with the potential (1.1), placed in the center of an homogeneous distribution of particles in a sphere of radius R and dimension d, with $\alpha \neq d$:

$$U = \int_{\delta}^{R} \frac{A}{r^{\alpha}} d^d r \sim \int_{\delta}^{r} r(d-1-\alpha) dr = R^{d-\alpha} - \delta^{d-\alpha} \,. \tag{1.6}$$

Here we are neglecting a small neighbourhood δ of the origin in order to avoid the divergence of the potential (which is unrelated to long-range features) and any constant coming from the integration. From the previous equation it is evident that, if A is constant, the energy U diverges as a power law with R, if $\alpha \leq d$, which makes the total energy non-extensive.
In the marginal case $\alpha = d$ the energy still diverges logarithmically:

$$E \sim \log(R) - \log(\delta) \,. \tag{1.7}$$

In order to recover extensivity it is customary to introduce factor scaling with the system size in front of the potential, as proposed by Kac et al. [26]. This procedure is quite common in mean-field physics, the most notable example being the Curie-Weiss model for ferromagnetic spin interaction, were particles interact with the mean potential generated by the system configuration. To better understand the effect of this scaling, let us consider as an example the simple case of the Hamiltonian Mean Field model (HMF), which we will introduce properly later and will become quite familiar to the reader, defined by the following Hamiltonian:

$$H = \sum_{i=1}^{N} p_i^2 + \frac{1}{2N} \sum_{i,j=1}^{N} (1 - \cos(\theta_i - \theta_j)) \,, \tag{1.8}$$

where p is the momentum and θ the angular coordinate of a particle moving on a circle.

Here the kinetic part of the energy is extensive, and thus the kinetic temperature T is an intensive quantity, while the sum in the potential grows like N^2, which is normalized by the factor $\frac{1}{N}$, thus making it extensive too.

An alternative way to recover extensivity without rescaling the potential would be to make the temperature extensive $T \to TN$, such that the terms of the free energy $F = E - TS$ have the same scaling (entropy S scales linearly with N and E scales with N^2). This approach is equivalent to rescaling velocities (assuming the temperature is the average kinetic energy per particle) and thus change the timescale. Both prescriptions shown above are equivalent from the point of view of the physical description of the system, but the rescaling of the potential is more widely used since it allows for a more intuitive physical insight.

1.2.2 Lack of Additivity

Even though it is possible to renormalise the interaction so to recover extesivity, long-range systems are by definition non-additive, meaning that they cannot be described as a sum of disjoint subsets.
Additivity is a key thermodynamic property. It implies that if we divide the ensemble Γ of all the elements of a system into k disjoint macroscopic sets Γ_i, each containing a smaller number of elements, with $\bigcup_{i=1}^{k} \Gamma_i = \Gamma$, then the total value of any extensive quantity computed for the whole ensemble Γ is given by the sum of the values relative to each set. For example the total energy E would read $E = \sum_{i=1}^{k} E_i$.

To make an example, let us consider the well known Curie-Weiss model described by the following Hamiltonian:

$$H = -\frac{J}{2N}(\sum_{i=1}^{N} S_i)^2 \,, \tag{1.9}$$

where N is the number of spins of magnetization $S_i = \pm 1$. This model is extensive thanks to the factor $\frac{1}{N}$. Let us consider a spin distribution which is split into two separate identical regions of different orientation, like the one displayed in figure (1.2).
The energy of the two areas is identical $E_1 = E_2 = -\frac{JN}{8}$. The total energy of the system is however $E = 0$. The system is hence non-additive since $E \neq E_1 + E_2$.

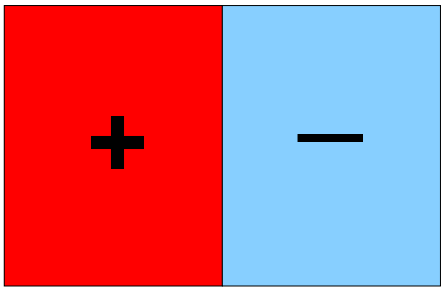

Figure 1.2: A spin distribution which shows the lack of additivity of the Curie-Weiss model (1.9). The two identical areas are homogeneously populated by spins of orientation $+1$ or -1, so that the total magnetization is zero.

1.3 Thermodynamics

The lack of additivity shown before has a relevant impact on the thermodynamic properties of a long-range system, resulting in unusual behaviours of the thermodynamic functions and yielding among the others to ensemble inequivalence, negative specific heat and temperature jumps.
As an example, let us suppose that we have a system which is characterized by two thermodinamic extensive macroscopic quantities, respectively the energy E and the magnetization M (this is the case of the HMF system, as we will show in chapter 2). If the system is additive, then we can identify two disjoint subsets and introduce a parameter λ such as:

$$\begin{aligned} E &= \lambda E_1 + (1-\lambda)E_2 \,, \\ M &= \lambda M_1 + (1-\lambda)M_2 \,. \end{aligned} \tag{1.10}$$

Of course λ measures the relative size of the two subsets.

Each state with $0 \leq \lambda \leq 1$ is accessible by simply varying the size of the two subsets. Property (1.10) is the mathematical definition of convexity for the macrostates space (E, M). A dynamical system can display the latter only by neglecting the interaction energy between the two subsets. This of course cannot be done for long-range systems.
In principle, the macroscopic phase space of a long-range system is not necessarily convex, and thus forbidden regions of macroscopic states may appear between two different accessible states. A schematic representation of this latter phenomenon is portrayed in figure (1.3). This in turn would mean that the space of macrostates is no longer connected and one may observe first order phase transitions (jumps) in the value of the thermodynamic variables, as well as ergodicity breaking.

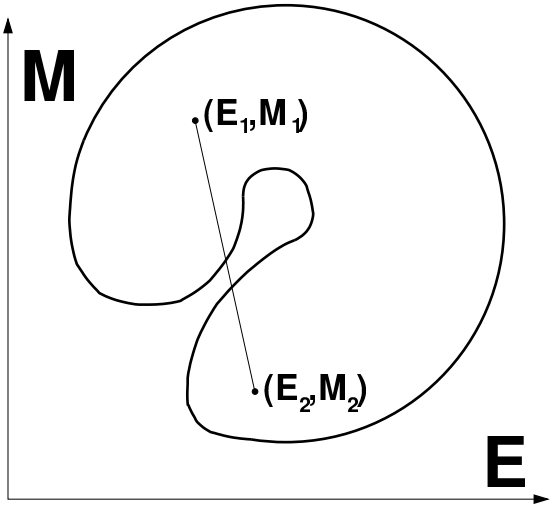

Figure 1.3: Schematic representation of a convex region in the macrostates (E, M) space for a long-range system.

Let us start by recalling the definition of statistical ensembles from statistical mechanics: a statistical ensemble is a collection of all the microscopic configurations (microstates) compatible with a given macrostate (identified by macroscopic measurables like temperature, total energy and so on). At the thermodynamic equilibrium, the measure of this ensemble, considering each microstate a point in the phase space, is proportional to the probability of the macrostate it represents. Usually the statistical relevance of these ensembles is accurate in the thermodynamic limit, which corresponds to having an infinite collection of microstates. This in turn implies that the number of degrees of freedom of the system is also infinite, and in a many body system this latter corresponds to sending the number of particles N to infinity. These key concepts are the basis of all the statistical mechanic theory.
The following are the main statistical ensembles that prove useful to construct a thermodynamic description of a physical system:

- The *microcanonical ensemble*, describing an isolated system in which each microstate corresponds to a configuration with fixed given energy and number of particles.

- The *canonical ensemble*, which describes to a system in contact with a large thermal bath (with fixed temperature T). The energy can be exchanged but the number of particles is fixed. This statistical ensemble is the most used in common thermodynamic problems.

- The *grand canonical ensemble*, corresponding to a system in which both energy and particles can be exchanged with the thermal bath.

1.3.1 The microcanonical description

Let us consider the simple case of a system with $d = 3$. Assume that each microstate is identified by position q and momentum p of the N particles, with total energy E and volume V. The microcanonical partition function, which gives the measure of the ensemble, is defined as:

$$\Omega(N, E, V) = \frac{1}{N!} \int_{\Gamma} \delta(E - H(q, p)) d^{3N} q d^{3N} p \,, \tag{1.11}$$

where the integral extends over the whole accessible phase space Γ and $H(p, q)$ is the Hamiltonian equation describing the system. From this, following Boltzmann's prescriptions, we define the microcanonical entropy function S:

$$S(N, E, V) = k_b \log \Omega(N, E, V) \,, \tag{1.12}$$

where k_b is the Boltzmann's constant (we will consider $k_b = 1$ for simplicity), and recover the thermodynamic limit sending $N \to \infty$, $E \to \infty$ and $V \to \infty$, while keeping finite all the intensive quantities like density $\rho = \frac{V}{N}$, energy density $\epsilon = \frac{E}{N}$ and entropy density $s = \frac{S}{N}$.

We define the microcanonical thermodynamic temperature of a system as

$$T = (\frac{\partial S}{\partial E})^{-1} = (\frac{\partial s}{\partial \epsilon})^{-1} \,, \tag{1.13}$$

and the microcanonical specific heat (at constant volume) as

$$c_v^{mic} = \frac{\partial \epsilon}{\partial T} = (\frac{\partial^2 s}{\partial \epsilon^2})^{-1} \,. \tag{1.14}$$

In the case of short-range systems, additivity implies that the entropy density s is a concave function in ϵ. Back to relations (1.10), it is easy to observe that

$$s(\rho, \lambda\epsilon_1 + (1 - \lambda)\epsilon_2) \geq s(\rho, \lambda\epsilon_1) + s(\rho, (1 - \lambda)\epsilon_2) \,, \tag{1.15}$$

is equivalent to

$$\log(\Omega(\rho, \lambda\epsilon_1 + (1 - \lambda)\epsilon_2)) \geq \log(\Omega(\rho, \lambda\epsilon_1)) + \log(\Omega(\rho, (1 - \lambda)\epsilon_2)) \,, \tag{1.16}$$

which is always true in the thermodynamic limit.

1.3.2 The canonical description

Additivity is a key property to construct the canonical ensemble for a system in contact with a thermal bath at temperature T. The classical procedure considers a system Λ_1 of energy E_1 which is in contact with a thermal bath Λ_2 of total energy $E_2 >> E_1$. The combination of the two systems results in a large isolated system with energy E that will eventually reach a microcanonical equilibrium. If additivity holds, we have $E = E_1 + E_2$. The microcanonical entropy of the isolated system is given by:

$$S(E) = k_b \log(\Omega(E)) \,, \tag{1.17}$$

where $\Omega(E)$ is the number of configurations (microstates) with total energy E.

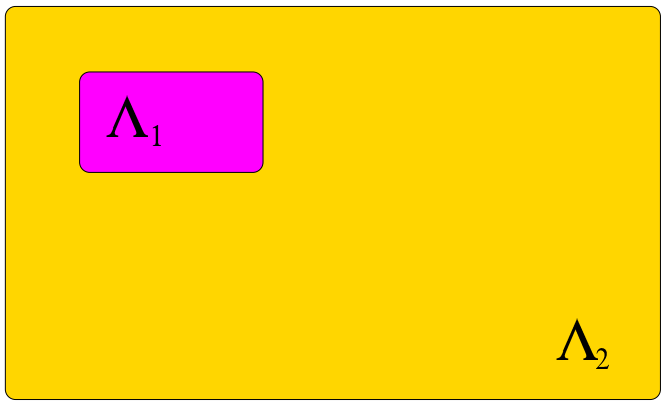

Figure 1.4: Pictorial representation of an isolated system $\Lambda = \Lambda_1 \bigcup \Lambda_2$ formed by a small system Λ_1 immersed in a thermal bath Λ_2.

The two subsystems reach equilibrium when

$$\frac{\partial S_1(E_1)}{\partial E_1} = \frac{\partial S_2(E_2)}{\partial E_2} \,, \tag{1.18}$$

$\frac{\partial S}{\partial E} = \frac{1}{T} = \beta$ being the inverse temperature.
Since $E_2 >> E_1$, The entropy of the heat reservoir can be expanded to the second order, yelding:

$$S_2(E - E_1) \simeq S_2(E) - E_1 \frac{\partial S_2(E)}{\partial E} = S_2(E) - \beta E_1 \,. \tag{1.19}$$

The probability p_1 of finding a system Λ_1 with energy between E_1 and $E_1 + dE_1$, while Λ_2 has energy E_2, is proportional to the number of microscopic configurations $\Omega(E_2)$:

$$p_1 = C\Omega(E - E_1) = C' \exp(-\beta E_1) \,, \tag{1.20}$$

where C and C' are constant factors. Indexing with γ all the possible energy configurations of system Λ_1, the normalization condition implies:

$$\sum_{\gamma} p_\gamma = 1 = C' \sum_{\gamma} \exp(-\beta E_\gamma) \,. \tag{1.21}$$

From this latter equation we obtain the partition function Z describing the statistics of the system Λ_1 in the canonical ensemble, while at equilibrium with the thermal bath:

$$Z(\beta) = \frac{1}{C} = \sum_{\gamma} \exp(-\beta E_\gamma) \,. \tag{1.22}$$

Consider now the case of simple 3-D gas in contact with a thermal bath characterized by the temperature $T = \frac{1}{\beta}$. The measure of the canonical ensemble can be described via the partition function:

$$Z(N, \beta, V) = \int \Omega(N, E, V) e^{-\beta E} dE = \frac{1}{N!} \int_{\Gamma} e^{-\beta H(q,p)} d^{3N} q d^{3N} p \,, \tag{1.23}$$

where the first integral is defined over the whole space of accessible energy configurations.
In the thermodynamic limit we define the free energy per particle f as

$$f(\beta, \epsilon) = -\frac{1}{\beta} \lim_{N \to \infty} \frac{1}{N} \log(Z(N, \beta, V)) \,. \tag{1.24}$$

In the following we will use more the practical definition of rescaled free energy, as $\phi = \beta f$.

In general the total energy of a system divided into two parts, as in the example considered above, can always be written as $E = E_1 + E_2 + E_{\text{int}}$, E_{int} being the interaction energy between the two parts.
For short-range systems the ratio $\frac{E_{int}}{E_1 + E_2}$ goes to zero in the thermodynamic limit ($N \to \infty$): the energy of a system is proportional to the volume of the system in d dimensions, while the interaction term is relative to dimension $d - 1$ of the contact surface between the two systems. The interaction is hence effective only between nearest neighbours.
With this latter consideration in mind, the procedure explained above always applies and allows one to construct a proper canonical ensemble for short-range systems.

In the case of long-range systems, energy is no more additive, as previously noticed. The potential is in fact coupling each particle belonging to the system

and the interaction energy is also proportional to the total volume. Recalling the generic potential (1.1), we obtain:

$$E_{\text{int}} = 2 \int_{\Lambda_1} \int_{\Lambda_2} V(r - r') d^d r d^d r' \,. \tag{1.25}$$

For $\alpha \leq d$, recalling the scaling coming from equation (1.6), the energy contribution that is associated to the interaction term, is no more negligible in the thermodynamic limit. Also, Kac renormalization does not alter the scaling ratio between E and E_{int}.

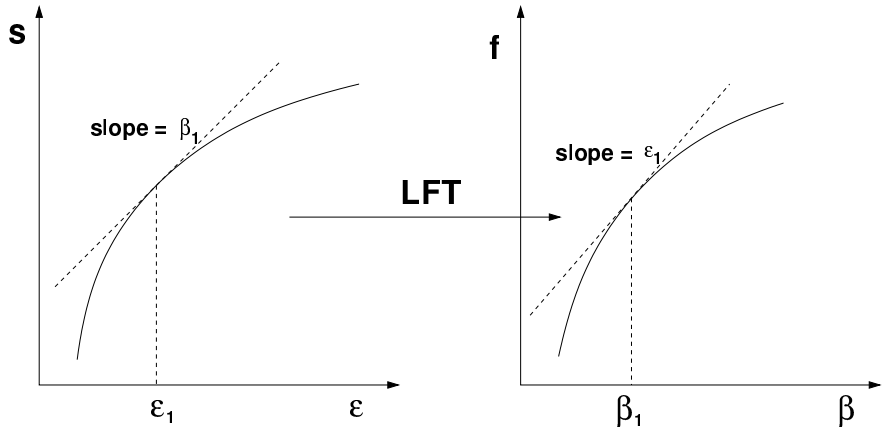

Figure 1.5: Relation between entropy density s and free energy per particle f through the LFT transform.

As a consequence, we cannot derive a canonical ensemble description in case of long-range interactions using the usual construction as explained above, and this poses serious problems in the study of their thermodynamics properties in case of open systems. Typically one can resort to the formal definition of a thermal bath [27, 28, 29, 30]. Assuming that the partition function Z exists, we can easily prove [9] that in the thermodynamic limit the following equality holds:

$$e^{-N\phi} = Z(N, E, V) = \int e^{-N[\beta\epsilon - s(\rho,\epsilon)]} dE \,, \tag{1.26}$$

so that, at equilibrium, ϕ can be obtained from the microcanonical entropy through a Legendre-Fenchel transform (LFT):

$$\phi = \inf_{\epsilon} [\beta\epsilon - s(\rho, \epsilon)] \,. \tag{1.27}$$

Since the LFT of a generic function is always concave, ϕ is concave.
This latter procedure is always valid and only assumes the existence of an

external thermal bath, whose action on the system is to keep the thermodynamic temperature $T = \frac{1}{\beta}$ fixed. We will return on the definition of the canonical ensemble in chapter 4, and discuss the problem that may arise in presence of long-range interactions.

1.3.3 Ensemble inequivalence and convexity of the entropy functional

In this section we will introduce a peculiar thermodynamic feature that can manifest for long-range interacting systems. This is the *ensemble inequivalence*, a phenomenon associated to the presence of unusual thermodynamic microcanonical properties, like negative specific heat [31, 32] and negative susceptibility (for magnetic-like systems) [33, 34].

In the case of short-range systems, entropy s is typically monotonic and concave, thus the inverse LFT can be applied and we can obtain a bijective way to map the canonical and microcanonical equilibrium thermodynamic functions onto each other, proving the equivalence of the two ensembles. The practical consequence of this latter property is that the same macrostate can be realized in both ensembles: this means that a microcanonical macrostate with an average temperature and constant energy, corresponds to a canonical macrostate with constant temperature and average energy, thus allowing a one to one mapping between energy and temperature.

Convex regions in entropy may appear in presence of a phase transition, were usually the equilibrium functions s and ϕ have some discontinuity in their derivatives.
Let us consider as an example figure (1.6), where we show a typical entropy function $s(\epsilon)$ in the case of a phase transition between liquid and gas, with a convexity in the energy range $[\epsilon_1, \epsilon_2]$. We recall that the first derivative of entropy is the inverse temperature $\beta = \frac{\partial s}{\partial \epsilon}$, so T may not monotonically increase with energy if s is convex.

In the case of short-range systems, thanks to additivity, an hypothetical convex region could be described as a mixing of two different phases of energy densities ϵ_1 and ϵ_2, so that the total energy density is $\epsilon = \lambda\epsilon_1 + (1-\lambda)\epsilon_2$, λ being the fraction of phase 1 present in the system. The entropy function s' describing the two phases has zero curvature for $\epsilon_2 > \epsilon > \epsilon_1$, and corresponds

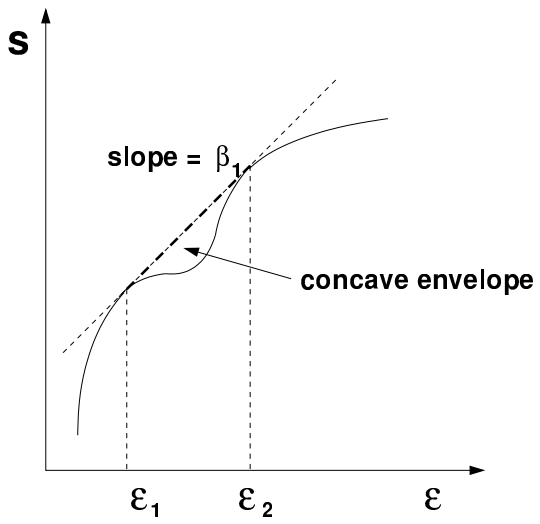

Figure 1.6: Concave envelope construction in a convex region of entropy $s(\epsilon)$.

to the concave envelope of the original convex entropy s. Hence $s' \geq s$, which in turn implies that s is an unstable solution and the system is naturally driven toward *phase separation* [35, 36, 37].

As schematically represented in figure (1.7), the LFT maps the entropy range $[s(\epsilon_1), s(\epsilon_2)]$ into a single point $\phi(\beta_1)$ were the first derivative $\frac{\partial \phi}{\partial \beta} = \epsilon$ is discontinuous. Increasing the temperature of the system, in the canonical ensemble, one obtains a first order phase transition with a finite jump in energy.
In the case illustrated above the microcanonical and canonical ensembles described by s and ϕ are not equivalent. Still the two functions can be mapped one to another with a bijective function, since the inverse LFT of ϕ reproduces the concave envelope s'. This latter is in fact a marginal case so it is referred to in the literature as to a partial inequivalence [38].

In a long-range system the lack of additivity implies that the entropy function is not necessarily concave, even far from phase transitions, and the states corresponding to points in any convex region of the entropy function are physically stable due to the impossibility to phase separate (which requires additivity). The derivation of the free energy from the Legendre-Fenchel transform (1.27) is still valid, and the function we obtain following this procedure is still concave The inverse LFT mapping would however reproduce the concave envelope of the microcanonic entropy, and not the original entropy function. In this case we do not have anymore a bijective mapping between the microcanonical and canonical ensemble, and ensemble inequivalence takes place.

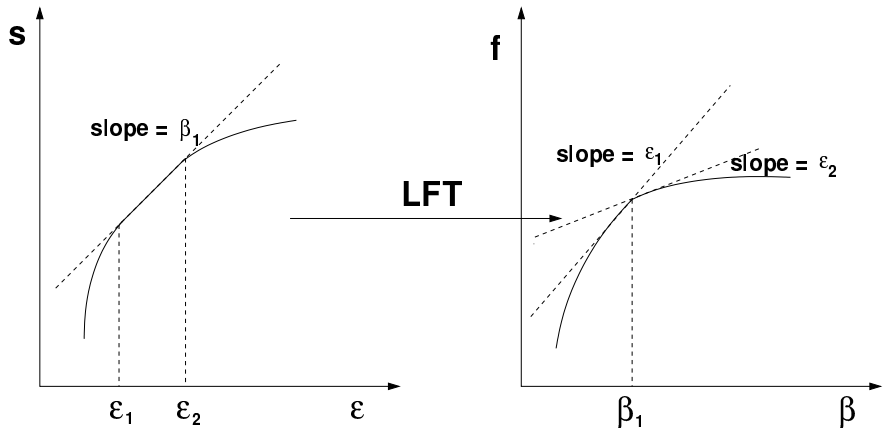

Figure 1.7: Entropy s and free energy f construction in presence of a first order phase transition.

As suggested above, the presence of stable convex regions in entropy can have a conceptually profound impact on the thermodynamic behaviour of a system. A striking consequence is that long-range systems can manifest negative micro-canonic specific heat, formally obtained from the second derivative of $s(\epsilon)$:

$$c_v^{\mathrm{mic}} = \frac{\partial \epsilon}{\partial T} = \frac{\partial^2 s}{\partial \epsilon^2}^{-1} . \tag{1.28}$$

In practical terms we the system will reduce its temperature while increasing the energy. This latter surprising condition is well known in scientific literature [31, 32].
Conversely the canonical specific heat is defined from the rescaled free energy ϕ as follows:

$$c_v^{\mathrm{can}} = \frac{\partial^2 \phi}{\partial \beta^2} \left(\frac{\partial \beta}{\partial T} \right) . \tag{1.29}$$

If we consider $T = \frac{1}{\beta}$ we have $\frac{\partial T}{\partial \beta} < 0$, and from the concavity of ϕ it follows that c_v^{can} must be always positive, independently on the nature of the system. This last result, which is quite intuitive and always true at equilibrium, may be reconsidered when one has to face out-of-equilibrium thermodynamics, as we will see more in detail in chapter 4.

1.4 Out-of-equilibrium quasi-stationary states (QSS)

Studying the dynamics of Hamiltonian systems with a large number of degrees of freedom and its connection to equilibrium statistical mechanics has been a long standing problem. The relaxation to statistical equilibrium has been under scrutiny ever since the pioneering work of Fermi and the FPU problem [40]. Moreover, since the advent of powerful computers and for specific systems within a class of initial conditions, integrating numerically Hamiltonian dynamics has proven to be competitive in regards to Monte-Carlo schemes for the study of statistical properties (see for instance [41, 42] and references therein). The assumption made is that since the system admits only a few conserved quantities for generic initial conditions, once the dimensions of phase space are large enough, microscopic Hamiltonian chaos should be at play and be sufficiently strong to provide the foundation for the statistical approach within the micro-canonical ensemble.
In order to attain thermodynamic equilibrium one typically has to wait a long enough time t for the system to relax to its final maximum entropy state.

However recent studies have shown that there is an increase of regularity with the system size in the microscopic dynamics when considering systems with long-range interactions [43, 44, 45, 46]. Indeed, the statistical and dynamical properties of these systems are still under debate. For instance we can measure negative microcanonical specific heat [47]. Moreover, phase transitions for one dimensional systems are also observed [9].

Given a vector $\vec{x}(t)$ representing the state of the system at time t, whose size depend on the number of degrees of freedom, the evolution of a generic dynamical system may be represented by an application $\Phi(t, \vec{x})$, called flux, that transforms the initial condition $\vec{x}_0$ at $t = 0$ into the evolved state $\vec{x}_t$:

$$\vec{x}_t = \Phi(t, \vec{x}_0) \, . \tag{1.30}$$

From the microscopic configuration $\vec{x}$ we can then compute macroscopic quantities $\Theta(\vec{x})$ (which can be every typical quantity like temperature or energy). A stationary equilibrium state requires that fluctuations of Θ would be negligible and, apart from integrable or strongly non-ergodic cases, this is generally true in the limit $N \to \infty$, where small contributions cancels out thanks to the increased statistics.

When a stationary equilibrium state is reached it means that:

$$\lim_{N\to\infty}\lim_{t\to\infty}\left[\Theta(\Phi(t',\vec{x}_0))-\Theta(\Phi(t,\vec{x}_0))\right]=0 \quad ,\forall t'>t\,, \tag{1.31}$$

so that Θ does not depend any longer on time.

A striking feature of the long-range class of systems is that, generally speaking, they show a weak convergence to equilibrium which is much slower than the typical exponential one common in the short-range case. For some choice of the initial conditions, far from equilibrium, after an initial fast relaxation, systems with long-range interaction can be trapped in out-of-equilibrium long lasting metastable quasi-stationary-states (QSS).
The lifetime τ of a QSS strongly depends on the number of degrees of freedom, and may diverge with the system size N as a power law [9]. For a long-range system, the limits (1.31) may not commute: if the size limit is performed before the time limit, the system may remain permanently trapped in a QSS, that actually becomes a proper equilibrium states, albeit possessing peculiar characteristic which are typical of nonequilibrium physics, like the strong dependence from the initial datum.
This observation is relevant for any large enough long-range system (e.g. galaxies [48]), for which the time needed to attain the thermodynamic equilibrium could be greater that the time accessible to the experiment (or the observation in the case of astrophysics).

Out-of-equilibrium QSS in long-range systems have been observed in numerical simulations, and have been analytically investigated for a wide range of different long-range potentials [50, 51, 52]. QSS emergence is found consistent with observations coming from many different fields of study, either from astrophysics [49, 48], charged systems e.g. plasmas [54] and magnetic dipolar systems [53]. Also out-of-equilibrium long-range physics was successfully used to interpret the behaviour of experimental systems based on wave-particle interactions, e.g. free-electron lasers [55, 56], and collective atomic recoil lasing (CARL) [57].
The HMF is the benchmark model for theory development targeted to the understanding of QSS. In chapter 3 and 4 we will analyse more deeply the QSS phenomenology. In the following chapter we will introduce and discuss the HMF model.

Chapter 2

Equilibrium solution of the HMF model

In the previous chapter we have reviewed the main theoretical picture of the long-range physics and its peculiarities. In this chapter we will focus on a paradigmatic example of long-range interacting systems, the so called Hamiltonian Mean Field (HMF) model, first introduced by Antoni and Ruffo in 1995 [58].
Usually long-range models are quite difficult to study, due to the numerical complexity coming from all-to-all interactions. The long-range potential effectively couples all the particles in the system, so it is impossible to reduce the dimension of the interaction matrix into smaller subsets. When computing the trajectory of a particle, in N-body simulations, calculations have to be performed considering the effect of all other particles constituting the system, and this makes the computational complexity to scale as $(Nd)^2$, where N is the number of particles and d is the dimension of the embedding space. Since one is generally interested in the large size ($N \to \infty$) limit, it can be easily understood how this poses problems that are beyond the capabilities of modern computers.
The HMF is a toy-model that was specifically designed in order to be easily implementable and analytically solvable, thus making it the ideal candidate to investigate the properties of long-range systems in the thermodynamic limit. Since its introduction it has been extensively studied, and has become a paradigmatic model for the study of out-of-equilibrium stationary states.

The HMF shows an interesting dynamic and thermodynamic behaviour. When performing numerical simulations, starting out-of-equilibrium, the system is usually trapped in long-lived QSSs, before relaxing to the Boltzmann equilibrium solution. The simplicity of the model allows one to develop a theoretical approach that explains the presence of QSSs as equilibrium solutions of the Vlasov

equation, as pioneered in [21] and as we shall review in chapter 3. Importantly, the HMF was also proposed to interpret the behaviour of wave-particle interacting systems: under specific conditions its nonequilibrium properties of can reproduce the dynamical aspects of the governing Hamiltonian of the Collective Atomic Recoil Laser (CARL) [57].
In the following sections we will briefly focus on the equilibrium thermodynamic description of the HMF model, revisiting results which were extensively studied in the literature (e.g. see [9]).

In statistical physics, it is very difficult to find models which allow for a straightforward computation of the canonical partition function, and, from that, of the microcanonical entropy function. In short-range systems it is customary to derive the micronanonical description from the canonical ensemble, thanks to ensemble equivalence, since in that case one needs to cope with simple integrals over the Boltzmann weights. As we observed in chapter 1.3.3, in long-range systems the microcanonical and canonical ensembles may be inequivalent. Hence it is important to derive a coherent description of each ensemble, without relying on the a priori supposed property of equivalence.

As we shall see, the HMF displays a second order phase transition at equilibrium, which divides between homogeneous to inhomogeneous states. In addition more complex out-of-equilibrium phase transitions are found, which interest the QSS states, as we will show in chapter 3.
In this chapter we will first introduce the dynamics of the HMF model, in section 2.1. Then we will turn to briefly discussing the thermodynamic equilibrium description in both canonical ensemble, section 2.2, and in the microcanonical one, section 2.3.

2.1 The HMF model

The governing Hamiltonian of the HMF model describes N identical particles that interact with a cosine-like potential:

$$H = \sum_{i=1}^{N} p_i^2 + \frac{C}{2N} \sum_{i,j=1}^{N} (1 - \cos(\theta_i - \theta_j)) \,. \tag{2.1}$$

The canonical coordinate θ_i identifies the position of particle i over the unitary circle $[0, 2\pi[$, with periodic boundary conditions, while p_i is the conjugated momentum.
Particles have the same mass, which we assume equal to one for simplicity. Particles cross each other, or equivalently experience perfectly elastic collisions, due

to the fact that masses are identical.
Depending on the value of the coupling constant C, the interaction can be either attractive ($C > 0$) or repulsive ($C < 0$). Both cases were studied in the past [9, 60], however all along this work we will assume $C = 1$ for simplicity.
The HMF potential can be also seen as the first harmonic in the expansion of the one-dimensional self-gravitating potential [61, 62], taking periodic boundary conditions.

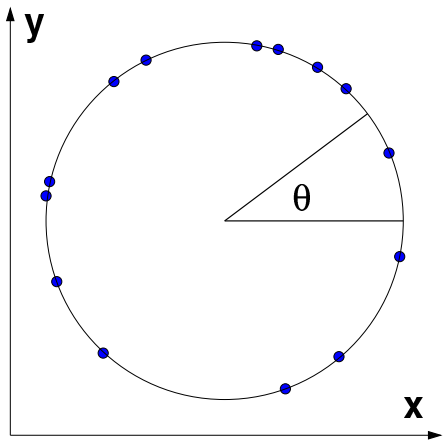

Figure 2.1: Pictorial presentation of the HMF system, where particles are identified by their angular position θ over a circle. The interaction is only sensitive the angular distance $\Delta\theta$ between each pair of particles.

The system obeys the following Hamilton equations:

$$\dot{\theta}_i = p_i \,, \tag{2.2}$$

$$\dot{p}_i = -\frac{\partial H}{\partial q_i} = -\frac{1}{N}\sum_{j=1}^{N} \sin(\theta_i - \theta_j) \,. \tag{2.3}$$

In analogy with spin-glass systems, we introduce a quantity that we identify with the single-particle magnetization vector $\vec{m}_i$, defined as:

$$\vec{m}_i = (\cos(\theta_i), \sin(\theta_i)) \;, \tag{2.4}$$

and define a global magnetization vector $\vec{M}$ with axial components M_x M_y as

$$\begin{aligned} M_x &= \frac{1}{N}\sum_i \cos(\theta_i) \,, \\ M_y &= \frac{1}{N}\sum_i \sin(\theta_i) \,. \end{aligned} \tag{2.5}$$

With the above notation we can simplify the previous Hamiltonian (2.1) into its mean-field version, which explicitly depends on the modulus M of the global magnetization

$$H = \sum_{i=1}^{N} p_i^2 + \frac{1 - M^2}{2} \,. \tag{2.6}$$

Recalling that $\phi = \arctan(\frac{M_x}{M_y})$, one obtains the following mean-field equations of motion:

$$\dot{\theta}_i = p_i \,, \tag{2.7}$$
$$\dot{p}_i = -M \sin(\theta_i - \phi) \,. \tag{2.8}$$

2.2 Canonical equilibrium solution

The HMF system can be easily solved in the canonical ensemble and we can obtain an analytical description of the equilibrium distribution function in the thermodynamic limit. In this section we will review the derivation of the canonical solution.

The canonical partition function is:

$$Z(\beta, N) = \int e^{-\beta H} d\theta_1 dp_1 \dots d\theta_N dp_N \,, \tag{2.9}$$

with $\beta = \frac{1}{k_b T}$ the inverse temperature and k_b the Boltzmann constant. In the following we will consider $k_b = 1$ for simplicity.
By integrating over the momenta we obtain:

$$Z(\beta, N) = \left(\frac{2\pi}{\beta}\right)^{\frac{N}{2}} e^{-\frac{N\beta}{2}} \int \exp\left[\frac{\beta}{2N} \sum_{i,j=1}^{N} \cos(\theta_i - \theta_j)\right] d\theta_1 \dots d\theta_N \,. \tag{2.10}$$

In the following we will use the Hubbard-Stratonovich transformation which, given two 2-dimensional vectors $\vec{x} = (x_1, x_2)$ and $\vec{y} = (y_1, y_2)$, reads:

$$e^{\frac{\mu}{2}\vec{x}^2} = \frac{1}{\pi} \int_{-\infty}^{\infty} \exp\left[-|\vec{y}|^2 + \vec{x} \cdot \vec{y}\sqrt{2\mu}\right] dy_1 dy_2 \,. \tag{2.11}$$

Recalling (2.5), and applying (2.11) to (2.10), we obtain:

$$Z(\beta, N) = \left(\frac{2\pi}{\beta}\right)^{\frac{N}{2}} e^{-\frac{N\beta}{2}} \frac{1}{\pi} \int d\theta_1 \dots d\theta_N \int_{-\infty}^{\infty} \exp\left[-|\vec{y}|^2 + N\vec{M} \cdot \vec{y}\sqrt{\frac{2\beta}{N}}\right] d\vec{y} \,. \tag{2.12}$$

By changing variables $\vec{y}' = \sqrt{\frac{2\beta}{N}}\vec{y}$, we can factorize the integration over the particle coordinates and go to polar coordinates $y' = |\vec{y}'|$. We finally obtain:

$$Z(\beta, N) = \left(\frac{2\pi}{\beta}\right)^{\frac{N}{2}} e^{-\frac{N\beta}{2}} \frac{N}{2\pi\beta} \int_{-\infty}^{\infty} \exp\left[-N\left(\frac{y'^2}{2\beta} + \ln(2\pi I_0(y')\right)\right] dy' \,, \quad (2.13)$$

where I_0 is the modified Bessel function of order 0:

$$I_0(y) = \frac{1}{2\pi} \int_0^{2\pi} e^{y'\cos(\theta)} \,. \quad (2.14)$$

In the thermodynamic $N \to \infty$ limit we can evaluate the integral (2.13) with saddle point technique, and obtain the rescaled free energy:

$$\phi(\beta) = -\lim_{N\to\infty} \frac{1}{N} Z(\beta, N) = \frac{\beta}{2} - \ln(\frac{2\pi}{\beta}) + \inf_{y'}\left(\frac{y'^2}{2\beta} - \ln(2\pi I_0(y')\right) \,. \quad (2.15)$$

In order to solve the minimization problem contained in the last term of equation (2.15), we search for its stationary points. Recalling that $I_1(y)$ is the first derivative of $I_0(y)$, we obtain the following condition:

$$\delta\left(\frac{|\vec{y}'^2|}{2\beta} + \ln(2\pi I_0(y'))\right) = \frac{y'}{\beta} - \frac{I_1(y')}{I_0(y')} = 0 \,. \quad (2.16)$$

The consistency equation that we obtained admits an homogeneous minimal free energy solution $y = 0$ for $\beta \geq 2$, while for $\beta < 2$ it yields a finite value which depends on β. The modulus M of the global magnetization is also obtained as the ratio of the Bessel functions:

$$M = \frac{I_1(y')}{I_0(y')} \,. \quad (2.17)$$

The derivative of the free energy (2.15) with respect to β gives the energy per particle ϵ:

$$\epsilon(\beta) = \frac{1}{2\beta} + \frac{1 - M^2}{2} \,. \quad (2.18)$$

The critical inverse temperature $\beta_c = 2$ corresponds to a second order phase transition between homogeneous ($M = 0$) states and inhomogeneous magnetized ($M > 0$) states, with a critical exponent that was shown to be $\frac{1}{2}$ [58]. The transition curve is represented in figure (2.2), and agrees very well with numerical finite-size simulations. The critical temperature correspond to a critical energy per particle $\epsilon_c = 0.75$.

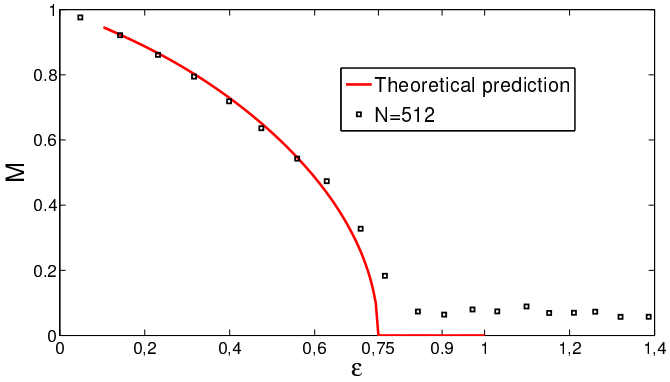

Figure 2.2: Second order phase transition between homogeneous and magnetized states for the HMF system at equilibrium, at a critical energy per particle $\epsilon_c = 0.75$. The predicted theoretical curve, displayed by the red thick line, is obtained from the minimization of the free energy in the canonical ensemble. It is consistent with the numerical microcanonical simulations carried out for finite N (the positive magnetization observed in the homogeneous phase is of the order of the finite-size fluctuations $\frac{1}{\sqrt{N}}$).

2.3 Microcanonical equilibrium solution

The particular form of the Hamiltonian (2.1) allows one to obtain directly the thermodynamic microcanonical density of states and derive consistently the entropy per particle $s(\epsilon)$. In this section we will revisit the procedure discussed in [9]. We define E_K and E_U respectively the kinetic an potential energy, while E is the total energy of the system. The number of microstates Ω is given by:

$$\begin{aligned}\Omega(E,N) &= \int \delta(E-H)\prod_{i=1}^{N} d\theta_i dp_i \\ &= \int \prod_{i=1}^{N} d\theta_i dp_i \int dE_K \delta\left(E_K - \frac{p^2}{2}\right)\delta\left(E - E_K - E_U(\{\theta_i\})\right) \\ &= \int dE_K \int \prod_{i=1}^{N} dp_i \delta\left(E_K - \frac{p^2}{2}\right) \int \prod_{i=1}^{N} d\theta_i \delta\left(E - E_K - E_U(\{\theta_i\})\right) \ .\end{aligned} \tag{2.19}$$

The integral over the momenta can be directly evaluated and yields:

$$\begin{aligned}&\int \prod_{i=1}^{N} dp_i \delta\left(E_K - \frac{p^2}{2}\right) = \frac{2\pi^{\frac{N}{2}}(2E_K)^{\frac{N-2}{2}}}{\Gamma(\frac{N}{2})} = \\ &\xrightarrow[N\to\infty]{} \exp\left[\frac{N}{2}\left(1 + \ln(2\pi) + \ln(\frac{2E_K}{N})\right)\right] \ ,\end{aligned} \tag{2.20}$$

where in the last passage use has been made of the expansion for the Γ function, $\Gamma(N) \simeq (N - \frac{1}{2})\ln(N) - N + \frac{1}{2}\ln(2\pi)$ for N large.
To solve the second configurational integral in (2.19) we exploit the simplicity of the HMF potential, which is function of the microscopic magnetization (2.4). There is a degeneracy in the direction of $\vec{m}$, so we can chose a magnetization vector laying along the x axis without loosing generality. We define m as the modulus of such vector, and we proceed to compute the integral (2.20) by making use of the Fourier representation of the δ function:

$$\begin{aligned}
&\int \prod_{i=1}^{N} d\theta_i \delta\left(E - E_K - E_U(\{\theta_i\})\right) = \\
&= (\frac{1}{2\pi})^2 \int_{-\infty}^{\infty} dk_1 \int_{-\infty}^{\infty} dk_2 \int \prod_{i=1}^{N} d\theta_i e^{ik_1(\sum_i \cos\theta_i - Nm)} e^{ik_2 \sum_i \sin\theta_i} \\
&= (\frac{1}{2\pi})^2 \int_{-\infty}^{\infty} dk_1 \int_{-\infty}^{\infty} dk_2 \exp\left[N\left(-ik_1 m + \ln J_0(\sqrt{k_1^2 + k_2^2})\right)\right] ,
\end{aligned} \tag{2.21}$$

where $J_0(k)$ is the Bessel function of order 0. We can solve the last integral with the saddle-point technique, by considering k_1 and k_2 as complex variables and remembering that $-J_i(k) = \frac{\partial J_0(k)}{\partial k}$. The saddle point has to satisfy the following conditions:

$$\begin{aligned}
&- im - \frac{J_1(\sqrt{k_1^2 + k_2^2})}{J_0(\sqrt{k_1^2 + k_2^2})} \frac{q_1}{\sqrt{k_1^2 + k_2^2}} = 0 , \\
&- \frac{J_1(\sqrt{k_1^2 + k_2^2})}{J_0(\sqrt{k_1^2 + k_2^2})} \frac{q_2}{\sqrt{k_1^2 + k_2^2}} = 0 .
\end{aligned} \tag{2.22}$$

This last system of equations admits a solution $q_2 = 0$ and $q_1 = i\gamma$, where γ is obtained by solving the following equation:

$$\frac{I_1(\gamma)}{I_0(\gamma)} = m , \tag{2.23}$$

were we used the properties $J_0(ik) = I_0(k)$ and $J_1(ik) = iI_1(k)$. The function $\frac{I_1(\gamma)}{I_0(\gamma)}$ is monotonic and decreasing, so we can define $\mathbb{J}_{inv}$ as the inverse of such function. Summing up the results from (2.19) and (2.21), we can then compute the microcanonical entropy per particle $s(\epsilon)$:

$$\begin{aligned}
&s(\epsilon) = \lim_{N\to\infty} \frac{1}{N} \ln \Omega(E, N) = \\
&= \frac{1}{2} + \frac{1}{2}\ln(4\pi) + \sup_m \left[\frac{1}{2}\ln(\epsilon - \frac{1}{2} + \frac{m^2}{2}) - m\mathbb{J}_{inv}(m) + \ln I_0(\mathbb{J}_{inv}(m))\right] .
\end{aligned} \tag{2.24}$$

The maximization problem can be solved graphically searching for solutions of the following equation:

$$\frac{m}{2\epsilon - 1 + m^2} - \mathbb{J}_{inv}(m) = 0 \,. \tag{2.25}$$

We obtain in this way the same transition curve already observed in the canonical ensemble (figure 2.2), with the same critical energy per particle $\epsilon_c = 0.75$. The first derivative of the entropy is the inverse temperature β:

$$\frac{ds(\epsilon)}{d\epsilon} = \beta(\epsilon) = \frac{1}{2\epsilon - 1 + m^2} \,. \tag{2.26}$$

Numerical solution of the previous equation shows that $\frac{d^2 s(\epsilon)}{d\epsilon^2} < 0$ for all values of m [9]. From the concavity of entropy, as observed in chapter 1.3.3, follows ensemble equivalence.

The latter observation concludes the discussion devoted to revisiting the equilibrium properties of the HMF. In the following section we shall turn to discussing the out-of-equilibrium dynamics of this paradigmatic model, and present some original results concerning the extension of the Lynden-Bell theory to a generalized family of initial conditions.

Chapter 3

Out-of-equilibrium thermodynamics

As we already anticipated in chapter 1.4, a long-range system experiences a very slow relaxation towards the deputed thermodynamic equilibrium. Indeed, it can be trapped in a long lasting out-of-equilibrium phase called Quasi Stationary State (QSS). The lifetime of the QSS was reported to diverge with the system size N. Interestingly, it displays different scaling behaviour versus N, which range from exponential to power law, being relic of the specific initial condition selected. As a consequence, searching for an equilibrium thermodynamic solution, the orders the limits $N \to \infty$ and $t \to \infty$ are taken do matter. Performing the continuum limit before the infinite time limit, implies preventing the system from eventually attaining its equilibrium and freezing it indefinitely in the QSS phase, the latter being typically described by a distribution which is non-Maxwellian [63, 64].

As a paradigmatic example we will discuss the time evolution of the HMF model (2.1), introduced in chapter 2. Consider an isolated system (microcanonical) initially set far from equilibrium. In this latter case, numerical simulations show that the HMF experiences a fast relaxation towards an intermediate regime [58, 65], before the final equilibrium is eventually attained (figure 3.1). These metastable states are indeed QSS, having a lifetime τ that diverges with system size, and bear distinctive traits that make them substantially different from the equilibrium solution, as we will discuss later in this chapter. It was estimated that the latter scaling has a power law $\tau \sim N^{\gamma}$ with a positive exponent $\gamma = 1.7$ [66].

In this chapter we will initially review how the QSS have been successfully interpreted as equilibria of the collisionless Vlasov equation. This latter appears

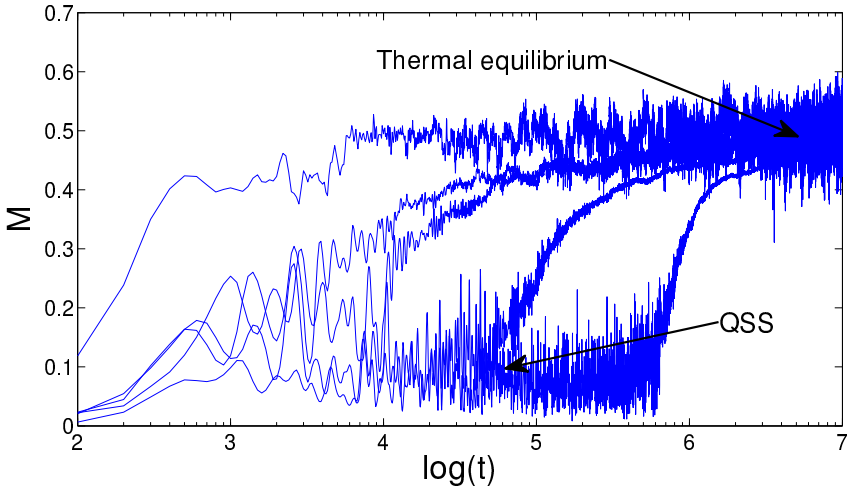

Figure 3.1: HMF model: relaxation of the global magnetization M respect to time t in logarithmic scale for different increasing systems sizes $N = 10^2, 5 \cdot 10^2, 10^3, 5 \cdot 10^3,\ 10^4$. There is evidence of a stationary metastable state before attaining equilibrium, which lifetime increases with N. The results are mediated over five different realizations.

to rule the dynamics of a broad family of long-range models, when recovering the continuum picture from the governing discrete formulation. A method exists that enables one to analytically predict the average characteristics of the QSS, including the emergence of out-of-equilibrium transitions [9]. This procedure follows a maximum entropy scheme and can be traced back to the Lynden-Bell work [8]. Section 3.2 is entirely devoted to presenting this approach.

Lynden-Bell theory was revisited by Antoniazzi et. al., with reference to paradigmatic long-range applications [20, 67, 68]. As we shall clarify in the forthcoming sections, the predictive adequacy of the Lynden-Bell violent relaxation theory has been so far solely assessed for a very specific class of initial conditions. These are the so called *water-bags*, were particles are assumed to initially populate a bound domain of phase space and therein be distributed with a uniform probability.
In this chapter, we will introduce an extension to the previous established theory that allows us to relax the strict constrain over the initial condition and apply Lynden-Bell theory to a generalized water-bag, which can in principle approximate continuous distributions. We will also show that our extended theory, original contribution of the thesis, works correctly when two levels are considered.

3.1 The Vlasov limit

Under some assumptions and in the limit of very large size, the dynamics of long-range systems can be described by the Vlasov equation. This latter describes the dynamical evolution of the single particle distribution function $f(p, q, t)$, moving from a trajectory based description to a field dynamics.
The fact that a N-body mean-field Hamiltonian system converges to a Vlasov equation in the limit $N \to \infty$ has been made rigorous in a theorem by W. Braun and K. Hepp [69, 70], which we will discuss in this section.

We can obtain the Vlasov limit by following a kinetic approach, which is similar to the Boltzmann's kinetic theory used in the case of perfect gases. In the latter case one deals with binary short-range collisions. When long-range interactions are to be accounted for, we must introduce a long-range collisional term which extends beyond the Boltzmann's one. Several approaches have been proposed to derive the Vlasov equation. Here we will follow the one that moves from the Klimontovich equation [71].

Let us consider a generic N-particles system described by an Hamiltonian in the form:

$$H = \sum_{i=1}^{N} \frac{p_i^2}{2} + U(q_i) \,, \tag{3.1}$$

where (q_i,p_i) are the canonical Lagrangian coordinates and momenta of the particle i, and $U(q_i) = \frac{1}{N} \sum_{j \neq i} V(q_i - q_j)$ is a mean-field potential which is given by the mean over the pair interactions $V(q_i - q_j)$. The dynamics of such system obeys to the Hamilton equations:

$$\begin{aligned} \dot{q}_i &= p_i \,, \\ \dot{p}_i &= -\frac{\partial U}{\partial q_i} \,. \end{aligned} \tag{3.2}$$

We introduce the discrete one-particle distribution function:

$$f_k(q, p, t) = \frac{1}{N} \sum_{i=1}^{N} \delta(q - q_i)\delta(p - p_i) \,. \tag{3.3}$$

This latter describes the state of the system at time t, as a function of the Eulerian coordinates q and p. Differentiating with respect to time, and using equations (3.2), we obtain:

$$\frac{\partial f_k}{\partial t} = \frac{1}{N} \sum_i \left[-p_i \frac{\partial}{\partial q} + \frac{\partial U}{\partial q_i} \frac{\partial}{\partial p} \right] \delta(q - q_i(t))\delta(p - p_i(t)) \,. \tag{3.4}$$

By using the property of the Dirac function $a\delta(a-b) = b\delta(a-b)$, we can rewrite the previous equation as:

$$\frac{\partial f_k}{\partial t} = \frac{1}{N}\sum_i \left[-p\frac{\partial}{\partial q} + \frac{\partial v}{\partial q}\frac{\partial}{\partial p}\right]\delta(q-q_i(t))\delta(p-p_i(t))\,, \tag{3.5}$$

with $v(q,t) = \int V(q-q')f_k(q',p',t)dq'dp'$. Equation (3.5) reproduces exactly the form of Klimontovich equation:

$$\frac{\partial f_k}{\partial t} + p\frac{\partial f_k}{\partial q} - \frac{\partial v}{\partial q}\frac{\partial f_k}{\partial p} = 0\,. \tag{3.6}$$

The previous equation is exact, and contains the microscopic information on every trajectory of the particles. It is therefore difficult to manage the limit $N \to \infty$. In order to obtain an averaged distribution function that encapsulates the sought statistical information, we must recover the mean-field limit of equation (3.6), through a perturbative calculation with respect to a small parameter that encodes the system size N.

Assume that the Klimontovich distribution function f_k can be described as an averaged distribution f, plus fluctuations that scales as $\frac{1}{\sqrt{N}}$:

$$f_k(q,p,t) = f(q,p,t) + \frac{1}{\sqrt{N}}\delta f(q,p,t)\,. \tag{3.7}$$

Here $f = \langle f_k \rangle$ is the averaged distribution function in the reduced phase space of single particle. We assume that the average is taken over a large ensemble of independent microstates, each corresponding to the same macrostate.
Using equation (3.7) we can rewrite the average potential as:

$$\langle v(q,t)\rangle = \int V(q-q')f(q',p',t)dq'dp'\,, \tag{3.8}$$

so to obtain:

$$v(q,t) = \langle v(q,t)\rangle + \frac{1}{\sqrt{N}}\delta v(q,t)\,. \tag{3.9}$$

Using both equations (3.7) and (3.9) into Klimontovich equation (3.6) one gets:

$$\begin{aligned}&\frac{\partial f}{\partial t} + p\frac{\partial f}{\partial q} + \frac{\partial \langle v\rangle}{\partial q}\frac{\partial f}{\partial p} = \\ &\quad -\frac{1}{\sqrt{N}}\left(\frac{\partial \delta f}{\partial t} + p\frac{\partial \delta f}{\partial q} - \frac{\partial v}{\partial q}\frac{\partial f}{\partial p} - \frac{\partial \langle v\rangle}{\partial q}\frac{\partial f}{\partial p}\right) + \frac{1}{N}\left\langle \frac{\partial \delta v}{\partial q}\frac{\partial \delta f}{\partial p}\right\rangle\,.\end{aligned} \tag{3.10}$$

Finally, by averaging over all initial microscopic configurations, yields to:

$$\frac{\partial f}{\partial t} + p\frac{\partial f}{\partial q} + \frac{\partial \langle v \rangle}{\partial q}\frac{\partial f}{\partial p} = \frac{1}{N}\left\langle \frac{\partial \delta v}{\partial q}\frac{\partial \delta f}{\partial p} \right\rangle . \tag{3.11}$$

In kinetic theory, (3.11) is the first equation of BBGKY hierarchy (see [72]).

In the case of short-range interactions, the right hand side of equation (3.11) gives the collisional term that we find in Boltzmann equation. If we neglect collisions, assuming that the latter term becomes negligible in the thermodynamic limit $N \to \infty$, the famous Vlasov equation is eventually recovered:

$$\frac{\partial}{\partial t} f(p,q,t) + p\frac{\partial}{\partial q} f(p,q,t) + \frac{\partial}{\partial q}\langle v(q,t) \rangle \frac{\partial}{\partial p} f(p,q,t) = 0 . \tag{3.12}$$

This equation has a wide range of applications in gravitational systems [73] and in plasma physics [72]. The Vlasov equation simply states that, in the absence of collisions, the distribution function f is conserved by the time evolution in phase space, which means $df/dt = 0$, in mathematical terms.

In a general case it is not easy to justify the above collisionless assumption. However, for a broad range of mean-field (long-range) potentials, Braun-Hepp theorem [69] rigorously proves that in the continuum limit $N \to \infty$ the solutions of equations (3.2) converges to the solutions of the Vlasov equation (3.12). In the last part of this section we shall briefly discuss the case of one-dimensional systems. The theorem can be however straightforwardly extended to higher dimensions.

Assume that the system is governed by a mean-field Hamiltonian which can be cast in the form (3.1), and $(q_i^0, p_i^0) = \vec{a}$ is the initial condition at $t = 0$, described by the discrete distribution $f_k(q,p,0)$ (3.3). We recall that the distribution function $f(q,p,t)$ is obtained from $f_k(q,p,t)$ in the $N \to \infty$ limit of equation (3.7). Consider the Newtonian equation:

$$\ddot{q} = -\int \mu(\vec{b})\frac{\partial}{\partial q} V\left(q(\vec{a},\mu,t) - q(\vec{a},\mu,t)\right) d\vec{b} . \tag{3.13}$$

The latter describes a single particle interacting through the 2-body potential $V\left(q(\vec{a},\mu,t) - q(\vec{a},\mu,t)\right)$ with other particles having initial conditions distributed over a real Borel measure μ on $\mathbb{R}^2$. Notice that equation (3.13) reduces to the N-body dynamics (3.2) if $\mu(\vec{b}) = f_k(q,p,0)$, while if $\mu(\vec{b}) = f(q,p,0)$ it reproduces the Vlasov equation (3.12). Hence, the two latter different dynamics represent disjoint specializations of (3.13), for different expressions of the measure μ.

Let $\mathcal{M}$ be the set of real Borel measures μ on $\mathbb{R}^2$, with $|\mu| < \infty$ and $\mathcal{M}_+^1$ the subset of probability measures. Let C_b^k be the set of all potentials $V(q) = V(-q)$ with continuous and bounded derivatives up to order k.

Theorem 3.1.1. (Braun-Hepp theorem) *Let $V \in C_b^2$. Then equation (3.13) has a unique solution $q(\vec{a}, \mu, t)$ for all $(\vec{a}, t) \in \mathbb{R}^2$ and $\mu \in \mathcal{M}$. Then $q(\vec{a}, \mu, t)$ is C^1 in $(\vec{a}, t)$ and weakly continuous in μ, uniformly for $\vec{a} \in \mathbb{R}^2$ and bounded sets in t. The mapping $q(\mu, t) : a \longrightarrow q(\vec{a}, \mu, t)$ is canonical and $T_i : (\vec{a}, \mu) \longrightarrow (q(\vec{a}, \mu, t), \mu \circ q(\vec{a}, \mu, t)^{-1}$ is a one-parameter group.*

The weak convergence in μ implies that whenever a discrete initial condition $f_k(q, p, 0)$ converges weakly to a normalized probability density $f(q, p, 0)$,

$$f_k(q, p, 0) = \frac{1}{N} \sum_{i=1}^{N} \delta(q - q_i^0)\delta(p - p_i^0) \longrightarrow f(q, p, 0) \,, \tag{3.14}$$

the Vlasov dynamics describes asymptotically the evolution of the system.

Searching for an equilibrium thermodynamic solution of a mean-field system in the above Vlasov approximation means performing the $N \to \infty$ limit before of the $t \to \infty$ limit. The Braun-Hepp theorem justify the use of Vlasov equation to model the evolution of large enough mean-field models, which may be the correct framework to understand the metastable regime of long-range dynamics. Lynden-Bell argued that QSS corresponds to statistical equilibria of the Vlasov equation (3.12). Is is however worth emphasizing that Vlasov equation has an infinite number of stationary solutions, depending on the initial condition $f(q, p, 0)$ [9].

3.2 Lynden-Bell approach to metastable QSS

The distribution function f of a system obeying the Vlasov equation (3.12) has a collisionless time evolution. The system undergoes an initial violent relaxation, governed by Landau damping [8], which develops through a peculiar process called *filamentation* due to the collisionless mixing: the fine-grained distribution function $f(q, p, t)$ will never reach a stationary state, but instead it will be stretched and stirred into filaments mixed at smaller and smaller scales [73].
From an observer point of view, this never-ending evolution is not physically relevant, since we have a limited resolution on our observation of the fine-grain of the phase space detail. An interesting approach to this problem was initially proposed by Lynden-Bell, in the framework of galactic dynamics [8]. At the

time there were experimental observations that the radiation signals emitted by elliptic galaxies were almost regular, implying that the galaxy was in an equilibrium state. However, these observations clashed with the analytical estimates for the typical relaxation times of the galaxies due to the two-body collisional effects. It was hence proposed that the manifest regularity could be due to a sort of out-of-equilibrium stationary state [74, 75].

With reference to cosmological applications, Lynden-Bell proposed a maximum-entropy approach to determine the stationary solutions of the Vlasov equation, pioneering the theory that it is nowadays referred to as to the violent relaxation theory. The very basic idea behind his work is to introduce a cutoff to the scale of observation. He first considered the coarse grained distribution $\bar{f}$, obtained by averaging the microscopic $f(q,p,t)$ over a finite grid. Each element of this grid will contain a large enough portion of phase space that encompass multiple filaments. The evolution will continue at smaller scales, but the coarse-grained distribution $\bar{f}(q,p,t)$ will reach an equilibrium state very fast. In order to analytically describe this equilibrium, the key passage is to associate to $\bar{f}$ a mixing entropy $S[\bar{f}]$, via a rigorous counting of the microscopic configurations that are compatible with a given macroscopic state.

While following the discussion that can be found in reference [8], we shall reformulate the original derivation in order to accommodate for the extended initial condition that we will introduce in the next section.

To apply the statistical mechanics machinery, we divide the phase space into a very large number of micro-cells each of volume $\tilde{\omega}$. The micro-cells define an hyper-fine support that can be invoked to obtain an adequate representation of the fine grained function f, provided the mass of the phase element that occupies each cell is given.
Consider a discretization of the original function f into n levels of phase density f_J , $J = 1, ..., n$. Then the phase element mass is $f_J\tilde{\omega}$ or 0. Under the effect of the equation (3.30), the distribution function $f(q', p', t)$ will be mixed and filamented. Still Vlasov dynamics conserve all the Casimirs $C_m[f] = \int f^m \, dqdp$, and, as a consequence, it will conserve independently the total mass of each level.
Lynden-Bell suggested to group these micro-cells into coarse grained macro-cells, very small, but sufficiently large to contain several micro-cells. Let us call ν the number of micro-cells inside the macro-cell, the latter having therefore volume $\nu\omega$. Define n_{iJ} the number of elements with phase density f_J that populate cell i, located in (q_i, p_i).
Clearly $\sum_i n_{iJ} = N_J$, where N_J stands for number of micro-cells occupied by

level J.

The sought entropy can be rigorously derived via the following steps. First, we quantify the number of ways of assigning the micro-cells to all $\sum_J n_{iJ}$ phase elements that are confined in the macro-cell i. A simple combinatorial argument yields to the estimate:

$$\frac{\nu!}{(\nu - \sum_J n_{iJ})!} \,. \tag{3.15}$$

Then, one needs to calculate the total number of microstates W that are compatible with the single macrostate defined by the numbers n_{iJ}. W is the product of (3.15) with the total numbers of ways of splitting the pool of available N_J elements into groups of n_{iJ}. In formulae:

$$W = \prod_J \frac{N_J!}{\prod_i (n_{iJ})!} \times \prod_i \frac{\nu!}{(\nu - \sum_J n_{iJ})!} \,. \tag{3.16}$$

Finally, the entropy $S = \log(W)$ can be cast in the form:

$$S = -\sum_J \sum_i \frac{n_{iJ}}{\nu} \log \frac{n_{iJ}}{\nu} - \sum_i \left(1 - \sum_J \frac{n_{iJ}}{\nu}\right) \log \left(1 - \sum_J \frac{n_{iJ}}{\nu}\right) \,, \tag{3.17}$$

were we have rescaled S by ν and neglected some unimportant constant contributions. The term $\sum_i (1 - \sum_J n_{iJ}/\nu) \log (1 - \sum_J n_{iJ}/\nu)$ reflects the exclusion principle that is being imposed in the combinatorial analysis. Two elements of phase cannot overlap, each micro-cell being solely occupied by one of the available density levels, including zero. As emphasized in [8] this procedure results in a novel type of statistics, which explicitly accounts for the mutual interference of distinguishable particles, at variance with the Fermi-Dirac one, that deals with indistinguishable entities. When only one level is allowed for, the Lynden-Bell and Fermi-Dirac statistics coincide.
This latter consideration can be viewed as a consequence of the conservation of the Casimirs, since in each microcell the fine-grained distribution function f will assume the value of only one of the initial levels. In a sense this is similar to a classical version of Pauli's exclusion principle, if we consider each level as populated by a different species of particles.

We now introduce the probability density ρ_{iJ} of finding the level of phase density f_J in cell i as:

$$\rho_{iJ} = \frac{n_{iJ}}{\nu} \,. \tag{3.18}$$

Notice that $\sum_i \sum_J \rho_{iJ} = 1$, as it should be. By inserting equation (3.18) into the entropy expression (3.17) one gets:

$$S = -\sum_J \sum_i \rho_{iJ} \log \rho_{iJ} - \sum_i \left(1 - \sum_J \rho_{iJ}\right) \log \left(1 - \sum_J \rho_{iJ}\right) . \tag{3.19}$$

Following Lynden-Bell, one can define the coarse grained distribution function $\bar{f}(q_i, p_i)$ as:

$$\bar{f}(q_i, p_i) = \sum_J \frac{n_{iJ}}{\nu} f_J = \sum_J \rho_{iJ} f_J . \tag{3.20}$$

The density ρ_{iJ} and the coarse grained distribution $\bar{f}(q_i, p_i)$ are the two main quantities upon which the description relies. However, these are not independent quantities. Let us write the density as $\rho_{iJ} = \alpha_J h_i$. The density factorizes hence into two terms: h_i depends on the i-th cell, while the other contribution, α_J, on the J-th level. By inserting this ansatz into the definition (3.20) for $\bar{f}(q_i, p_i)$ we get:

$$\bar{f}(q_i, p_i) = \sum_J \alpha_J j_i f_J , \tag{3.21}$$

from which we straightforwardly obtain:

$$h_i = \bar{f}(q_i, p_i) , \tag{3.22}$$

together with the normalization condition

$$\sum_J f_J \alpha_J = 1 . \tag{3.23}$$

Hence, summarizing we can rewrite the density (3.18) as:

$$\rho_{iJ} = \bar{f}(q_i, p_i) \alpha_J , \tag{3.24}$$

which admits a simple interpretation. The probability of finding an element of phase density f_J in cell i is given by the probability of finding any element in such a cell, $\bar{f}(q_i, p_i)$, times the probability that the selected element is actually of type f_J. Reasoning along this lines, α_J can be seen as the relative fraction of phase space volume that hosts the elements of phase density f_J.

Finally, one can obtain a compact expression for ρ_{iJ} that explicitly evidences all allowed levels:

$$\rho_{iJ} = \sum_L \bar{f}(q_i, p_i) \alpha_L \delta_{LJ} . \tag{3.25}$$

By taking the continuum limit both in the spatial variable $(q_i, p_i) \to (q, p)$, and in the level distribution $f_J \to \eta$, one obtains the generalized density function $\rho(q, p, \eta)$. Operating under this conditions, (3.20) rewrites:

$$\bar{f}(q,p) = \int_{\text{levels}} \rho(q,p,\eta)\eta d\eta \,, \tag{3.26}$$

and (3.25) takes the form:

$$\rho(q,p,\eta) = \int_{\text{levels}} \bar{f}(q,p)\alpha(x)\delta(x-\eta)\, dx \,, \tag{3.27}$$

where $\alpha(x)$ is the volume of the set of points (q, p) such that $\bar{f}(q, p) = x$.

In the following, we will be concerned with the intermediate situation where the levels are discrete in number. In this case, by using the spatially continuous version of equation (3.25) in the entropy (3.19), one gets:

$$\begin{aligned} S = -\int d\tau' \Bigg[& \sum_J \alpha_J \bar{f}(q,p) \log \sum_J \bar{f}(q,p) \\ & + \left(1 - \sum_J \alpha_J \bar{f}(q,p)\right) \log \left(1 - \sum_J \alpha_J \bar{f}(q,p)\right) \Bigg] \end{aligned} \tag{3.28}$$

where $d\tau' = dqdp/(\tilde{\omega}\nu)$ and the $\sum_J$ cumulates the contribution of all levels that insists on cell i.

The equilibrium coarse grained distribution function $\bar{f}$ maximizes the entropy functional $S[\bar{f}]$, while imposing the constraints of the dynamics. These latter are the energy, momentum and normalization, as well as the phase space volumes α_J associated to each of the allowed levels.

3.3 Lynden-Bell microcanonical solution for the HMF model

As we already seen in section 3.1, thanks to the Braun-Hepp theorem, mean-field models can be approximated in the large size limit by the Vlasov equation. It may be argued that Vlasov equation provide the correct framework to address the problem of QSS emergence. The procedure exposed in the previous section allows us to search for an equilibrium solution of a Vlasov system, by maximizing

Lynden-Bell entropy. The problem is not easily solvable in a generic context, and one must resort to strict assumptions on the form of the initial condition in order to obtain an equilibrium solution of the distribution function.

Lynden-Bell theory was successfully applied in the past to obtain a solution that explains the QSS regime of the HMF model [20]. Such a solution was recovered by using a peculiar initial distribution function known as "water-bag", which is flat over a bounded domain of phase space (usually called a "level") and zero outside of it.

In the following we will discuss the multi-level water-bag class of initial conditions, which naturally extends beyond the single water-bag case study, so far explicitly considered in the literature. It is our intention to test the predictive ability of the Lynden-Bell theory within such generalized framework. The theory will be developed with reference to the general setting, including n levels. The benchmark with direct simulations will be instead limited to the two-levels case, i.e. $n = 2$.

3.3.1 The HMF out-of-equilibrium dynamics (QSS) regime in the single level case

First let us briefly review the main results already present in literature and discuss the general features of HMF's QSS states. As we already mentioned the HMF model describes N identical particles identified by the set of coordinates θ, p, where $\theta \in [0, 2\pi[$ is the angular coordinate over the ring and p is the conjugated momentum.
For convenience, we shall rewrite here the Hamiltonian equation that describes the model:

$$H = \sum_{i=1}^{N} p_i^2 + \frac{1}{2N} \sum_{i,j=1}^{N} (1 - \cos(\theta_i - \theta_j)) \,. \tag{3.29}$$

The HMF model has a continuous C^∞ potential, and so the Braun-Hepp theorem (3.1.1) states that in the limit $N \to \infty$ the system converges to the Vlasov equation (3.12):

$$\frac{\partial f}{\partial t} + p\frac{\partial f}{\partial \theta} - (M_x[f] \sin\theta - M_y[f] \cos\theta) \frac{\partial f}{\partial p} = 0 \,, \tag{3.30}$$

where M_x and M_y represent the total magnetization along the x and y axis respectively:

$$M_x[f] = \int f\cos(\theta)\,d\theta dp\,, \tag{3.31}$$
$$M_y[f] = \int f\sin(\theta)\,d\theta dp\,, \tag{3.32}$$
$$M[f] = \sqrt{M_x^2[f] + M_y^2[f]}\,. \tag{3.33}$$

The Vlasov limit of the HMF dynamics was tested rigorously in [51]. The system conserves the energy density ϵ, total initial momentum P and total mass γ:

$$\epsilon[f] = \int \tfrac{p^2}{2} f(\theta,p)\,d\theta dp - \tfrac{M[f]^2-1}{2}\,, \tag{3.34}$$
$$P[f] = \int f(\theta,p)p\,d\theta dp\,, \tag{3.35}$$
$$\gamma[f] = \int f(\theta,p)\,d\theta dp = 1\,. \tag{3.36}$$

The mass conservation is equivalent to the normalization condition (3.23). In the Vlasov approximation the system conserves also all the Casimirs of the distribution f, as a property of Vlasov equation.

The original water-bag initial condition f_{wb} considered in the paper by Antoniazzi et. al. [20] takes a constant value f_1 within a finite portion of the phase space, and zero outside of it. Although this is the only prescription to be accommodated for, rectangular domains are usually chosen for practical computational reasons. We shall label $[\Delta\theta, \Delta p]$ the widths of such a rectangle, as calculated respectively along θ and p directions. A second simplification is also customarily assumed: the rectangle is centred in the origin, so that $\theta \in [-\frac{\Delta\theta}{2}, \frac{\Delta\theta}{2}]$ and $p \in [-\frac{\Delta p}{2}, \frac{\Delta p}{2}]$.

$$f_{init} = \begin{cases} f_1 & \text{if } \theta \in [-\frac{\Delta\theta}{2}, \frac{\Delta\theta}{2}] \text{ and } p \in [-\frac{\Delta p}{2}, \frac{\Delta p}{2}], \\ f_0 = 0 & \text{otherwise.} \end{cases} \tag{3.37}$$

This region has an area $\alpha_1 = 4\Delta\theta\Delta p$, and imposing the total mass to be one, we obtain the normalization condition (3.23) which gives:

$$f_1 = \frac{1}{4\Delta\theta\Delta p}\,. \tag{3.38}$$

With the previous choice, we can express the energy density $\epsilon = \frac{E}{N}$ and the initial magnetization M_0 as functions of $\Delta\theta$ and Δp:

$$M_0 = 2\tfrac{\sin(\frac{\Delta\theta}{2})}{\Delta\theta}\,, \tag{3.39}$$
$$\epsilon_0 = \tfrac{\Delta p^2}{24} + \tfrac{1-M_0^2}{2}\,. \tag{3.40}$$

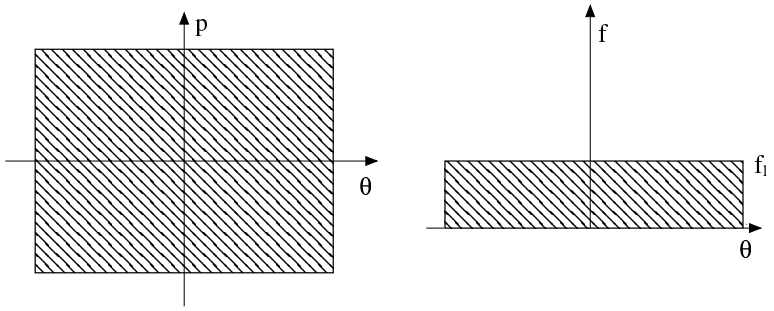

Figure 3.2: Pictorial representation of a 1-level ($n = 1$) water-bag initial condition. The background level is $f_0 = 0$.

Although quite simple, for systems characterized by small energy dispersions, the 1-level water-bag initial conditions represent a good approximation of a more natural Gaussian initial distribution [67].

Starting from the water-bag initial condition, as depicted in figure (3.1), numerical evidences show that the HMF system develops a QSS, which is reminiscent of the Vlasov evolution. The QSS become stationary stable in the limit $N \to \infty$, justifying the approach based on the Lynden-Bell maximum entropy principle.

An extensive study of the solution to Lynden-Bell problem, in the single water-bag case, was already performed in [39], and it was shown that the Lynden-Bell theory is capable to reproduce the QSS states observed in finite-size numerical simulation to a satisfying precision. The stable solution $\bar{f}_{eq}$ depends on the initial choice of the energy density ϵ_0 and initial magnetization M_0. Depending on the initial condition, the theory predicts two distinct QSS regimes. One characterized by a finite positive total magnetization, with a single-cluster distribution, and the other by an almost zero total magnetization, with a two-cluster formation, the two phases being separated by an out-of-equilibrium phase transition.
Also the tricritical point that separates the two transitions can be identified with precision. This results are reported in figure (3.3). An extended description of this out-of-equilibrium phase transition can be found in [78], where the theory also validates versus numerical simulations.

With the previous assumptions, the form of the equilibrium distribution function that maximizes Lynden-Bell entropy is fermionic-like:

$$\bar{f}_{eq} = \frac{f_1}{1 + e^{f_1\left[\beta\left(\frac{p^2}{2} - \vec{M}\cdot\vec{m}\right) + \lambda p + \mu\right]}} \,, \tag{3.41}$$

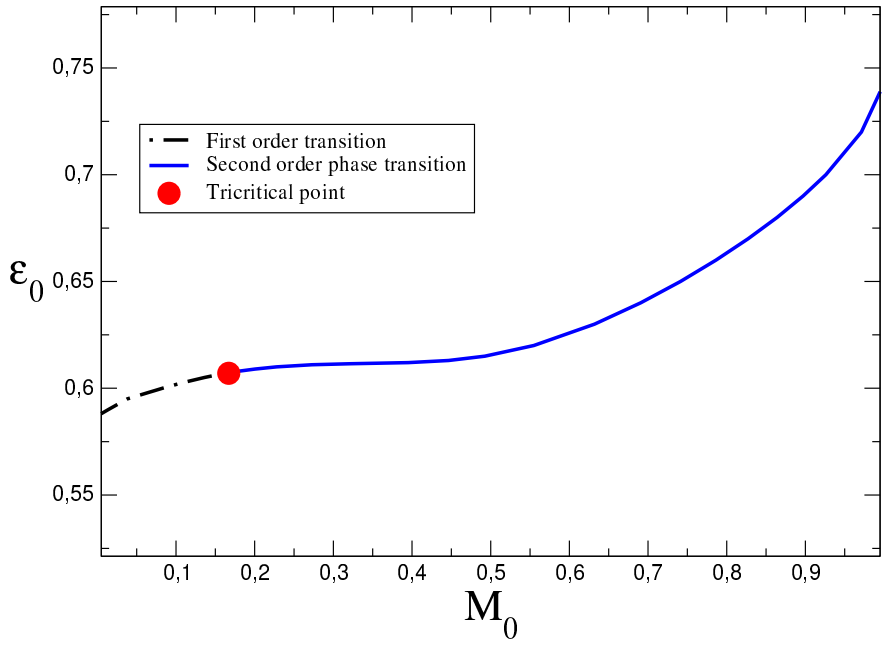

Figure 3.3: Phase diagram in the (ϵ_0, M_0) plane of the transition predicted from Lynden-Bell theory in the QSS states of the HMF model. The full line corresponds to a first order transition, while the dashed line corresponds to the first order one. The red marker evidences the tricritical point separating the two transitions.

where $\vec{M}$ is the global magnetization vector (2.5) and $\vec{m} = [\cos(\theta), \sin(\theta)]$. β and μ are the Lagrange multiplies coming from the maximization problem. β is identified with the inverse thermodynamic temperature of the system.
In the phase where the total equilibrium magnetization vanishes, we recover a simple form for the equilibrium distribution:

$$\bar{f}_{eq} = \frac{f_1}{1 + e^{f_1 \beta \left(\frac{p^2}{2} + \frac{\mu}{\beta} \right)}} \,. \tag{3.42}$$

Also, in the limit $f_1 \to \infty$, the normalization forces the support of the initial distribution to $\alpha_1 \to 0$, so f_{init} reduces to a δ-like function. In this approximation one recovers the usual Maxwellian distribution function:

$$\bar{f}_{eq} \simeq f_1 e^{-f_1 \beta \left(\frac{p^2}{2} + \frac{\mu}{\beta} \right)} \,. \tag{3.43}$$

In both phases, homogeneous or magnetized, in the low temperature limit $\beta \to \infty$ we observe that the value $\epsilon_f = \vec{M} \cdot \vec{m} - \frac{\mu}{\beta}$ plays the role of the Fermi energy, and for $|p| \leq \sqrt{2\,(\epsilon_f)}$ we recover the Fermi step equilibrium distribution where:

$$\bar{f}_{eq} = \begin{cases} f_1 & \text{if } |p| \leq \sqrt{2\,(\epsilon_f)}\,, \\ 0 & \text{if } |p| > \sqrt{2\,(\epsilon_f)}\,. \end{cases} \tag{3.44}$$

3.3.2 N-levels extended solution

Now we will take one step forward and challenge the validity of the theory presented in section 3.2, when particles are instead distributed so to uniformly fill more levels. In principle, any smooth profile could be approximated by a piecewise function, made of an arbitrary number of collated water-bags [79].
As observed above, the general philosophy that inspires the Lynden-Bell theory is broader than the specific realm to which it was relegated and its potentiality deserves to be further clarified. We will here extend the treatment to the multi-levels water-bag initial condition, a step that opens up the perspective to eventually handle more realistic scenarios, where smooth distributions could be considered.

Following the notation introduced above, the arbitrary integer n quantifies the total number of distinct levels, other than the background one $f_0 = 0$, that are to be allowed for when considering the generalized initial distribution function f_{mwb}. Arguably, by accounting for a large enough collection of independent and discrete levels, one can approximately mimic any smooth profile. A pictorial representation of the family of initial conditions to which we shall refer to is depicted in figure (3.4).
The initial distribution function f_{mwb} can be written as:

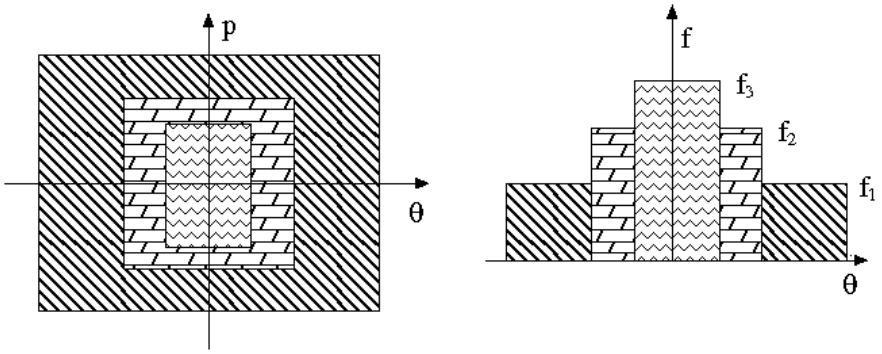

Figure 3.4: Pictorial representation of a 3-levels ($n = 3$) water-bag initial condition. The background level is $f_0 = 0$.

$$f_{mwb}(\theta, p) = \begin{cases} f_J & \text{if } \theta \in \mathbf{\Theta_J} \text{ and } p \in \mathbf{P_J}\,, \\ f_0 = 0 & \text{elsewhere}\,. \end{cases} \tag{3.45}$$

Here $\Gamma_J = [\Theta_J, P_J]$, $J = 1, \ldots, n$ identifies the domain in phase space associated to level f_J. The corresponding volume is labeled α_J.

We have already seen that the normalization condition (3.23) links together the $2n$ constants, f_J and α_J, that are to be assigned to fully specify the initial con-

dition. In other words, only $2n-1$ scalars are needed to completely parametrize the initial condition. Importantly, the 1-level water-bag limit is readily recovered once the phase space support of the levels indexed with $J>1$ shrinks and eventually fades out. This condition implies requiring $\alpha_J \to 0$ for $J>1$. In formula:

$$\rho_1 = \lim_{\alpha_J \to 0, J>1} \rho_n = \bar{f}\alpha_1 \delta\left(\eta - f_1\right) + \left(1-\bar{f}\,,\alpha_1\right)\delta\left(\eta\right)\,. \tag{3.46}$$

Moreover, by making use of the normalization condition one gets $\alpha_1 = \frac{1}{f_1}$, which, inserted (3.46), returns immediately the well known form of the one level density distribution function. Notice that the initial value of the macroscopic observables can be computed from the explicit knowledge of ρ_1.

The QSS distribution function $\bar{f}_{eq}(\theta,p)$ for the HMF model, relative to the generalized n-levels water-bag initial condition, is found by maximizing the Lynden-Bell entropy, under the constrains of the dynamics. This in turn implies solving a variational problem. The solution is relative to the microcanonical ensemble, since the Vlasov equation implies that we work with fixed total energy.
As we already observed, the generic n-levels entropy (3.28) takes the following functional form:

$$s_{LB}[\bar{f}] = -\int \{\sum_{J=1}^{n} \bar{f}\alpha_J \ln(\bar{f}\alpha_J) + (1-\sum_{J=1}^{n}\bar{f}\alpha_J)\ln(1-\sum_{J=1}^{n}\bar{f}\alpha_J)\}\, d\theta dp\,. \tag{3.47}$$

The conserved quantities are respectively the energy density ϵ:

$$\epsilon\left[\bar{f}\right] = \int \frac{p^2}{2}\bar{f}(\theta,p)\, d\theta dp - \frac{M[\bar{f}]^2-1}{2} \equiv \epsilon_0\,, \tag{3.48}$$

and the total momentum P:

$$P[\bar{f}] = \int \bar{f}(\theta,p) p\, d\theta dp \equiv P_0\,. \tag{3.49}$$

The initial energy density ϵ_0 relates to the geometric characteristics of the bounded domains that define our initial condition. Conversely, as we will be dealing with patches Γ_J symmetric with respect to the origin, one can immediately realize that the total initial momentum $P_0 = 0$.

The n volumes of phase space, each deputed to hosting one of the considered levels, are also invariant of the dynamics. We have therefore to account for the conservation of n additional quantities, the volumes $\Omega_J[\bar{f}]$ for $J=1,...,n$, defined as:

$$\Omega_J[\bar{f}] = \int \bar{f}(\theta,p)\alpha_J\, d\theta dp\,. \tag{3.50}$$

Moreover using the normalization condition (3.23) for the coarse grained distribution function $\bar{f}(\theta, p)$, we get $\Omega_J[\bar{f}] = \alpha_J$. Equivalently, by imposing the above constraints on the hypervolumes, we also guarantee the normalization of the distribution function, which physically amounts to impose the conservation of the mass.

Summing up, the variational problem that needs to be solved to eventually recover the stationary distribution $\bar{f}_{eq}(\theta, p)$ reads:

$$\max_{\bar{f}} \{ s_{LB}[\bar{f}] \mid \epsilon \left[\bar{f}\right] = \epsilon_0; P \left[\bar{f}\right] = P_0; \Omega_J \left[\bar{f}\right] = \alpha_J \} \,, \tag{3.51}$$

where the entropy functional $s_{LB}[\bar{f}]$ is given by equation (3.47). This immediately translates into:

$$\delta s_{LB} - \beta \delta \epsilon - \lambda \delta P - \sum_{J=1}^{n} \mu_J \delta \Omega_J = 0 \,, \tag{3.52}$$

where β, λ and μ_J stands for the Lagrange multipliers associated respectively to energy, momentum and volumes (or equivalently mass) conservations.

A straightforward calculation yields to the following expression for $\bar{f}_{eq}(\theta, p)$:

$$\bar{f}_{eq} = \frac{1}{B + A e^{\beta' \left(\frac{p^2}{2} - \vec{M}[\bar{f}_{eq}] \cdot \vec{m} \right) + \lambda' p + \mu'}} \,, \tag{3.53}$$

where

$$B = \sum_{J=1}^{n} \alpha_J \;;\; A = \left(\prod_{J=1}^{n} \alpha_J^{\alpha_J} \right)^{\frac{1}{B}} \,, \tag{3.54}$$

and we redefined the Lagrange multipliers in the following way:

$$\begin{aligned} \beta' &= \frac{\beta}{B} \,, \\ \lambda' &= \frac{\lambda}{B} \,, \\ \mu' &= \frac{\sum_{J=1}^{n} \mu_J}{B} \,. \end{aligned} \tag{3.55}$$

The above solution is clearly consistent with that obtained for the 1-level water-bag case study [20]. This latter (3.41) is in fact recovered in the limit ($\alpha_J \to 0$ for $J > 1$ while $\alpha_1 = \frac{1}{\bar{f}_1}$).

As we have shown for the previous case, also with this extended n-levels water-bag initial condition we end up with an implicit form for $\bar{f}_{eq}$ which depends

on itself. Also, we observe that the equilibrium distribution only depends on μ', and not on the complete collection of μ_J: this means that, in order to solve $\bar{f}_{eq}$, we can hereafter focus just on the conservation of the global mass, i.e. the normalization.
The number of unknowns total therefore to four (M_x, M_y, β', μ') and the system of implicit equations that we have to solve is equivalent to the 1-level case.

$$\epsilon_0 = \frac{\tilde{A}}{2\beta'^{3/2}} \int e^{\beta' \vec{M}\cdot\vec{m}} F_2(y)\, d\theta - \frac{M^2-1}{2} \tag{3.56}$$

$$1 = \frac{\tilde{A}}{\sqrt{\beta'}} \int e^{\beta' \vec{M}\cdot\vec{m}} F_0(y)\, d\theta \tag{3.57}$$

$$M_x = \frac{\tilde{A}}{\sqrt{\beta'}} \int e^{\beta' \vec{M}\cdot\vec{m}} F_0(y)\cos(\theta)\, d\theta \tag{3.58}$$

$$M_y = \frac{\tilde{A}}{\sqrt{\beta'}} \int e^{\beta' \vec{M}\cdot\vec{m}} F_0(y)\sin(\theta)\, d\theta \tag{3.59}$$

Here we have expressed the relations as function of the Fermi integrals $F_h(y) = \int \frac{p^h e^{-p^2/2}}{1+ye^{-p^2/2}}\, dp$, $y = \tilde{A}Be^{\beta'\mathbf{M}\cdot\mathbf{m}}$ and $\tilde{A} = A^{-1}e^{-\mu'}$.

The system of equations (3.56, 3.57, 3.58, 3.59) can be solved numerically with a Newton method, in a way which is analogous to the 1-level case. We numerically checked (data not shown) that in the limit of a single water-bag $\alpha_{j>1} \to 0$ the solution reported in [20] is indeed recovered. In the following section we turn to discussing the theory predictions with reference to the simple case of 2-levels water-bag ($n = 2$), validating the results versus direct numerical simulations.

3.3.3 The case $n = 2$: theory predictions and numerical simulations.

We here consider the simplifying setting where two levels ($n = 2$) water-bag are allowed for ($f_0 = 0$ being the background level). We are in particular interested in monitoring the dependence of $M = \sqrt{M_x^2 + M_y^2}$ versus the various parameters that characterize the initial condition. We recall in fact that, for the case of a 1-level water-bag, out of equilibrium transitions have been found, which separates between homogeneous and magnetized phases.
A natural question is thus to understand what is going to happen if one additional level is introduced in the initial condition. The level f_1 is associated

to a rectangular domain Γ_1 of respective widths $\Delta\theta_1$ and Δp_1. The level f_2 insists instead on an adjacent domain Γ_2, whose external perimeter is delimited by a rectangle of dimensions $\Delta\theta_2$ and Δp_2. The corresponding surface totals hence $\Delta\theta_2\Delta p_2 - \Delta\theta_1\Delta p_1$.

Recall that the energy ϵ_0 can be estimated as dictated by formula (3.48) and reads in this specific case:

$$\begin{aligned}\epsilon_0 = &\frac{1}{24}\left(f_1\Delta\theta_1\Delta p_1^3 + (f_2 - f_1)f_2\Delta\theta_2\Delta p_2^3\right) \\ &+ \frac{1 - 16(f_1\Delta p_1 \sin\Delta\theta_1/2 + (f_2 - f_1)\Delta p_2 \sin\Delta\theta_2/2)}{2} .\end{aligned} \tag{3.60}$$

The 1-level limit is readily recovered by simultaneously imposing $\Delta\theta_2 \to 0$ and $\Delta p_2 \to 0$ (which also implies $\alpha_2 \to 0$). By invoking the normalization condition (3.23) the following relation holds:

$$\lim_{\Delta\theta_2, \Delta p_2 \to 0} \epsilon_0 = \frac{1}{6}\Delta p_1^2 + \frac{1}{2}(1 - M_0^2) , \tag{3.61}$$

where $M_0 = 2\sin(\Delta\theta_1/2)/\Delta\theta_1$. The above relation coincides with the canonical expression obtained in the 1-level case (3.40).

Relation (3.60) enables us to estimate the energy associated to the selected initial condition and can be used in the self-consistency equations (3.56). Before turning to illustrate the predicted solution, let us note that the normalization (3.23) reduces for $n = 2$ to:

$$\alpha_1 f_1 + \alpha_2 f_2 = 1 . \tag{3.62}$$

To explore the parameter space we have decided to monitor the dependence of M on f_1, which therefore acts as a control parameter. To this end, we proceed by fixing the quantity $\Delta f \equiv f_2 - f_1$, the difference in hight of the considered levels. Furthermore, we specify the quantity α_1, while α_2 is calculated so to match the normalization constraint.

The analysis is then repeated for distinct choices of Δf, so to eventually elaborate on the importance of such crucial parameter. The results are displayed in figure (3.5). The curves collapse towards a point that corresponds to the limiting condition $\alpha_2 \to 0$ ($f_1 = 1/\alpha_1$): this special solution is met when the hypervolume populated by the level f_2 shrinks to zero, so driving the system towards the standard one level setting. By progressively reducing f_1 the predicted magnetization first increases and subsequently decreases to eventually

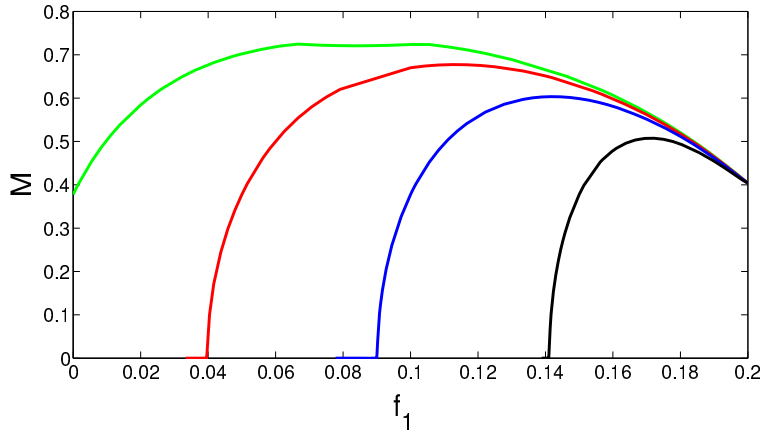

Figure 3.5: Analytical predictions for the equilibrium magnetization $M[\bar{f}_{eq}]$ as obtained for different values of the initial 2-levels water-bag distribution. The two levels are respectively labeled f_1 and f_2, while $f_0 = 0$ is the background level. We here work at constant $\alpha_1 = 5$ and $\Delta f = f_2 - f_1$, while moving the control parameter f_1. The analysis is repeated for distinct values of Δf (from left to right $\Delta f = 0.2, 0.15, 0.1, 0.05$). α_2 is computed according to eq. (3.23). For $f_1 \to 1/\alpha_1 = 0.2$ the normalization condition yields to $\alpha_2 \to 0$, and the distribution collapses to the limiting case of a 1-level water-bag.

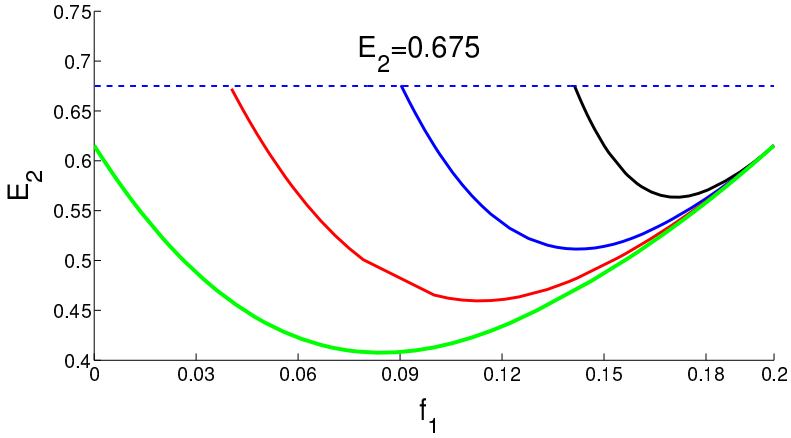

Figure 3.6: The analytical curves (same setting as in figure (3.5)) are now plotted in the plane (ϵ, f_1) (from left to right $\Delta f = 0.2, 0.15, 0.1, 0.05$). We here only represent the points that are associated to positive $M[\bar{f}_{eq}]$. The transition occurs at constant energy density $\epsilon \simeq 0.675$, regardless of the specific domains that result in the 2-levels water-bag distribution.

reach zero at a critical threshold f_1^c. For $f_1 > f_1^c$ the system is predicted to evolve towards a magnetized, hence non homogeneous phase.
Alternatively, for $0 < f_1 < f_1^c$ a homogeneous phase is expected to occur. Interestingly, the transition point f_1^c depends on the selected Δf: the larger Δf the smaller the value of the transition point, corresponding to a shift to the left in figure (3.5). Notice that above a limiting value of Δf, which self-consistently corresponds to imposing $\alpha_2 > 1/\Delta f$, the value of f_1 has to forcefully become

negative so to respect the normalization condition.
A *well* hence opens up in phase space, an intriguing scenario that can be formally handled within the descriptive Vlasov framework but that we have here deliberately omitted to deepen any further.
The smooth phase transition as depicted in figure (3.5) is therefore lost above a threshold value of Δf, when the predicted value of M associated to $f_1 = 0$ turns out to be greater than zero.

To elucidate the specificity of the outlined transition, we plot in figure (3.6) the energy ϵ, associated to each of the selected initial conditions, versus f_1, for the same selection of parameters as employed in figure (3.5). As suggested by visual inspection of the figure, the transitions, which we recall take place within a finite window in f_1, always occur for an identical value of the energy (in this case $\epsilon^c \simeq 0.675$). The transition point is hence insensitive to the specificity of the two levels f_1 and f_2, being neither dependent on their associated volumes nor relative heights. It is in principle possible to extend the above analysis and so reconstruct the complete transition surface in the (f_1, f_2, ϵ) space, a task which proves however demanding from the computational viewpoint and falls outside the scope of the present treatment.

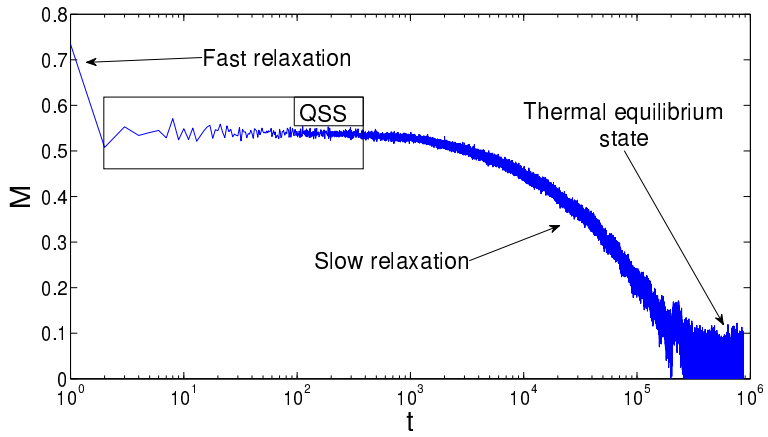

Figure 3.7: Magnetization M as a function of time t, as seen in a typical simulation. The system experiences a fast relaxation and then settle down into the lethargic QSS phase, whose duration (data not shown) increases with N. Later on the system moves towards the deputed equilibrium. In this simulation a two levels water-bag is assumed with $f_1 = 0.14$, $f_2 = 0.1$, $\alpha_1 = 0.2$, $\alpha_2 = 0.3$. The energy density is $\epsilon = 1.0$ and $N = 10^4$.

To test the validity of the theory we have run a series of numerical simulations of the HMF model. The implementation is based on fifth order McLachlan-Atela algorithm [80] with a time-step $\delta t = 0.1$. The initial condition is of a 2-levels

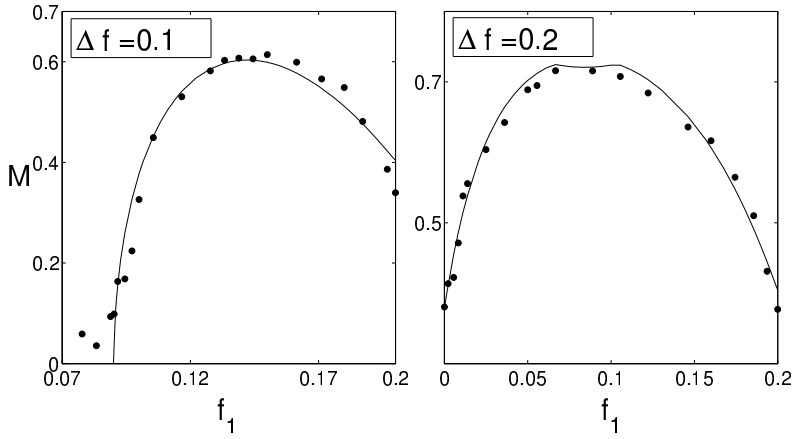

Figure 3.8: The analytical predictions (solid line) for the QSS magnetization as a function of f_1 in the 2-levels water-bag case, are compared (filled circles) to the numerical simulations performed for $N = 10^4$. The comparison is drawn for two distinct values of Δf ($\Delta f = 0.1$ (left) and $\Delta f = 0.2$ (right)). $\alpha_1 = 5$ and α_2 follows the normalization condition. Numerical values of M are computed as a time average over a finite time window where the QSS holds. The data are further mediated over 4 independent realizations. Expected uncertainties are about the size of the circle.

water-bag type, with respective domains assigned as follows the aforementioned prescriptions. As a preliminary check we have monitored the approach to equilibrium, figure (3.7).

As expected and generalizing the conclusion that have been shown to hold for the simpler 1-level water-bag family of initial conditions, the system settles down into a QSS, whose lifetime grows with the number of simulated particles. The QSS are indeed the target of our analysis and it is the magnetization as recorded in the QSS phase that needs to be compared to the Lynden-Bell predictions. The comparison between theory and simulations is reported in figure (3.8). Filled symbols refer to the simulation while the solid line stand for the theory, for two distinct choice of Δf. The agreement is certainly satisfying and points to the validity of the Lynden-Bell interpretative framework, beyond the case of the single water-bag, so far discussed in the literature.
Motivated by this success, we argue that the Lynden-Bell approach could be adapted to more complex, and so realistic, family of initial conditions.

Chapter 4

Out-of-equilibrium canonical description of the HMF model

Despite the great effort profused in the past years [81, 82, 83], the practical definition of a canonical thermal bath for a long-range system in a QSS regime is still an open problem. In particular we cannot straightforwardly follow Boltzmann's theory, since the partition function that is used in e.g. chapter 2.2 is weighted on the Maxwellian distribution which, as we have seen in the previous chapter, is inadequate to describe the out-of-equilibrium states [63, 64]. Other problems may arise from inequivalences among different equilibrium statistical ensembles [17, 85], as observed in chapter 1.3.3.
Because of the above difficulties, the microcanonical approach was so far the privileged playground to test theoretical predictions. In fact most results present in literature restrict to studies made on an isolated system.

The importance of a definition of a canonical out-of-equilibrium thermodynamic theory is the starting point to question the reproducibility of QSSs in real physical experiments, where the external interaction with a thermal bath, e.g. in the form of an an external noise source, induce perturbations that cannot be taken into account in the microcanonical ensemble. It was shown that the presence of such noise can induce complex phenomena such as phase transitions from the Vlasov-stable states [86].
As already shown numerically in past works, in the case of an HMF in contact with a short-range bath, if the contact interaction is weak enough, the system still relaxes violently to a QSS, while a strong interaction destroys the out-of-equilibrium state [81, 82].
Since an explicit derivation of the canonical partition function would require the knowledge of the practical implementation of the bath, which is still a matter of debate [84].

In this chapter we will present an original result of this thesis that aims to deriving a canonical description of a long-range system from a formal approach. We will see how such procedure can lead to problems and violations of fundamental thermodynamic principles, eventually pointing to the necessity of a generalized thermodynamic theory to tackle the study of a long-range system in contact with a thermal bath.

Almost all thermodynamic quantities, which are measurables in the canonical ensemble, can be obtained from the knowledge of the free energy function F. As discussed in chapter 1.3.2, following the accepted thermodynamic theory, this latter quantity can be always recovered from the knowledge of the microcanonical entropy S through a Legendre-Fenchel transform (LFT). This translates into a viable strategy to study a generic system in contact with the thermal bath without any knowledge of the latter (apart from its temperature T).
In the previous chapter we have shown how Lynden-Bell mixing entropy (3.28), obtained in the Vlasov limit (3.12), is capable to produce a valid prediction for the QSS states of the HMF model. Starting from this setting we will try to apply the canonical thermodynamic formalism to out-of-equilibrium stationary states of this paradigmatic model.
Before proceeding further, it is worth emphasizing that while we will use the HMF example, the results exposed in this chapter are relevant for a quite large class of systems and for many practical physical situations showing QSS with non-Gaussian equilibria, as observed in chapter 1.4.

In section 4.1 we will outline how the formal canonical approach may force us to reconsider the very definition of temperature, in the light of the non-Maxwellian nature of the equilibrium distribution function.
When proceeding in deriving the standard formal canonical free energy, we can end up with a system that possess a negative kinetic specific heat while in contact with a thermal reservoir. This latter evidence will lead to counterintuitive consequences, and rises questions on the validity of present thermodynamic theory to describe a long-range system out of the microcanonical formalism.
Conversely in chapter 4.2 we will show how, if we assume the validity of the formal definition of the thermodynamic temperature obtained from the thermodynamic functions, we could end up conceiving a thermal cycle that violates the second law of thermodynamics. To reconcile the last result with the thermodynamic principles, we could end up modifying the Fourier law of heat transport, with profound implications in long-range thermodynamics.

4.1 Out-of-equilibrium thermal bath: questioning temperature definition

In classical thermodynamics, specific heat is defined as the energy required to *increase* the temperature of a unit quantity of a substance by a unit of temperature. Such a definition follows common sense: providing energy to a physical system should induce heating, that is an increase of the system temperature.
In fact, this is normally the case of physical systems obeying the Boltzmann statistics [87] and being characterized by short-range interactions. However, less intuitive thermodynamic properties may be displayed by long-range interacting systems.

In that case, experiments realized on isolated systems, described by the micocanonical statistical ensemble, may give different results from similar experiments performed on systems in contact with a thermal bath, for which the canonical ensemble is the appropriate one.
As observed in chapter 1.3.3, one of the most striking features of such ensemble inequivalence is the presence of a negative specific heat in the microcanonical ensemble: increasing the energy of an isolated long-range system may lead to a decrease of its thermodynamic temperature. On the other hand, as mentioned in chapter 1.3.3, it is generally recognized that the specific heat in the canonical ensemble is always positive, even if interactions are long-range.

Hence, it is a generally shared opinion that one can not *measure* negative specific heat in a system in contact with a thermal bath. As we will see, such a result relies on the assumption that the thermodynamic temperature, defined as $T_{\text{th}} = (\partial s/\partial \epsilon)^{-1}$ (where s and ϵ are, respectively, the system entropy and the energy per particle), coincides with the kinetic temperature, T_{kin}, defined in terms of the average of the system kinetic energy. In fact, as we will show, the latter true only for Boltzmannian systems, and generally not for systems following a different statistics.

As a paradigmatic example for our investigation, we consider the so-called Hamiltonian Mean Field (HMF) model (2.1). With the notation introduced in chapter 3.3.

As already discussed in chapter 3, starting from an initial condition far from equilibrium, the system may be trapped in a "quasi-stationary state" (QSS), whose lifetime diverges with the system size N. In this regime the system is

described by a non Gaussian distribution. It has been shown that in the limit $N \to \infty$ QSSs can be related to the stable steady states of the Vlasov equation describing the system, and Lynden-Bell's theory can be used to define a mixing entropy s_{LB}. Its explicit form is obtained from a water-bag initial condition.
For simplicity in the following we will consider a 1-level water-bag (3.37), in which case the entropy per particle reads:

$$s_{LB}[\bar{f}] = -\int \left[\frac{\bar{f}}{f_1}\ln\frac{\bar{f}}{f_1} + \left(1-\frac{\bar{f}}{f_1}\right)\ln\left(1-\frac{\bar{f}}{f_1}\right)\right] \mathrm{d}p\mathrm{d}\theta \,. \tag{4.1}$$

As already seen in chapter 3.3.1, maximizing this entropy yields a "fermionic" solution $\bar{f}_{eq}(\theta, p)$ (3.41). While QSSs represent out-of-equilibrium states of the N-body dynamics, they could be equally interpreted as equilibrium configurations of the corresponding continuous description: in this respect, the conclusions of our analysis applies to both equilibrium and non equilibrium dynamics, provided the latter bears distinctive non-Boltzmannian traits.

In chapter 1.3 we have seen that the specific heat in the canonical ensemble is always positive, but here we will challenge that confidence and discuss in which respects such an argument does not apply to our case.
Consider a generic (long-range or short-range) system. Given the microcanonical entropy $s(\epsilon, n)$, where n is the particle density, the canonical rescaled free energy, $\phi(\beta, n) = \beta f(\beta, n)$, can be calculated as the Legendre-Fenchel Transform (LFT) of $s(\epsilon, n)$:

$$\phi(\beta, n) = \inf_\epsilon \left[\beta\epsilon - s(\epsilon, n)\right] \,. \tag{4.2}$$

Here β is a free parameter to be related to the system temperature.
As we already noted in chapter 1.3.2 the LFT of a generic function is always a concave function. If $s(\epsilon, n)$ is also concave, the inverse LFT can be applied: $s(\epsilon, n) = \inf_\beta \left[\beta\epsilon - \phi(\beta, n)\right]$. This is always the case of short-range systems, for which the equivalence of statistical ensembles holds true. Using the previous relation one can write:

$$\frac{\partial^2 s}{\partial \epsilon^2} = \frac{\partial \beta}{\partial \epsilon} = \frac{\partial \beta}{\partial T}\frac{1}{c_v^{\mathrm{mic}}} \,, \tag{4.3}$$

where

$$c_v^{\mathrm{mic}} = \frac{\partial \epsilon}{\partial T} = \frac{1}{\left(\dfrac{\partial^2 s}{\partial \epsilon^2}\right)\left(\dfrac{\partial T}{\partial \beta}\right)} \tag{4.4}$$

is the specific heat (at fixed volume) calculated in the microcanonical ensemble and T is either the thermodynamic (T_{th}) or the kinetic (T_{kin}) system temperature.

Making use of the LFT, the specific heat can be also calculated in the canonical ensemble and expressed in terms of the rescaled free energy:

$$c_v^{\rm can} = \frac{\left(\dfrac{\partial^2 \phi}{\partial \beta^2}\right)}{\left(\dfrac{\partial T}{\partial \beta}\right)} \, . \tag{4.5}$$

Using the thermodynamical definition of temperature: $T_{\rm th} = (\partial s/\partial \epsilon)^{-1} = 1/\beta$, one gets:

$$\left(c_v^{\rm mic}\right)_{\rm th} = -1/T_{\rm th}^2 \left(\partial^2 s/\partial \epsilon^2\right) \, . \tag{4.6}$$

The sign of $\left(c_v^{\rm mic}\right)_{\rm th}$ depends on that of the second derivative of the entropy respect to energy:

$$\begin{cases} \text{If } \partial^2 s/\partial \epsilon^2 < 0 \, , \text{then } \left(c_v^{\rm mic}\right)_{\rm th} > 0 \, , \\ \text{If } \partial^2 s/\partial \epsilon^2 > 0 \, , \text{then } \left(c_v^{\rm mic}\right)_{\rm th} < 0 \, . \end{cases} \tag{4.7}$$

As already noted in chapter 1.3.3, in the case of long-range systems, the entropy function can have a convex region in energy in presence of first order phase transitions, while this cannot happen in case of short-range interactions due to phase separation [9].
In the canonical ensemble we have:

$$(c_v^{\rm can})_{\rm th} = -\frac{1}{T_{\rm th}^2} \left(\frac{\partial^2 \phi}{\partial \beta^2}\right) \, . \tag{4.8}$$

As we have already mentioned, ϕ is always concave and, as a consequence, $(c_v^{\rm can})_{\rm th}$ is always positive.

Consider now the definition of kinetic temperature, which is the one experimentally accessible [63] (we cannot directly measure a thermodynamic potential):

$$T_{\rm kin} = \int p^2 F(\theta, p) d\theta dp \tag{4.9}$$

(we assume unitary mass in the definition of kinetic energy). Here $F(\theta, p)$ is the normalized equilibrium distribution function of the system. Equation (4.9) furnishes the link between $T_{\rm kin}$ and the thermodynamical temperature $T_{\rm th} = 1/\beta$.
For a Boltzmannian system: $F(\theta, p) = C \exp(-\beta p^2/2)$, where C is a normalization constant [87]. Substituting the latter expression into equation (4.9) one gets:

$$T_{\rm kin} = 1/\beta = T_{\rm th} \, . \tag{4.10}$$

In this case the statistical and kinetic definitions of specific heat provide the same result: $(c_v)_{\text{th}} = (c_v)_{\text{kin}}$.

From the above, one can conclude that, for a Boltzmannian system, the canonical specific heat is always positive, regardless the definition of temperature. As a consequence, for a Boltzmannian long-range system, the presence of negative specific heat in the microcanonical ensemble is the signature of ensemble inequivalence.
A completely different scenario may arise in the case of non-Boltzmannian or out-of-equilibrium long-range systems. As we shall demonstrate, for those systems one can expect to measure negative specific heat in the canonical ensemble.

Consider the "fermionic" system characterized by the entropy (4.1), paradigmatic example of a long-range system "trapped" in a QSS. Following the procedure outlined above, one can perform the LFT of $s[\bar{f}]$ and calculate the rescaled free energy $\phi[\bar{f}, \beta]$. Requiring the free energy to be stationary, one have to solve the following variational problem:

$$\delta s_{LB} - \beta \delta \epsilon = 0 \tag{4.11}$$

and gets the following distribution:

$$\bar{f}_{eq}(\theta, p) = \frac{f_1}{1 + e^{\beta f_1 (p^2/2 - M_x[\bar{f}_{eq}] \cos\theta M_y[\bar{f}_{eq}] \sin\theta) + \mu}} \,. \tag{4.12}$$

Here μ plays the role of a Lagrange multiplier associated to mass conservation, while $M_x[\bar{f}] = \int \bar{f} \cos(\theta) d\theta dp$, $M_y[\bar{f}] = \int \bar{f} \sin(\theta) d\theta dp$ stand for the two components of magnetization in the $N \to \infty$ limit.
It is worth stressing that the expression (4.12) for the stationary distribution in the canonical ensemble is formally identical to the one obtained by requiring the entropy (4.1) to be stationary in the framework of the microcanonical ensemble (3.41). In that case, β and μ are Lagrange multipliers associated to energy and mass conservation.

Figure (4.1) shows the entropic curve, $s_{LB}(\epsilon)$, for a given initial condition f_1. The curve is calculated in the framework of the microcanonical ensemble, using the following procedure. Once fixed ϵ and f_1, one first determines the corresponding values of M_x, M_y, μ and β in the expression (4.12) for $\bar{f}_{eq}$. This can be done by imposing energy and mass conservation and by using the definition of M_x and M_y (see chapter 3.3.1).
In general, one obtains several possible distributions $\bar{f}_{eq}$, corresponding either to

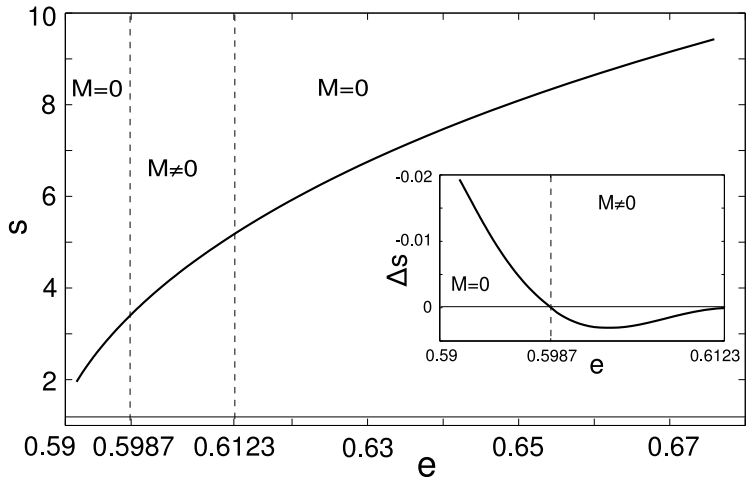

Figure 4.1: Lynden-Bell entropic curve, $s_{LB} = s_{LB}(\epsilon)$, calculated for the initial condition $f_1 = 1.1096$, in the framework of the microcanonical ensemble. Inset: difference, Δs_{LB}, between magnetized and non-magnetized branches of the entropic curve, as a function of energy. A change of sign in $\Delta s_{LB}(\epsilon)$ is the signal of a phase transition, see also [88]. There is a second-order phase transition at $\epsilon = 0.6123$ and a first-order phase transition at $\epsilon = 0.5987$. Note that the latter cannot be noticed on the (too large) scale used to plot the entropic curve.

magnetized (i.e., $M = \left(M_x^2 + M_y^2\right)^{1/2} \neq 0$) or to non-magnetized (i.e., $M = 0$) states. The value of $s(\epsilon)$ is found by substituting the possible solutions into (4.1) and by solving numerically the integral: the retained value is the one corresponding to maximum. This also selects the expected (magnetized or non-magnetized) stable equilibrium distribution.

The Lynden-Bell entropic curve $s(\epsilon)$ is always concave (see figure 4.1): such a result is a clear indication of ensemble equivalence.
Assuming $F(\theta, p) = \bar{f}_{eq}(\theta, p)$ in equation (4.9), one gets a formal nonlinear relation between the kinetic temperature; T_{kin}, and the Lynden-Bell Lagrange multiplier $\beta = 1/T_{\rm kin}$ (inverse thermodynamic temperature).

Reconsidering now equations (4.4) and (4.5), with $T = T_{\rm kin}$, one is led to the surprising conclusion that the measured kinetic specific heat can be negative both in the microcanonical and in the canonical ensembles, no matter the convexity of the entropy and of the free energy functions. In fact, in both cases the sign of the specific heat also depends on that of the derivative of the function $T_{kin} = T_{kin}(\beta)$.

The curve $T_{kin} = T_{kin}(\beta)$ can be calculated in the framework of the canonical ensemble, as follows. Once fixed β and f_1, one determines the stable equilibrium distribution by finding out the corresponding values of M_x, M_y and μ. This can

be done by imposing the normalization constraints and by using the definition of magnetization.
Note that finding the equilibrium distribution in the framework of canonical ensemble requires to determine three parameters (and, thus, to solve three equations), instead of four, as required in the case of the microcanonical ensemble. This is due to the fact that energy does not explicitly enter the expression (4.12) for the stationary distribution.
The obtained result is then substituted into equation (4.9) and the integral solved numerically. The curve $T_{\rm kin} = T_{\rm kin}(\beta)$ is shown in figures (4.2) and (4.3).

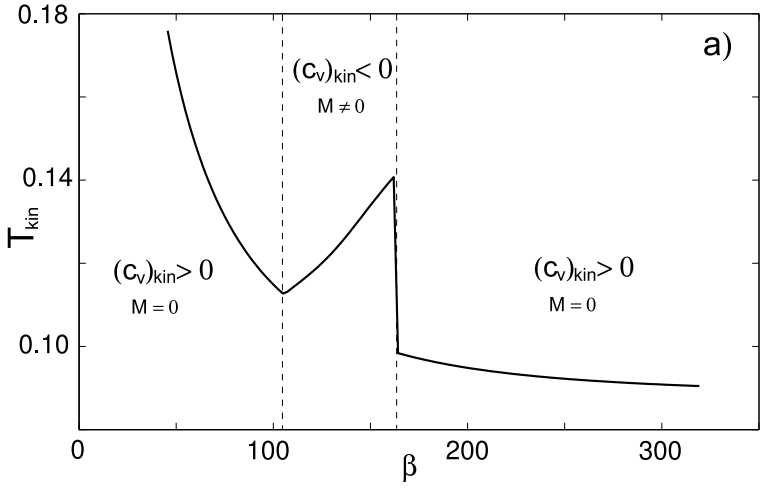

Figure 4.2: Kinetic temperature, $T_{\rm kin}$, as a function of the Lynden-Bell Lagrange multiplier β, calculated for the initial condition $f_1 = 1.1096$.

As it can be seen, one gets $\partial T_{kin}/(\partial\beta) > 0$ and, thus negative specific heat, $(c_v)_{\rm kin} < 0$, in both ensembles, in the magnetized region. The change of sign occurs in correspondence of phase transitions: from positive to negative in correspondence of a second-order phase transition, at smaller β values, and from negative to positive in correspondence of a first-order phase transition, at larger β values, where the curve displays a discontinuity.
Note that this behaviour is fundamentally different from that displayed by Boltzmannian long-range systems. Indeed, as already mentioned, in that case the change from positive to negative (thermodynamical) specific heat may occur only in correspondence of a first-order phase transition [85]. Phase transitions are also signaled by a change of stability of the magnetized and non-magnetized branches of the entropic curve, as shown in the inset of figure (4.1).

The presence of a negative kinetic specific heat in the magnetized region

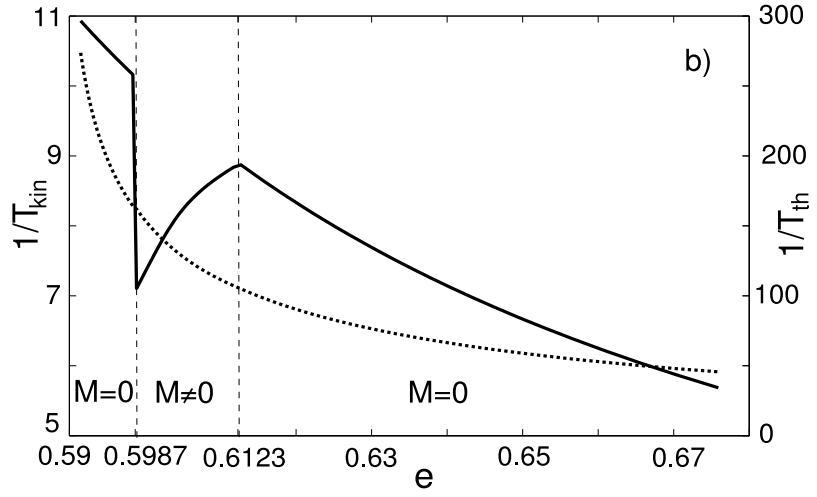

Figure 4.3: Kinetic caloric curve, $1/T_{\rm kin}$ vs. ϵ (continuous line), and thermodynamic caloric curve, $1/T_{\rm th} = \beta$ vs. ϵ (dotted line), calculated at $f_1 = 1.1096$.

can be also noticed by looking at the kinetic caloric curve shown in figure (4.3) (continuous line). As expected on the basis of the result shown in figure (4.1), the thermodynamic caloric curve (dotted line in figure 4.3), is instead characterized by a negative derivative over the whole energy range, corresponding to $(c_v)_{\rm th} > 0$ in both ensembles.
It is worth stressing that the occurrence of negative specific heat in the microcanonical ensemble when the system is magnetized is confirmed by the results of direct N-body simulations, based on the HMF Hamiltonian (2.1) [88].

As we anticipated, a further surprising result is that the presence of negative specific heat is associated to equivalent statistical ensembles. A clear indication of ensemble equivalence can be obtained by inspection of figure (4.1), showing a concave entropic curve, and of figure (4.2), showing the occurrence of positive and negative canonical and microcanonical specific heats in the same interval of β values.
The same indication can be drawn by the thermodynamical caloric curve shown in figure (4.3).
However, the curves displayed in figures (4.1) and (4.2) have been obtained for a particular initial condition f_1. In order to investigate ensemble equivalence for any f_1, we have compared the values of M obtained by solving the Lynden-Bell problem in the two ensembles for different initial conditions, following the above outlined procedures. Results (not reported here) show that the magnetized and unmagnetized regions perfectly coincide, and this confirms ensemble equivalence.

The results previously exposed demonstrate the unexpected possibility to

measure negative specific heat in the statistical canonical ensemble. As we argued above, this conclusion does not contradict any fundamental law of thermodynamics but ultimately originates from the non-Boltzmannian features that are possibly associated to non-equilibrium, as well as equilibrium, dynamics. We want to stress that this issue is strictly related to the concept of "measure". In fact we used a formal thermal bath with a constant β (thermodynamic temperature), but we assume that the real measurable temperature is the kinetic one, having no instrument to measure a thermodynamic potential or even to obtain the direct knowledge of the entropy functional.

With reference to the case at hand, and for a specific window of the parameter space that we traced back to magnetized QSS, the particles gain in kinetic energy when an energy quota is passed from the system to the heat reservoir. This surprising effect arises spontaneously and it is driven by the inherent ability of the system to self-organize at the microscopic level. The average particle velocity is enhanced at the detriment of the potential energy, and this yields in turn to an increase of the experimentally measurable kinetic temperature. The opposite holds if the energy flows towards the system: the particles cool down, while the potential contribution grows so to guarantee for the needed energy balance.
This phenomenon, that we have here demonstrated with reference to the HMF model, is in principle general and can potentially extend to all those settings where non-Boltzmannian effects play a role.

The question that arises from these evidences is how to define the temperature of a long-range system in contact with a thermal bath, and how to define the heat transfer between the bath and the system. In past works [81, 82] the attention was put onto short-range thermal baths (with $T_{th} \equiv T_{kin}$). In this latter case the interaction with the system (where $T_{th} \not\equiv T_{kin}$) cannot keep a constant β, and a new theory must be developed in order to define appropriate thermodynamic potentials that take into account the inequivalence in the two temperature definitions.

Conversely, if a standard thermal bath is indeed realizable, it would be particularly attractive to speculate on the possibility of realizing efficient thermal devices, working with a non-Boltzmannian fluid. Given the particular interplay between the potential and kinetic energy, one can expect that such a machine would have surprising features. In the next section we will show that this latter possibility would naturally lead to the violation of key thermodynamic principles, pointing out the necessity of a global revision of present thermodynamic theory for long-range systems.

4.2 A thermal machine working with non-Maxwellian fluid

According to standard thermodynamics, the efficiency of a cyclic machine is strictly lower than one. Such a result is a straightforward consequence of the second principle of thermodynamics. However, as we observed in the previous chapters, long-range interacting system report on a rather intricate zoology of peculiar behaviors, which are occasionally in contrast with customarily accepted scenarios, dueling with intuition and common sense. In this section we will try to assemble a thermodynamical cycle for an ideal device working with non-Boltzmaniann long-range fluid and operating in contact with two thermal reservoirs.
Assuming the microcanonical or canonical temperature T_{th} to be the correct thermodynamic temperature, the system is analytically shown to violate the second principle of thermodynamics. This phenomenon ultimately relates to the existence of regions in the canonical ensemble where $c_v^{kin} < 0$. We argue that the validity of the second principle of thermodynamics can be possibly restored, by revisiting the definition of canonical ensemble, as well as the Fourier law of heat transport, and consequently relaxing the constraint on the maximal efficiency as imposed by the Carnot theorem.
This latter possibilities, however, would eventually lead to the development completely new thermodynamics for non-Boltzmannian systems in equilibrium with a thermal bath.

The second principle of thermodynamics represents a fundamental milestone of physics [89]. Its validity is however supported by an impressively large gallery of experimental facts and consequently assurged to the status of inviolable universal law. It admits different formulations, the first of which is credited to the German physicist Rudolf Clausius [90]: *No process is possible whose sole result is the transfer of heat from a body of lower temperature to a body of higher temperature.* This in turn traces back to the concept of irreversibility: the heat cannot flow from cold to hot regions without external work being performed on the system, as e.g. it happens in a refrigerator. An alternative formulation of the second principle due to the Irish physicist Lord Kelvin [91] recites instead: *No process is possible in which the sole result is the absorption of heat from a reservoir and its complete conversion into work.* In practice, one cannot entirely transform the heat absorbed by a reservoir into work, without dissipating part of it. Rephrasing the latter statement: it is thermodynamically impossible to obtain a 100 % efficiency from a cyclic heat engine.

Indeed, Carnot's theorem [92] limits the maximum efficiency η for any possible engine, and can be seen as a direct byproduct of the second principle. All irreversible heat engines operating between two heat reservoirs, respectively characterized by thermodynamic temperatures T_C (cold) and T_H (hot), are less efficient than a Carnot engine working in contact with the very same reservoirs. The Carnot maximal efficiency can be straightforwardly quantified in $\eta = 1 - T_C/T_H$ as discussed in any basic textbooks.

As already emphasized, the above picture is at the core of our current understanding of physics, it appears to be solidly grounded on experiments and no doubt is cast on its correctness. Problems may emerge, however, when dealing with thermodynamics of long-range systems.

4.2.1 Vlasov fluid in an external field

Let us consider an HMF system in its Vlasov limit $N \to \infty$ (3.30), and lets put it in contact with a thermal bath, as already explained in chapter 4.1. For the sake of simplicity, and to allow for relatively straightforward analytical progress, we solely consider the case of a 1-level water-bag initial condition (3.37), and we will chose the initial energy density ϵ_0 and magnetization M_0 in order to end up in a magnetized QSS phase. In this condition we will measure a negative kinetic specific heat also in the canonical ensemble.
We will of course suppose that the standard thermodynamic theory can be applied also in this case, and a free energy function can be successfully obtained through a Legendre-Fenchel transform of the microcanonical Lynden-Bell entropy s_{LB}.
In this latter hypothesis, the effect of the thermal bath is to maintain a constant temperature T_{th}, while energy and kinetic temperature T_{kin} can variate.

In order to accommodate the necessity of performing external work on the system (and thus construct an adiabatic transformation) we will suppose that the system will interact with be subject to an external magnetic forcing of strength h. In its original formulation, the HMF is a discrete model composed of N particles (spins) in mutual interaction, and has been thoroughly studied in the previous chapters in the unperturbed limit $h = 0$.
In the continuum limit $N \to \infty$, we will redefine the interaction potential $V(\theta)[f]$ with an additional external term:

$$V(\theta)[f] = 1 - M[f]\cos(\theta) + h\cos(\theta)\,, \tag{4.13}$$

where $f(\theta, p, t)$ is the one particle distribution function. For simplicity, and

without loss of generality, we will assume that the total magnetization M of the system will be directed along the y axis:

$$M[f] = \int_{-\pi}^{\pi} \int_{-\infty}^{\infty} f(\theta, p, t) \cos\theta \mathrm{d}\theta \mathrm{d}p \,. \tag{4.14}$$

Including the kinetic contribution, the specific energy reads:

$$\epsilon[f] = \int \int (p^2/2) f(\theta, p, t) \mathrm{d}\theta \mathrm{d}p - (M^2 - 1)/2 + hM \,. \tag{4.15}$$

Within the previous approximations, the entropy reads:

$$s[\bar{f}] = -\int \mathrm{d}p \mathrm{d}\theta \left[\frac{\bar{f}}{f_1} \ln \frac{\bar{f}}{f_1} + \left(1 - \frac{\bar{f}}{f_1}\right) \ln \left(1 - \frac{\bar{f}}{f_1}\right) \right] \,, \tag{4.16}$$

where $\bar{f}$ is the coarse-grained distribution function (4.12) obtained though Lynden-Bell procedure.
By maximizing the entropy functional, one obtains the microcanonical solution in terms of a fermionic distribution $\bar{f}_{eq}$ (3.41), which coincides with a particular class of stable stationary solutions of the Vlasov equation.

Given the microcanonical entropy (that self-consistently depends on the energy ϵ), one can always calculate the canonical rescaled free energy, $\phi(\beta, \bar{f}_{eq})$, as the Legendre-Fenchel transform (4.2). β is a free parameter which we assume to be equal to the inverse of the (constant, in the canonical ensemble) thermodynamic temperature T_{th} of the system. Requiring the free energy to be stationary, under the dynamical constraints, one recovers a closed mathematical prediction for the particles distribution (4.12), which again is fermionic.
In the case of an external magnetic field h we have:

$$\bar{f}_{eq}(\theta, p) = \frac{f_1}{1 + e^{\beta f_1 (p^2/2 - M[\bar{f}] \cos\theta - h\cos\theta) + \mu}} \,, \tag{4.17}$$

where μ is a Lagrange multiplier associated to mass conservation, which can be calculated by solving the self-consistent system of equations obtained by imposing the constraints conditions. Consequently, the coarse grained distribution function $\bar{f}_{eq}$ and the magnetization M can be calculated, for any fixed initial condition, i.e. given f_1, h β.

The thermodynamic temperature is defined as:

$$T_{th} = \begin{cases} (\partial s/\partial \epsilon)^{-1} & \text{in the microcanonical ensemble} \,, \\ 1/\beta & \text{in the canonical ensemble} \,. \end{cases} \tag{4.18}$$

A system and a thermal reservoir are said to be in equilibrium (no heat is exchanged) if their respective thermodynamic temperatures match. The canonical ensemble, as defined by the above LFT, provides hence the appropriate descriptive scenario for the system dynamics, β being fixed as the inverse of the thermostat thermodynamic temperature.
If a difference in temperature manifests between two adjacent systems, the heat flows against (proportional to) the temperature gradient so to eventually restore the equilibrium condition. This is the celebrated Fourier's law. With reference to both microcanonical and canonical pictures, one can alternatively consider the definition of kinetic temperature [63]:

$$T_{\rm kin} = \int p^2 \bar{f}_{eq}(\theta, p)\, d\theta dp \,. \tag{4.19}$$

We are purposely omitting any constant factor in the definitions of both temperatures.

As already observed in the previous section, for a Boltzmannian system $\bar{f}_{eq}(\theta, p) \propto \exp(-\beta p^2/2)$ [93] and it is therefore immediate to see that $T_{\rm kin} = 1/\beta = T_{\rm th}$. When instead the system displays non-Boltzmannian traits, $T_{\rm k} \neq T_{\rm th}$.
Unintuitive phenomena can thus set in as the emergence of negative kinetic heat in the canonical ensemble, a possibility demonstrated in chapter 4.1. Moreover, for a non-Boltzmannian fluid, a word of caution should be exercised on the usage of Fourier's heat law: does the heat flow proportional to the kinetic or thermodynamic temperature gradient? Is the proportionality scaling correct? We shall return later on this crucial point.

4.2.2 Constructing the thermodynamic cycle

Having reviewed the definition of canonical and microcanonical ensembles, we can formally construct a thermodynamic cycle, reminiscent of Carnot's one, for an hypothetic device working with the Vlasov fluid introduced above. We will in particular consider two isothermal transformations, the reservoirs being characterized by the (thermodynamic) temperatures T_H (hot) and T_C (cold). The cycle is then closed by assuming two adiabatic transformations. As concerns the latter transformation, we recall [94] that the first principle of thermodynamics reads:

$$\delta Q = de - h dM \,. \tag{4.20}$$

Here, Q is the heat provided by the environment to the system. The adiabatic transformation $\delta Q = 0$ is hence realized by tuning the field strength as

$h = d\epsilon/dM$ along the path. A representative cycle obtained by implementing the procedure outlined above is depicted in figure (4.4). Each point displayed in the three dimensional space (h, M, ϵ) is either a stationary solution of the entropy functional s (microcanical, adiabatic lines) or of the free energy ϕ (canonical, isothermal). Notice that one needs to circulate the cycle in figure (4.4) (lower panel) counter-clockwise, so to extract a positive work amount ($L_{HMF} = -\int_{cycle} h dM$). The heat exchanged with the hot and cold reservoirs, labeled respectively Q_H and Q_C, can be readily evaluated as an application of the first principle (4.20) and upon calculation of the work performed along the isothermal tracks.

Surprisingly, and as a straightforward application of the above procedure[1], we obtain $Q_H < 0$ and $Q_C > 0$. Moreover, $Q_C > |Q_H|$.
This is at odds with the physical constraints imposed by the second law of thermodynamics. The virtual machine that we have constructed works in fact as a refrigerator, cooling down the reservoir with the lower temperature. In doing so, it however generates a *positive* work load, which violates Clausius formulation of the second law of thermodynamics.
In principle, and admitting this conclusion to be correct, one could insert between the two considered reservoirs a standard thermal machine that, in a cycle, receives from the hotter bath the heat quota Q_H (i.e. the very same released by our Vlasov device), and returns to the colder reservoir the heat Q'_C, such that $|Q'_C| < Q_H$, while producing a positive work L.
The machine obtained by pairing together the two considered devices, subtracts heat from a single reservoir ($Q_C - |Q'_C| > 0$) and returns the positive work $L_{tot} = L_{HMF} + L$, against the second law of thermodynamics in the Kelvin-Planck formulation.

In other words, the machine that we have assembled, and which intimately exploits the unintuitive features of long-range systems, is characterized by an efficiency $\eta = L_{tot}/(Q_C - |Q'_C|)$ equal to one. This is so unexpected that, at first sight, it would be tempting to reject the results as a whole.
It is however possible to elaborate on a thermodynamic interpretation of the results and pinpoint to the specific, and highly unconventional phenomenon, that is ultimately responsible for such an astonishing behavior. Then we will come back to discussing the foundation of the theory, especially the customarily adopted definition of canonical ensemble, and suggest that the validity of the

[1]Let us recall that the solution of the Lynden-Bell variational problem (4.11) cannot be cast in a closed analytical form. In fact, the equations for the constraints which enable one to quantify the Lagrange multipliers, are to be solved numerically, at sought precision, with an iterative numerical scheme.

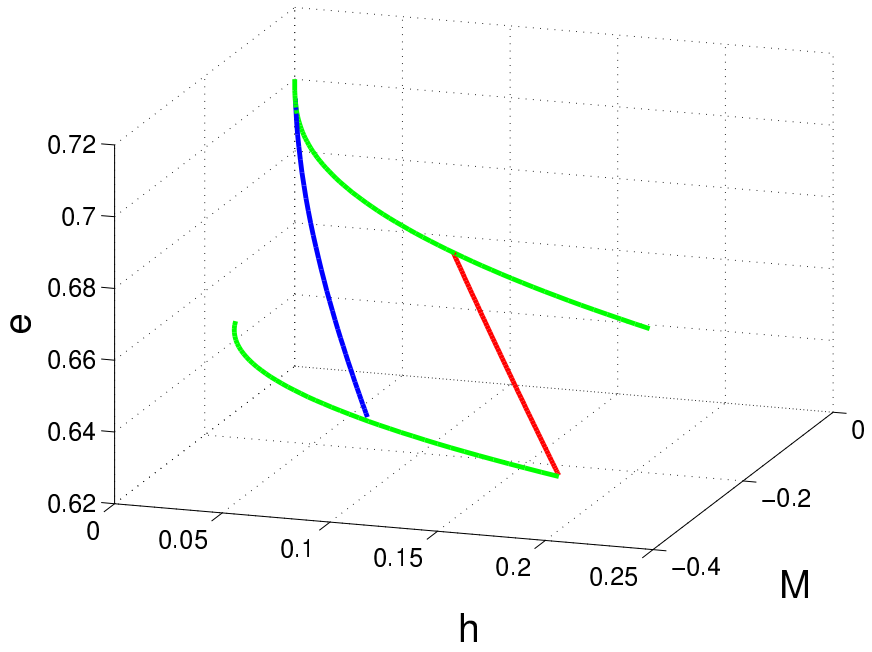

Figure 4.4: The thermodynamics cycle is represented in the three dimensional space (h, M, ϵ). The red line stands for the isothermal transformation carried out at T_H, while the blue line refers to the choice $T_C < T_H$. Here $T_H = 1/\beta_H = 0.33$ and $T_C = 1/\beta_C = 0.26$. The adiabatic transformations that close up the cycle are depicted in green. The heat exchanged with the reservoirs are respectively: $Q_H = -0.0363$ (heat flows out the system) and $Q_C = 0.0416$ (the heat flows towards the system). Here, $f_1 = 0.12$: this choice is purely representative. We have in fact repeated the calculation for different values of f_1, observing the same type of violation as described in the main body of the paper.

second principle could be eventually restored provided the kinetic temperature and *not* the thermodynamic one is employed in the law of Fourier for the heat transport.

4.2.3 Negative kinetic heat capacity and the violation of the second principle of thermodyamics

The cycle reproduced in figure (4.4) extends within a domain of the parameters space yielding magnetized states, where the system is characterized by negative (kinetic) specific heat in both canonical and microcanonical ensemble, i.e. along the isothermal lines of the cycle, when the magnetization is different from zero. This fact is indeed responsible for the apparently unphysical conclusions reached above. Consider in fact the first law and isolate the two terms that enter the right hand side of equation (4.20). The second term is related to the actual physical work: when proceeding counter-clockwise along the isothermal transformation, in contact with the hot reservoir, the quantity $-hdM$ is positive as can be

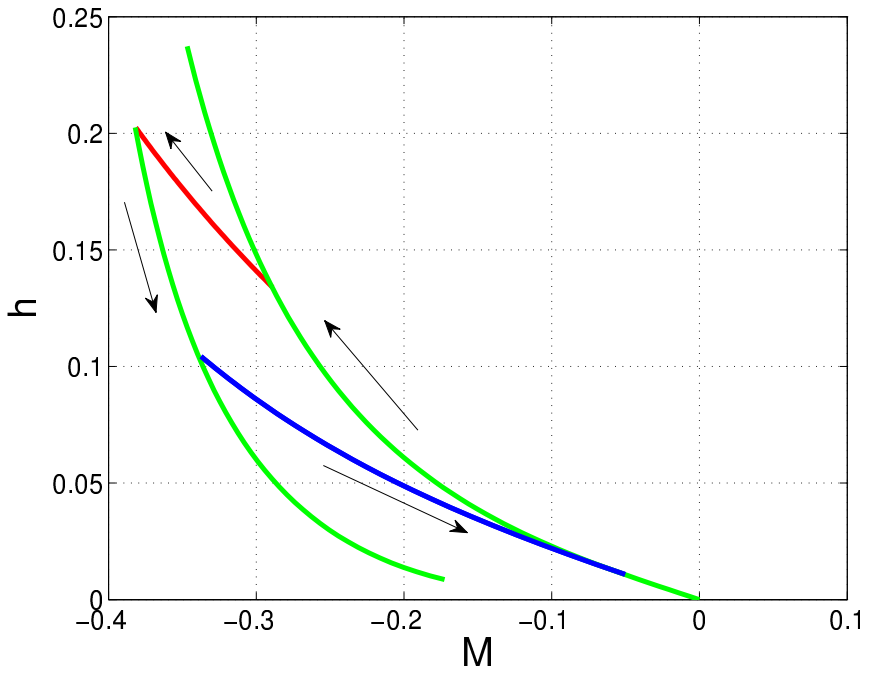

Figure 4.5: The cycle in figure 4.4 is projected in the (M, h) subspace. The arrows indicate the direction of circulation that produces a positive work.

deduced by looking at figure (4.4) (lower panel, red line).
In practice, and as it happens for an ideal gas performing an isothermal transformation, the work applied perturbs the system from its equilibrium condition, while constraining it to the same thermodynamic temperature of the bath.
A (positive) heat quota $(-hdM)$ is consequently transferred from the bath to the system, when circulating counter-clockwise. The opposite clearly holds when the cold isothermal is considered, together with the chosen direction of circulation: $-hdM$ is negative, see figure (4.4) (upper panel, blue line).
While the thermodynamic temperature is kept constant, the kinetic one T_{kin} changes along the considered transformation: in particular, T_{kin} increases along the isothermal at T_H, decreases when the system is evolved in contact with the colder bath T_C.

The other contribution to the heat δQ, the first term $(d\epsilon)$ on the right hand side of equation (4.20), gets also modulated along the transformation. In figure (4.6), the energy ϵ is shown to decrease when T_{kin} increases, for both cold and hot isothermals (resp. red and blue). The kinetic specific heat is thus negative, a condition that realises because of the non-Boltzmannian character of the system. Increasing the kinetic temperature, as the system does when in contact with

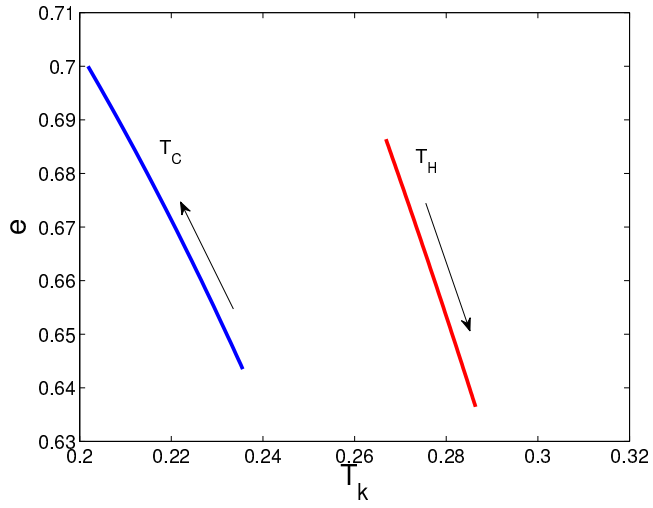

Figure 4.6: The energy ϵ of the system is plotted versus the kinetic energy T_{kin}, along the two isothermal transformations (in red $T_H = 0.33$, in blue $T_C = 0.26$). The transformations proceed along the directions highlighted by the arrows. Here, $f_1 = 0.12$.

the hot bath T_H, implies decreasing the energy e, and so contributing with a negative term to the global heat exchanged with the reservoir. Incidentally, the latter contribution turns out to be larger in absolute value, than the positive contribution associated to the magnetic work.
The total contribution is hence negative and for this reason the system cedes heat to the hot reservoir. Similar conclusions can be drawn when looking at the other isothermal transformation: now $d\epsilon$ is positive (the kinetic temperature decreases) and overcomes the negative $-hdM$ contribution.
When kinetic and thermodynamics temperature are equal (as they should for conventional Boltzmannian short range systems) the (kinetic) specific heat has to be necessarily positive, and the above surprising condition cannot realize.

4.2.4 Reconciling theory and experience: alternatives to the violation of second law

Summing up we have analytically shown that non-Boltzmannian systems can apparently violate the second law of thermodynamics, and explained such an astonishing ability in terms their peculiar statistical mechanics. It is however hard to accept such a conclusion, which would revolutionize our current understanding of the laws of nature.

However our derivation, though rigorous, relies on the formal definition of free energy. This latter follows naturally from the entropy functional, as emphasized

in the literature [88, 95, 9], and makes it possible to carry out the mathematical study here reported.
The actual implementation of a long-range dynamics in contact with a heat reservoir is still an open and controversial issue, that deserves to be carefully considered when challenging the possible practical relevance of our speculations.

When operating in the proposed scenario several way out in our view exists which potentially allows one to respect the second principle and confirm its validity for the class of systems being here considered. The critical point has to do with the definition of the canonical ensemble, that we have here mutuated from equilibrium classical statistical mechanics, by performing the Legendre-Fenchel Transform of the entropy functional.
In doing so, one requires that the canonical dynamics preserves the thermodynamic temperature of the system, setting it to a constant value imposed by the external reservoir.
First, and as anticipated before, we here assume that statistical mechanics and thermodynamics temperature coincide. Although this is a natural and well founded assumption for short-range systems, its extension to long-range systems should be critically questioned.
Moreover, one could imagine that non-Boltzmannian systems, when placed in contact with a thermal bath, would organize so to freeze their *kinetic temperature* to the temperature [2] of the bath.

As a natural consequence of this latter assumption, already stressed before, the Fourier law [96] should require that the heat flows proportionally to the *kinetic temperature gradient*, not the thermodynamic one, as the definition of canonical thermodynamical equilibrium would indirectly imply.
Pushing further this proposal, we could possibly ends up with a cyclic non-Boltzmannian engine which meets the second law requirement, while still exceeding the Carnot upper bound of efficiency, since the thermodynamic temperature is related to the kinetic one by a non linear functional relation:

$$T_{kin} = g(T_{th}) \, . \tag{4.21}$$

This is an important issue that touches the foundation of modern physics and that deserves to be carefully addressed in future works.
More substantial modification of the Fourier law of heat conduction can be also foreseen where e.g the heat flux is not solely influenced by the kinetic contributions but also forced by the configurational degrees of freedom stored

[2] Kinetic temperature, in general. If one deals with a Boltzmannian bath, kinetic and thermodynamics temperature clearly coincide.

in the potential terms. Preliminary N-body simulations of two coupled HMF systems encourage to insist along this line of investigation, which is out of the scope of the present work.

To conclude, we would like to stress that our study is relevant for a quite large class of systems and for many practical physical situations. In fact, the Vlasov equation is often invoked as the reference model for several experimental systems, as already observed in chapter 3. The modifications involved to the presently accepted thermodynamic theory are not simple, and working with unconventional non-Boltzmannian fluids could alter our current perception of the concept of efficiency, beyond the standard Boltzmann picture to which predictive tools are at present indirectly anchored.
In particular, it can be shown that, under some hypotheses, the governing Hamiltonian of CARL dynamics can be formally reduced to the HMF (2.1) [97]. This important observation will open up the perspective to eventually test our predictions versus direct experiments.

Chapter 5

Quasi-stationary states at the short-range threshold

The HMF system introduced before is a paradigmatic model of long-range interactions and has been widely studied in past literature. In the preceding chapters we have focused on discussing its main dynamic and thermodynamic features. Other models however exist which present an especially rich zoology of peculiar behaviours. This is for instance the case of the α-HMF model, a generalization of the HMF (2.1) which has been originally proposed in [98].
The interaction between two rotators has the same form as in the HMF model, but now the coupling constant is a weakly decaying function of the distance between the two lattice sites where the rotators sit. Thanks to a parameter α, which determines the decay with distance of the coupling constant between rotators, we can tune the strength of the interaction. This latter feature makes it possible to investigate long-range physics ranging from the mean-field limit $\alpha = 0$ up to the threshold α_c after which the model becomes technically short-range.
This model displays identical equilibrium features as the HMF. In fact it was rigorously proven that all stationary states of the HMF model are also stationary solutions of the α-HMF model [99, 9, 46].

In this chapter, we shall concentrate on a numerical study of the α-HMF model. We shall consider here one-dimensional cases for which the exponent α is next to the threshold value $\alpha = 1$, when the α-HMF potential model makes a transition from long to short-range interaction. Also, we shall discuss the presence of long-range dynamic and thermodynamic signatures in the range $1 \leq \alpha < 2$, where the system is technically short-range, according to the classification reported in figure (1.1). As observed in section 5.1, the peculiarity of the α-HMF interaction makes the model difficult to define on the basis of the scaling law of the potential, allowing some long-range features to persist in the short-range

regime.
This latter observation eventually points out the necessity to extend the definition given in chapter 1, in order to take into account the decay with the distance of the force, acting between pairs of particles.

5.1 The α-HMF model

The α-HMF describes N particles in a periodic space, and obeys to the following governing Hamiltonian:

$$H = \sum_{i=1}^{N} \left[\frac{p_i^2}{2} + \frac{1}{2\tilde{N}} \sum_{j \neq i}^{N} \frac{1 - \cos\left(q_i - q_j\right)}{\|i-j\|^{\alpha}} \right] , \tag{5.1}$$

where q_i stands for a spin angle located on the lattice site i and p_i is its canonically conjugate momentum. The distance $\|i-j\|$ between the two lattice sites where the rotators sit, is defined as the shortest distance on the circle of perimeter $N-1$, so that the systems can be isolated and still translational invariant along the lattice. The mean-field HMF model is eventually recovered for $\alpha = 0$.

Recalling definition (1.1), systems are considered long-range when the two body interacting potential $V(r)$ decays at most as $1/r^{\alpha}$ with $\alpha < d$, where d stands for the dimension of the embedding space. Having only one degree of freedom, $d = 1$ for the α-HMF model.
To make the system extensive, we assume N even and write:

$$\tilde{N} = \left(\frac{2}{N}\right)^{\alpha} + 2 \sum_{i=1}^{N/2-1} \frac{1}{i^{\alpha}} . \tag{5.2}$$

The equations of motion of each element i are derived from the Hamiltonian (5.1):

$$\dot{p}_i = -\sin(q_i) C_i + \cos(q_i) S_i = M_i \sin(q_i - \varphi_i) , \tag{5.3}$$

$$\dot{q}_i = p_i , \tag{5.4}$$

where

$$C_i = \frac{1}{\tilde{N}} \sum_{j \neq i} \frac{\cos q_j}{\|i-j\|^{\alpha}} , \tag{5.5}$$

$$S_i = \frac{1}{\tilde{N}} \sum_{j \neq i} \frac{\sin q_j}{\|i-j\|^{\alpha}} . \tag{5.6}$$

C_i and S_i identify the two components of a magnetization per site, with modulus $M_i = \sqrt{C_i^2 + S_i^2}$, and phase $\varphi_i = \arctan(S_i/C_i)$. For large N, and assuming $0 < \alpha < 1$, we have:

$$\tilde{N} \approx \frac{2}{1-\alpha}(N/2)^{1-\alpha} \,. \tag{5.7}$$

Then we can use (5.7) in equation (5.5) and perform the $N \to \infty$ limit while introducing the continuous variables $x = i/N$ and $y = j/N$ to arrive at:

$$C(x) = \frac{1-\alpha}{2^\alpha} \int_{-1/2}^{1/2} \frac{\cos\left(q(y)\right)}{\|x-y\|^\alpha} dy \,, \tag{5.8}$$

where $\|x - y\|$ represents the minimal distance on a circle of perimeter one.
In the above equation we can recognize the fractional integral $I^{1-\alpha}$ and consequently write:

$$C(x) = \frac{1-\alpha}{2^\alpha}\Gamma(1-\alpha) I^{1-\alpha}\left(\cos q(x)\right) \,. \tag{5.9}$$

In this large size limit, the α-HMF dynamics implies studying the evolution of the scalar fields $q(x,t)$ and $p(x,t)$ which are ruled by the fractional (non-local) partial differential equations:

$$\frac{\partial q}{\partial t} = p(x,t) \,, \tag{5.10}$$

$$\frac{\partial p}{\partial t} = \frac{\mu}{2^\alpha}\Gamma(\mu)\left(-\sin(q) I^\mu\left(\cos(q)\right) + \cos(q) I^\mu\left(\sin q\right)\right) \,, \tag{5.11}$$

where $\mu = 1 - \alpha$. It has then been shown in [46] that stationary states are solutions of the following equation:

$$\mathcal{D}^\alpha \cos q = \frac{d^\alpha \cos q}{dx^\alpha} = 0 \,, \tag{5.12}$$

where the operator D^α stands for the fractional derivative, and that this property is shared by non stationary QSS's. All these results were obtained for the model in its long-range version, meaning when α is smaller than one.

Considering situations where $1 < \alpha < 2$ implies studying short range models. In fact $\tilde{N}$ is finite so there is no need of system size renormalization of the coupling constant for $\alpha > 1$. However something is peculiar about the α-HMF lattice model. The force F acting between particles is obtained from the gradient of the interaction potential:

$$F = -\nabla V(r) \,. \tag{5.13}$$

When considering the dynamics of a long-range system, we would expect the force between particles to be ruled by a $1/r^\beta$ decay with $\beta = \alpha + 1$. In the case

of the α-HMF model, the distance is defined over a fixed lattice and does not come into play in the above derivation. In this latter case the decay exponent is unchanged ($\beta = \alpha$).

Moreover given the particular importance of the microscopic dynamics and possible ergodicity breaking, it is legitimate to ask whether the long-range nature of a system is ruled by the dynamics, rather then by the energy scaling. This would then imply that a system is long-ranged if $\beta < d+1$, which for the α-HMF, corresponds to requiring $\alpha < 2$. Past investigations targeted to the α-HMF model have assumed $\alpha < 1$, and cannot be simply extended to $1 < \alpha < 2$. A first numerical analysis is therefore necessary.

5.2 Equilibrium phase transitions in the short-range regime

One peculiarity of one dimensional systems is that they should not admit phase transitions, if the interaction is short ranged. We do know from literature that the α-HMF is equivalent to the HMF model in the long-range regime ($\alpha < 1$) [99, 9], so one recovers the equilibrium phase transition in figure (2.2) with a transition energy density $\epsilon_c = 0.75$.
In this section we perform a first numerical study of the magnetization versus density of energy for $\alpha = 1.5$. Discarding any possible metastable regime, to be assimilable to the aforementioned QSS, we shall hence obtain a description of the relation $M(\epsilon)$ for the system at equilibrium. The numerical integration of the microscopic dynamics is performed using a simplectic scheme (optimal fifth order see [80]), the time step used is $\delta t = 0.05$, and the initial conditions are Gaussian distributed.

As can be seen in figure (5.1) an equilibrium phase transition is displayed at a transition point $\epsilon_c \approx 0.6$ which is then different from previous value obtained in the HMF limit. Preliminary results show that the critical point depends on the value of α and approaches $\epsilon = 0$ for $\alpha = 2$.

The existence of a phase transition beyond the "classical" long-range threshold in one dimension, already noticed for the Ising model by Dyson in the sixties, seems to suggest that the system maintains a long-range nature when the potential of the interaction is short-ranged. Recent results [100], seem to point out that the scaling of the force must be taken into account. However an important feature to assert this new definition would be to find as well quasi-stationary

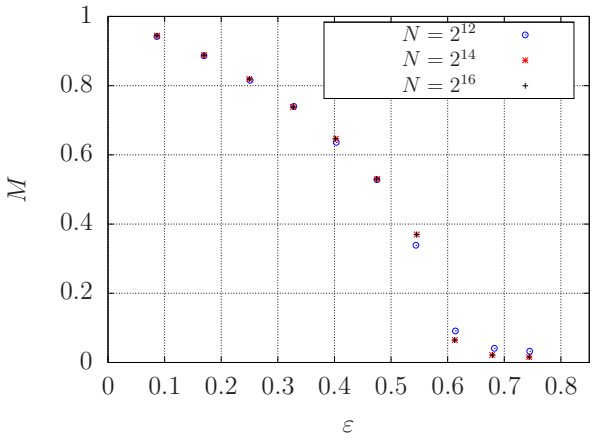

Figure 5.1: Magnetization vs energy, for $\alpha = 1.5$. A phase transition is displayed with $\epsilon_c \approx 0.6$. The transition point seem to be different from the long-range one which is $\epsilon_c = 0.75$, but the qualitative behaviour of curve is the same.

states in this region of α's.

5.3 QSS lifetime

As we already observed in chapter 1.4, in long-range interacting systems, the limit $N \to \infty$ and $t \to \infty$ may not commute, so the thermodynamic equilibrium is not unequivocally defined and one may end up in different states depending on the order in which the previous limits are taken. The divergence of the lifetime τ clearly indicates that QSS become indeed equilibrium states (that in general do not obey Boltzmann's statistics [9]) in the infinite N limit.

In this section we focus on studying how the QSS lifetime scales with the exponent α, which, we recall, controls the decay of the potential.
First we study the behaviour of the lifetime τ around the crucial value $\alpha = 1$ to better understand the transition between a long-range system and a supposedly short range one. As mentioned above in the case of α-HMF there are convincing arguments that the requirement for the emergence of long-range behavior could be relaxed, and we can expect some long-range features to survive above $\alpha = 1$.

We considered the initial condition already used in [46] which resulted in a magnetized QSS above the critical energy. We consider all the particles initially placed in a single point $q_i = 0$, while the momenta p_i's are Gaussian. To characterize the QSS lifetime we monitor the behaviour of the global macroscopic parameter magnetization $M = |\sum_j e^{iq_j}|$, in analogy with what already done for the case of the HMF. In figure (5.2) we show the behaviour of M as a function

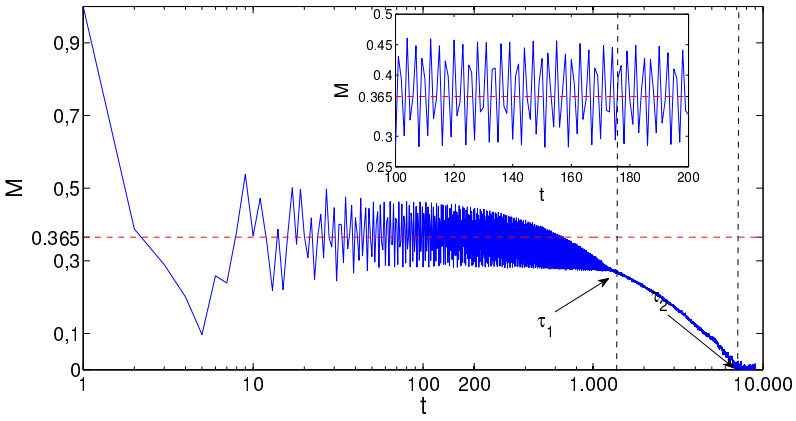

Figure 5.2: Magnetization curve vs time for $\alpha = 1.0$, $N = 2^{18}$ and $\epsilon = 1.2$. During the QSS the magnetization is oscillating for a time τ_1, then it relaxes down to its equilibrium value in a time τ_2.

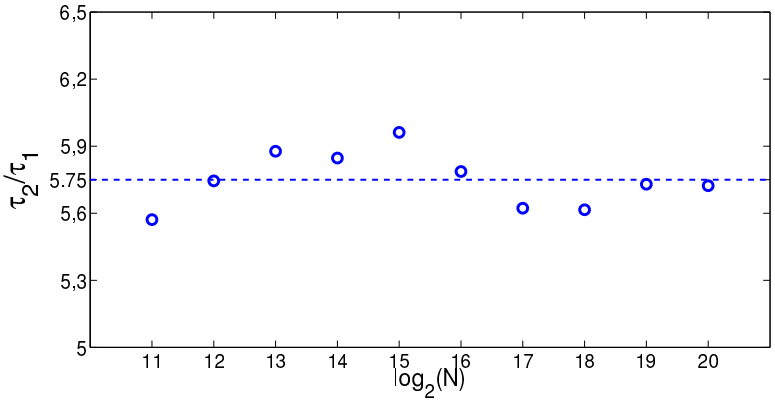

Figure 5.3: $\frac{\tau_2}{\tau_1}$ for different values of N, $\alpha = 1$ and $\epsilon = 0.6$. The two times are approximately proportional, so τ_1 returns a good approximation for τ_2. This proportionality is respected for all α values examined in this work, even if the proportionality constant may vary.

of time, for $\alpha = 1$, which is qualitatively representative for the all the values of α considered in this work.
A first transition at $t = \tau_1$ can be identified. Before this threshold in time the system oscillates around an almost constant magnetization value. Then the system starts to relax towards the equilibrium value $M = 0$. A second transition at $t = \tau_2$ is as well identified: it corresponds to the time at which the system finally reaches its equilibrium state. As it can be seen in figure (5.3), we find that these two values are almost linearly proportional for each α-value that we took into consideration. Hence, we shall refer to the first lifetime τ_1 as the lifetime of the QSS, since it is an order of magnitude faster to compute it and we are interested only in the qualitative form of the scaling law for the lifetimes.

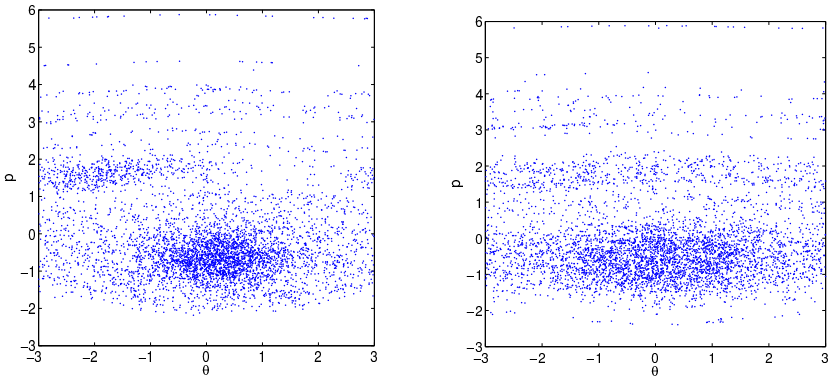

Figure 5.4: Poincarè sections for $\alpha = 1$, $\epsilon = 1.2$ and $N = 2^{20}$. Left panel refers to the QSS, while right panel represent intermediate relaxation between the QSS and the equilibrium state ($\tau_1 < t < \tau_2$). It can be easily seen that the second small island disappears during the relaxation and the phase space becomes symmetric in q, thus ending the oscillations of the magnetization.

The difference of the two dynamical regimes defined by the above thresholds are better understood when looking at the Poincarè section captured in each of this regimes, as displayed in figure (5.4). At first the system forms two distinct islands in the phase space, which start moving around and create the oscillations in the magnetization that characterize the QSS. Then, one of the islands disappears during the relaxation period, while the phase space becomes symmetric in q, thus causing the end of the oscillations.

Now we turn to analysing the lifetime of the QSS versus the size of the system, close to the classical long-range threshold $\alpha = 1$. If the system is long-range, it should diverge with N. The cases $\alpha = 0.9$, $\alpha = 1$ are displayed in figure (5.5), while in figure (5.6) we show the case $\alpha = 1.1$, beyond the long-range threshold. We can see that around $\alpha = 1$ the scaling of τ with N is well interpolated by a logarithmic curve, meaning that the QSS survives at least until $\alpha = 1$ and maybe beyond. In fact a logarithmic scaling appears to be valid also for $\alpha = 1.1$.
However, when looking at the data for larger value of α, namely $\alpha = 1.5$ the scaling of τ appears to saturate as displayed in figure (5.7): the magnetization curves obtained for $\alpha = 1.5$ appear to be all identical, no matter the size of the system. At this value of α, a phase exists which exhibits an oscillation in M, typical of the QSS. Now, the associated lifetime seems to be independent of N and finite, so the system will eventually reach the equilibrium state in a long enough time.

Conversely we may expect to observe a saturation in τ_1 also for $\alpha = 1.1$. We

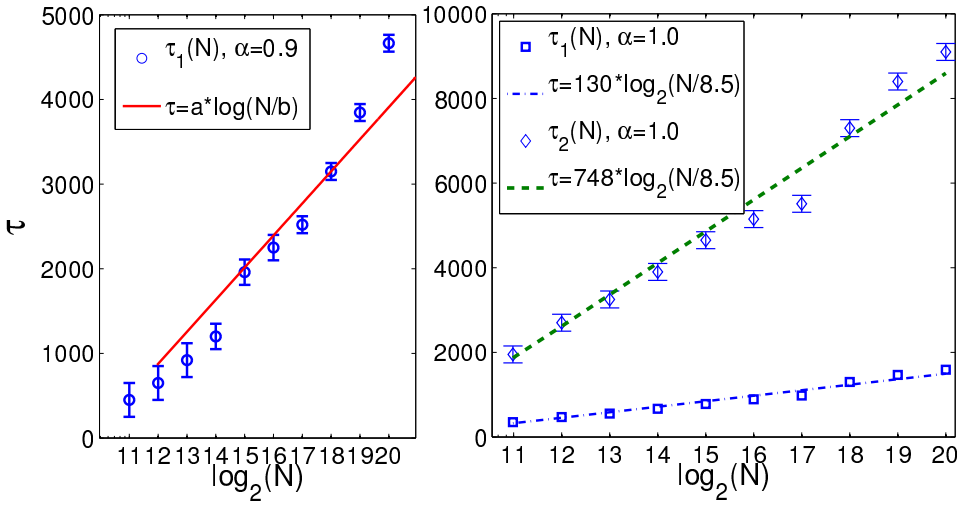

Figure 5.5: Right: scaling of τ_1 with N for $\alpha = 0.9$ and $\epsilon = 1.2$. Left: scaling of τ_1 and τ_2 with N for $\alpha = 1.0$ and $\epsilon = 1.2$.

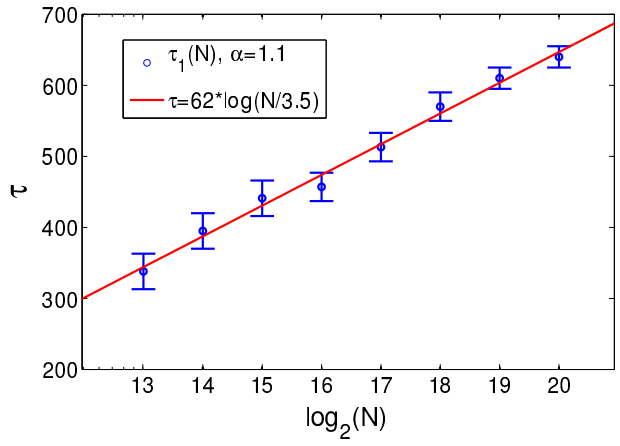

Figure 5.6: Scaling of τ_1 respect to N for $\alpha = 1.1$ and $\epsilon = 1.2$.

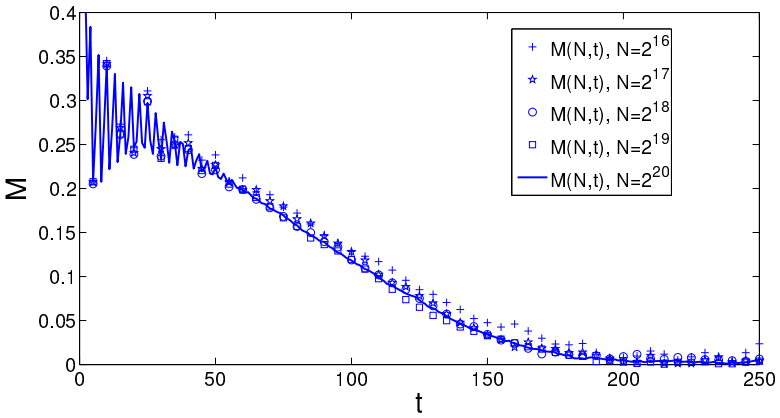

Figure 5.7: Magnetization curve vs time for $\alpha = 1.5$, $\epsilon = 1.0$ and increasing N values. The initial oscillation lifetime τ_1 is independent of N and the system relaxes to equilibrium in a time which should be constant in the continuous limit.

cannot in fact exclude that our observation reflects the limited (although large) size of the numerical simulations, due to computing time restrictions. We are therefore brought to conclude that, right now, we do not have enough proofs in support of a transition, that can presumably occur between $1.1 < \alpha < 1.5$, where the system can become suddenly short-range dropping the logarithmic growth of $\tau_1(N)$. It may be possible that even for $\alpha = 1.1$ the scaling time could saturate at some larger value of $N > 2^{20}$. Preliminary results show that this saturation becomes quite fast for $\alpha \sim 1.2, 1.3$ where even for lower values of N, it may still be possible to observe a scaling which is sub-logarithmic. Nevertheless, given the large size that would eventually reproduce the saturation, we may expect that QSS could be observable for a time which, from the "experimental" point of view, could be long enough to be relevant only for systems with an astronomical scale of constituents.

However even if the QSS lifetime seems to saturate at some point, so that the system dynamics change into a short range one, the phase transition from a magnetized to an homogeneous state, typical of the long-range regime, is still present (figure 5.1).
The evidences collected so far seem to suggest that the dynamical definition of long-range interaction, based on the decay with distance of the force, may be relevant. A similar conclusion was also independently proposed in a recent work by A. Gabrielli et al. [100].
The presence of QSS-like metastable behaviour (even with a finite lifetime) or one-dimensional phase transition for a wider range of potentials, encourages us to search for more complex and realistic models. The aim is to eventually be able

to interpret the out-of-equilibrium behaviour of real long-range physical systems in the framework of the rigorous theoretical results obtained in the context of mean-field systems.

Chapter 6

Self organization in a model of long-range rotators

Many long-range (LR) models exist in literature, that made it possible to elucidate several key aspects of both equilibrium and out-of-equilibrium dynamics. Still, due to their inherent complexity and number of degrees of freedom involved, the study of these phenomena is nowadays limited to toy-model systems and paradigmatic case studies, which cannot reproduce the whole complex behaviour that we observe in real experimental settings, for example the emergence of self-organized LR structures.

Typically many-body systems experiencing long-range forces, exhibit many peculiar self-organization properties displaying for instance the emergence of collective dynamics. On the other hand, the instabilities generated by random thermal motion tend to destroy the collective structures. The force of the interaction is typically the key factor that allows one to observe such behaviours. There is currently a great effort targeted to understanding the origin and robustness of such structures. This activity is crucial to eventually clarify the underlying dynamics of galaxy formations and plasma collective properties, among other things.
In past years there were many experimental confirmations of the emergence of crystal-like ordered structures in many long-range physical systems, as for example dusty charged plasmas [101, 102], Coulomb-interacting cold atoms [103] or Bose-Einstein condensates [104]. The phenomenology of these latter states is not clearly understood: there are experiments that seems to suggest the presence of an intermediate phase during the melting of the solid structure, which displays additional ordering at different scales [101]. In presence of a long-range interaction, the interplay between potential and kinetic energy terms give rise to correlations that do not decay rapidly with distance. This

latter effect may eventually translates into the emergence of complex thermodynamic transitions and peculiar symmetries. Long-range thermodynamics may prove the correct framework in which to interpret such debated observations.

The main problem that we encounter, while trying to model complex spatial phenomena using the long-range models that are made available in literature, is that their phase space presents a relatively modest degree of complexity. This latter feature is of course welcomed in order to allow one to find exact analytical solutions, as it is the case for the HMF model. However such simplifications do not allow for the formation of complex structures with extended spatial symmetries. For instance in the HMF the spatial extension of the phase space is limited in size, each coordinate being mapped onto the circle $\theta \in [0, 2\pi[$. The notion of interparticles' distance is not explicitly accounted for.
Other long-range solvable systems, albeit spatially extended, may lack of translational invariance, like the ϕ^4 model [9], or encode for a term defined on a peculiar lattice metric, see for example the discussion in the previous chapter devoted to α-HMF model. This latter has a predetermined structure that is embedded in the model itself, and which reflects in the observed structures as a natural imprint.

In order to describe the behaviour of crystal-like long-range structures, we will introduce and characterize in this chapter a more complex model, inspired to the α-HMF and to the paradigmatic HMF model. Such system was first proposed in [105] and was never extensively studied in the literature.
We will show that the system under scrutiny reproduces the same equilibrium thermodynamic curves and phase transitions as observed for the HMF, for a wide range of parameters. Under few assumptions we will prove analytically that in the thermodynamic limit the models can be considered equivalent. The dynamics is however different, as we shall discuss in the following.
In section 6.1 we will introduce the new rotators model, obtain its governing equations and highlight its basic features.
In section 6.2 we will set down to study the dynamic features of the model at equilibrium, showing the emergence of self-organized crystal phases, which eventually mutate into disordered gaseous phases at high energies. This extended model enables one to observe a new self-organized equilibrium state, which is intermediate between a crystal phase and a gaseous phase. This newly observed state is identified as a disordered soft crystal.
In section 6.3 we will derive an equilibrium distribution function for the model being examined and discuss the limit of its applicability due to finite-size corrections.
In section 6.4 we will show that, taking advantage of the strong properties of symmetry of the above distribution, we can formally reduce the rotator model

to the HMF and α-HMF in the infinite size limit.
Finally, in section 6.5 we will describe the phase transition between the crystal ferromagnetic phase and the homogeneous gaseous phase, which is found to be equivalent to the HMF equilibrium transition for a wide range of parameters.

6.1 An extended model of rotators

We introduce a 1-D Hamiltonian model describing N rotators that interact with a cosine-like potential similar to the HMF. The interaction is however scaled by a factor $d^{-\alpha}$, d being a measure of the interparticle distance and α an appropriate positive exponent that will play the role of an external parameter. Notice that d is a continuous parameter, that depends on the dynamical state of the system rather than on the initial lattice ordering of the particles. This marks a fundamental distinction with respect to the α-HMF case study discussed in the previous chapter 5.
The model is defined in a 1-dimensional space of arbitrary length L, with an average particle density $\rho_0 = N/L$. In this extended phase space we are not a priori forced to choose a particular metric or boundary condition. In this work, however, we will always consider periodic boundary conditions, in order to eventually recover the HMF setting in the limit $\alpha = 0$. Then we will consistently define the distance between two particles of position q and q' as

$$d = \min\{|q - q'|, L - |q - q'|\} := \|q - q'\| \,. \tag{6.1}$$

With the previous conditions, by denoting with p_i the canonical momentum of the particle with position q_i, the Hamiltonian equation describing the system can be written in the following way:

$$H = \sum_{i=1}^{N} \frac{p_i^2}{2} + A(\rho_0, L) \sum_{i,j=1}^{N} \frac{1 - cos(q_i - q_j)}{||q_i - q_j||^\alpha} \,. \tag{6.2}$$

When $0 \leq \alpha < 1$ the system is formally a long-range interacting one.
We can use the α parameter to tune the strength of the long-range effects. Notice that in the limit $q_i \to q_j$ the potential term goes to zero with continuity, and the whole Hamiltonian is a C_1 function. This latter property means that the potential does not satisfy the Braun-Hepp theorem, as stated in chapter 3.1. As a consequence the system dynamics is not necessarily described by the Vlasov equation in the limit $N \to \infty$. This observation marks an important distinction with respect to both HMF and α-HMF models.
$A(\rho_0, L)$ is a constant introduced to ensure extesivity, obeying Kac prescription.

Its value is obtained by requiring that the energy density ϵ does not depend on N. It is difficult to compute the analytical integral of the potential in equation (6.2), but we can estimate the scaling of ϵ as follows:

$$\epsilon \sim T_{kin} + \lim_{\delta \to 0} \int_{\delta}^{L/2} \rho_0 \frac{2A}{r^\alpha} dr = \frac{2\rho_0 A}{(1-\alpha)} (\frac{L}{2})^{1-\alpha} . \tag{6.3}$$

In order to make ϵ independent on N, we set:

$$A = \frac{(1-\alpha)}{N} (\frac{L}{2})^{\alpha} . \tag{6.4}$$

We then checked through numerical simulations that the latter choice correctly makes the potential extensive up to a precision in energy density of order 10^{-5}. In the HMF limit, $\alpha = 0$, we have $A = 1/N$, and so recover the correct HMF scaling.
For simplicity, we will consider L as an integer multiple of 2π, $L = 2\pi l$, so we will also avoid any finite-size effect due to non periodicity of phase space. It can be argued that this effect becomes eventually negligible in the limit of large L.

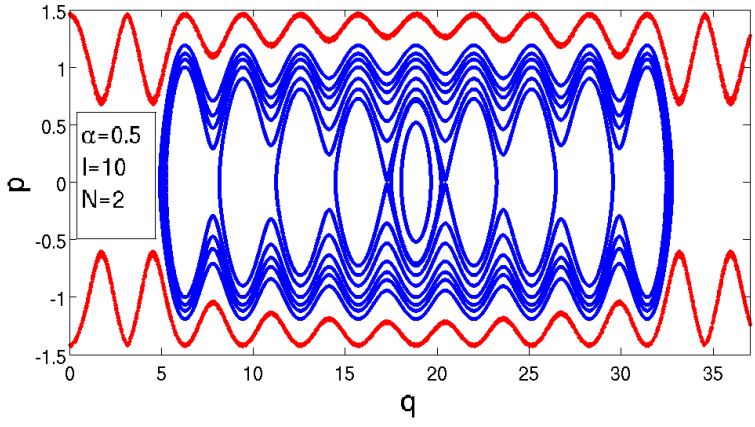

Figure 6.1: Phase space portrait in the case of $N = 2$, $l = 10$ and $\alpha = 0.5$. The different curves are obtained for different energies: blue ones represent bounded solutions while red ones represent free particle solutions for high energy.

From the previous Hamiltonian (6.2) we derive the following equations of

motion:

$$\dot{q_i} = p\,, \tag{6.5}$$

$$\dot{p_i} = 2A\sum_{j=1}^{N}\{-sin(q_i)\frac{\cos(q_j)}{||q_i - q_j||^{\alpha}} + \cos(q_i)\frac{\sin(q_j)}{||q_i - q_j||^{\alpha}} + \\ + \alpha\frac{(q_i - q_j)(1 - \cos(q_i - q_j))}{||q_i - q_j||^{\alpha+2}}\}\,. \tag{6.6}$$

The above equation closely resembles the one obtained for the α-HMF model previously studied (5.3), except for the presence of the third additional coupling term that complicates the dynamics and prevents a simple mean-field description. For $N = 2$ the equation of motion can be easily decoupled and the system becomes integrable. Phase space portrait can be computed analytically (figure 6.1), showing a striking similarities with the pendulum portraits.

6.2 Equilibrium dynamics

In this chapter we will focus on the study of the equilibrium dynamic and thermodynamic properties of the previously introduced system. We deliberately ignore possible quasi-stationary-states (QSSs). To this end we considered in our simulations a sufficiently long transient to make sure that the system has relaxed to the deputed equilibrium.

To help characterizing the system it is useful to define a bunching parameter (magnetization) analogous to the HMF case $\vec{M} = \frac{1}{N}\sum_i(\cos(q_i), \sin(q_i))$. This global parameter serves as an indicator of the degree of organization present in the phase space. In fact, one observes $M = ||\vec{M}|| = 1$ if all particles are placed in the local extrema of the potential, where $(q_i - q_j) = k\pi$, while $M \sim 0$ if the particles are spread along the space.

N-body simulations are run with a fifth-order Mclachlan-Atela symplectic algorithm [80], with a timestep of $\delta t = 0.05$. The presence of the distance term in the equation significantly increases the computation time with respect to the HMF case study, or even compared to the α-HMF, where the fixed condition of the lattice sites allows for a simplified approach and makes the computational effort scale with $N \log N$ [105]. Due to the enhanced computational costs we consider systems of sizes smaller than $N = 10^3$.

All simulations presented in this thesis are run with an initial distribution which is Gaussian over momenta p with total momentum $P = 0$, and 2π-symmetric, uniformly distributed, over positions q. However, we numerically tested other initial conditions and we observed convergence to the same equilibrium state in most cases. Choosing a function which is inhomogeneously peaked over few positions q makes the time necessary to attain the equilibrium much longer than our computational capability, for large N. However, we observe a convergence to the same equilibrium, independently of the selected initial condition. We shall therefore assume in this work that the system has only one thermodynamic equilibrium state.
Starting with a 2π-periodic initial distribution, following the modulation induced by the cosine term of the potential, allows us to greatly shorten the time that is needed to converge to equilibrium. $t \sim 10^4$ has proven to be an adequate choice in most of the cases. The magnetization M settles down to an asymptotic state, as shown in figure (6.2), which is kept unchanged over time.

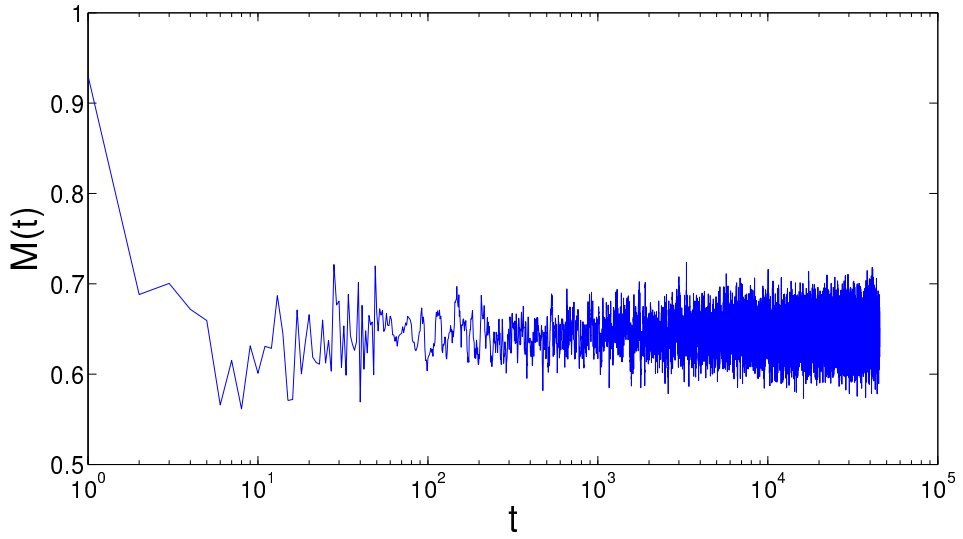

Figure 6.2: Convergence in time of the total magnetization M toward its equilibrium value. Results were obtained through an N-body simulation with $N = 100$, $l = 100$, $\alpha = 0.5$ and $\epsilon = 0.45$. The initial distribution is 2π-periodic and Gaussian over the local minima of the potential ($q = 2k\pi$).

Let us start by simply looking at the equilibrium trajectories $q(t)$ obtained through N-body simulations in figure (6.3): this is the easiest and quickest way to discover that the system presents self-organization. Three different equilibrium dynamical states are in particular identified.
At very low energy densities $\epsilon < \epsilon_c$, the system forms a regular crystal phase in which particles are bounded to their lattice wells corresponding to the symmetries

of the potential.
The solid eventually melts at higher energies $\epsilon_c < \epsilon < \epsilon_m$ and enters a partially disordered phase: the particles are still bound for finite times, thus preserving a sort of soft crystal ordering and a finite positive magnetization.
At high energy densities $\epsilon > \epsilon_m$ the system looses this partial ordering and displays a dynamical phase similar to a gaseous state which is homogeneous in space, with no bunching ($M \simeq 0$).

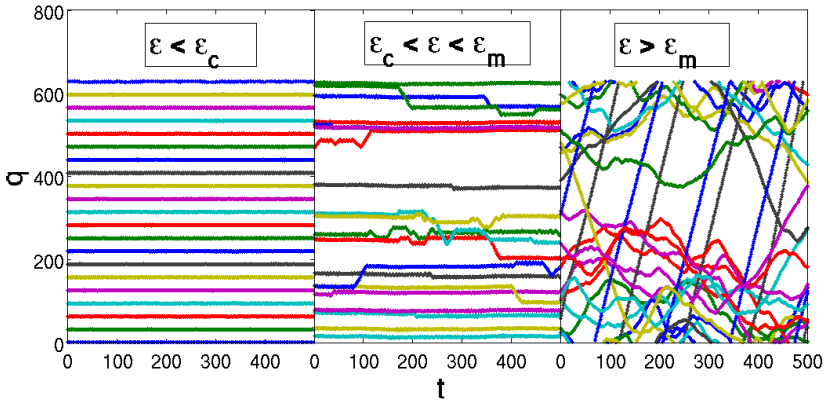

Figure 6.3: Position of particles in the q-space versus time. The trajectory of few particles is depicted. A visual inspection clearly show that three different dynamical regimes occur. The simulations are obtained for $N = 500$, $l = N$ and $\alpha = 0.5$. A numerical estimation of the thresholds in energy separating different phases gives $\epsilon_c \leq 0.2$ and $\epsilon_m \simeq 0.75$.

The critical threshold ϵ_m, which separates between magnetized ferromagnetic ($M > 0$) and homogeneous paramagnetic ($M = 0$) phases presents dependency on both α and L. We were not able to observe a dependency on the average density ρ_0, as we will show in section 6.3. According to the numerical simulations, the first energy threshold ϵ_c is estimated $\epsilon_c \lesssim 0.3$ for all values of $\alpha < 1$. In this work we did not investigate in detail the scaling of ϵ_c versus the latter parameter, due to the computational effort that would be eventually needed to achieve a satisfying precision. For $\alpha = 0.5$ the upper bound for the value of ϵ_c is numerically estimated to be 0.2.

The lattice ordering becomes evident if we analyse the spatial Fourier power spectrum of the distributions of inter-particle distances (6.1) $\mathcal{C}(d)$, in figure (6.4). We formally define $\mathcal{C}(d)$ as:

$$\mathcal{C}(d) = \int \int \rho(q+d)\rho(q)\, dq\,, \tag{6.7}$$

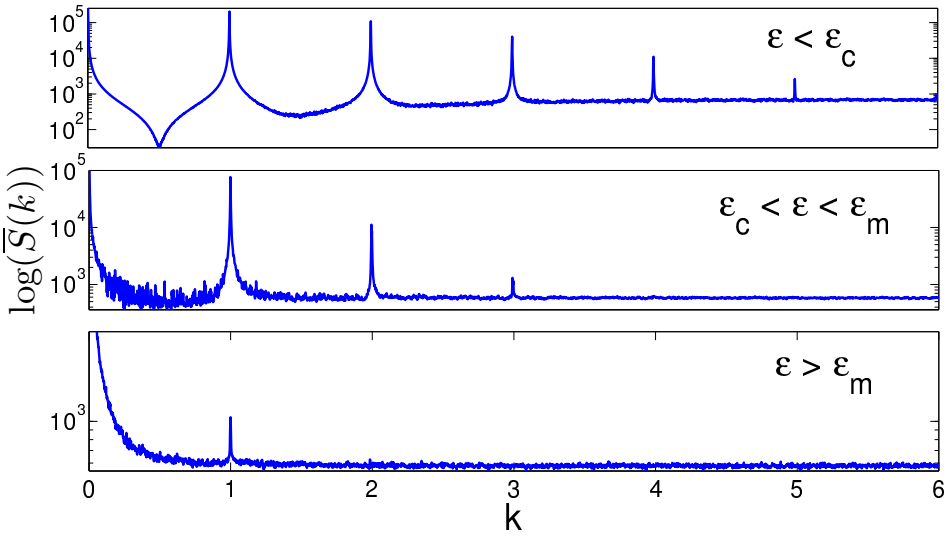

Figure 6.4: $\overline{S}(k)$ is the average over time of the Fourier power spectrum obtained from the distance distribution $\mathcal{C}(d)$. Results are displayed for three different energy density regimes. For $\epsilon < \epsilon_c$ there is a clear crystal structure, with some order preserved in the range $\epsilon_c < \epsilon < \epsilon_m$ and an almost disordered state for $\epsilon > \epsilon_m$. The data are obtained with $N = 500$, $l = N$ and $\alpha = 0.5$, discarding an initial transient time of order $t \sim 10^3$.

where $\rho(\cdot)$ represents the probability distribution of particles in space. It is easy to estimate the latter two quantities from numerical simulations. Notice that $\mathcal{C}(d)$ has the advantage of being translational invariant by construction.
The clear peaks in the wave number k for $\epsilon < \epsilon_c$ shows an ordering with a wavelength $\lambda = 2\pi$, which corresponds to the periodicity induced by the cosine term of the potential.
This very same ordering is still present in the energy range $\epsilon_c < \epsilon < \epsilon_m$, even if some of the harmonics are destroyed by the emerging noise. This means that the particles distribution still displays a uniform crystal ordering, on the same wavelength as observed in the energy range $\epsilon < \epsilon_c$.
The order eventually disappears in the high energy regime $\epsilon > \epsilon_m$. The global magnetization is in fact zero, and this corresponds to an absence of structures in the phase space and a flat noisy Fourier power spectrum. The small residual peak, that we observe in this energy regime, can be interpreted as a finite size effect around the transition ϵ_m and disappears at higher energies.

The disordered nature of the dynamics in the intermediate phase can be visually appreciated in figure (6.5), which displays the phase space portraits of the particles for $\epsilon = 0.5, \alpha = 0.5, l = 100$ and $\rho_0 = \frac{1}{2\pi}$.
For any finite time the particles live in small regions of size comparable to the dimension of the lattice, as observed in the crystal phase. They can occasion-

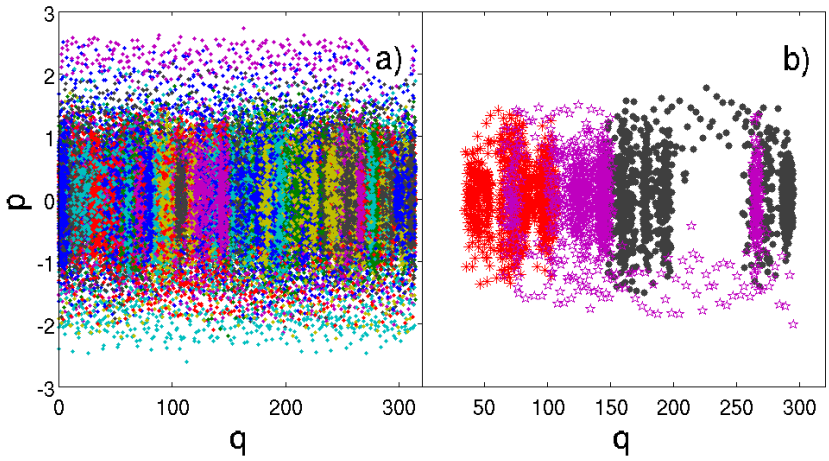

Figure 6.5: This is the phase space portrait of particle trajectories obtained with $\epsilon = 0.5, \alpha = 0.5, l = 100$ and $\rho_0 = \frac{1}{2\pi}$. It corresponds to the intermediate phase between the regular crystal and the gas phase. Different colors correspond to different particles. We can visually identify the soft lattice regions that correspond to disordered crystal wells. In figure (a) we represent the whole phase space, while in figure (b) we show few tracer particles for a finite time $T \sim 1000$.

ally escape from these clusters and move around for a while before falling again in local potential well. The corresponding phase is assimilated to a sort of *soft crystal*.

In figure (6.6) we show the mean period τ_i of each particle q_i computed along the time evolution. This was obtained by recording the time interval between an inversion in the sign of the momenta p_i. We observe that moving from ϵ_c to the transition energy ϵ_m the mean period increases, consistently with the increase in the free path of each trajectory. By monitoring the behaviour of the standard deviation of the value τ_i, we notice that the stability of these periods drops while approaching the gaseous phase. For any finite time it is still possible to observe free particles which corresponds to a diverging value of τ_i in figure (6.6-c). The number of free particles was observed to decrease with time with a law $1/t$. This suggests that the phenomenon originates from a finite-size effect. A collapse in a trapping region is hence expected to occur the thermodynamic limit. However, it takes a long time to observe convergence close to a phase transition, which explains while we still observe free particles after a time $t = 10^4$ for $\epsilon = 0.65$.

The above evidences strengthen our interpretation of the phase $\epsilon_c < \epsilon < \epsilon_m$ as a generalized disordered lattice phase, which is generated by the collective distribution of the particles.
The presence of this disordered crystal with soft lattice wells emerges from the long-range nature of the system and was never observed in simplified long-range

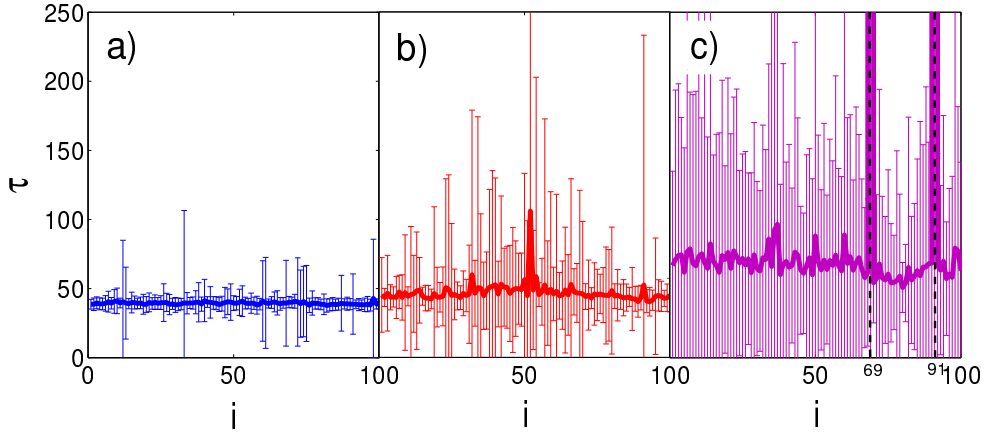

Figure 6.6: Mean period of particles of index i computed as the time interval between inversions in the sign of momenta. These data were obtained from N-body simulations performed with $l = 100$, $\rho_0 = 1/2\pi$ and $\alpha = 0.5$. Figure (a) corresponds to $\epsilon = 0.3$, figure (b) to $\epsilon = 0.45$ and figure (c) to $\epsilon = 0.65$. In last picture, two free particles can be identified (which correspond to the peaks at $i = 69$ and $i = 91$), which never exhibit a change of sign in their momenta during the total time $t = 10^4$ of the evolution. The error bars correspond to the standard deviation computed over the time evolution. Such values reflect the relative stability of the trapping regions.

models. This can be seen as an extension of crystal lattices to the case of purely long-range interacting systems.

6.3 Equilibrium distribution in the thermodynamic limit

With respect to the HMF and α-HMF models, we have one more degree of freedom in choosing our thermodynamic limit. The system now depends on both the length L and the average particle density $\rho_0 = \frac{N}{L}$. When performing the limit $N \to \infty$ we can consider $\rho_0 \to \infty$ and fixed L, or the limit $L \to \infty$ with constant ρ_0. We can manipulate the rescaling constant A in order to make the system explicitly dependant on respectively ρ_0 or L.
The infinite density limit is performed for the case of the HMF and α-HMF, where the volume of the accessible space is limited to the bounded region $[0, 2\pi[$. Let us emphasize that the latter limit is a priori different from the typical thermodynamic one, usually investigated in statistical mechanics, which aims to consider an infinite volume. However, both limits are legitimate and have

potential physical interest.

In the infinite density case, it is easy to compute and obtain the corresponding Hamiltonian equation for single particle, by simply performing the limit $N \to \infty$ with L constant, since we can integrate over a bounded region in space:

$$\mathcal{H}(q,p) = \frac{p^2}{2} + \frac{1-\alpha}{2\pi L}(\frac{L}{2})^\alpha \int_L \frac{1-cos(q-q')}{||q-q'||^\alpha} dq' \,. \tag{6.8}$$

In the case of constant density and $L \to \infty$ it is not so straightforward to recover analytically an analogous Hamiltonian, and so it is not rigorously proven that such a limit actually exists. The problem lies in the fact that the potential is modulated by the cosine with a periodicity of 2π, but it is not periodic. So we are not allowed to perform trivial simplifications without any knowledge on the form of the distribution function. Still we can solve the system for finite length, and observe the scaling of thermodynamic quantities for $L \to \infty$.

Let us consider $q \in [0,\ 2\pi l]$, $\rho_0 = \frac{N}{2\pi l}$ and perform the limit $N \to \infty$. We will restrict for now to the infinite density case and we will keep l constant. Let us call $f(q,p,t)$ our single particle distribution function, such as $f(q,p,t)dqdp$ is the fraction of particles in the interval $[q.q+dq][p,p+dp]$ at time t. The system conserves the energy density $\epsilon[f]$

$$\epsilon[f] = \int_\Gamma f(q,p,t)\mathcal{H}(q,p)dqdp \,, \tag{6.9}$$

where $\mathcal{H}(q,p)$ is obtained from equation (6.8). Also the total momentum $P[f]$ is conserved

$$P[f] = \int_\Gamma f(q,p,t)pdqdp \,, \tag{6.10}$$

together with normalization condition

$$\mathcal{G}[f] = \int_\Gamma f(q,p,t)dqdp = 1 \,, \tag{6.11}$$

where Γ represents the whole phase space domain.
We assume the entropy S has the following functional form which is strictly Boltzmannian:

$$S[f] = -\int_\Gamma f(q,p,t)\log(f(q,p,t))dqdp \,. \tag{6.12}$$

To obtain the equilibrium function $f(q,p)$ which maximizes the entropy $S[f]$ with the constrains obtained from the conserved quantities, we have to solve this

maximization problem:

$$\max_f \{S[f] | \int_\Gamma f(q,p,t)dqdp = 1, \epsilon[f] = E, P[f] = P\} \,. \tag{6.13}$$

Requiring stationarity of the entropy functional, the latter problem translates into solving the following equation:

$$\delta S[f] + \beta\delta\epsilon[f] + \gamma\delta P[f] + \mu\delta\mathcal{G}[f] = 0 \,, \tag{6.14}$$

where β, γ and μ are Lagrange multipliers. A straightforward derivation of equations (6.12), (6.9), (6.10) and (6.11) yields the following:

$$\log(f(q,p)) = -\beta(\frac{p^2}{2} + V(q)) - \gamma p - \mu - 1 \,, \tag{6.15}$$

where $V(q)$ reads:

$$V(q) = \int\int f(q',p)\frac{1-\alpha}{2\pi L}(\frac{L}{2})^\alpha \frac{1-cos(q-q')}{||q-q'||^\alpha}\, dpdq' \,. \tag{6.16}$$

Since we initially chose $P[f] = 0$, the Lagrange multiplier γ vanishes from equation (6.15), yielding to the following equilibrium distribution function:

$$f(q,p) = De^{-\beta(\frac{p^2}{2}+V(q))} \,, \tag{6.17}$$

where $D = e^{-1-\mu}$. This is the standard Maxwellian distribution function, where $\beta = 1/T$ is the inverse temperature and μ is the chemical potential. In analogy with what we observed in the case of the HMF solution (3.41), we have to deal with an implicit system, since $V(q)$ depends on $f(q,p)$. To solve the problem we use an iterative numerical scheme explained in [106], which, with respect to the standard Newton technique, has the advantage of ensuring that entropy increases toward the maximum value at each iteration step.

From equation (6.17) we define the equilibrium density function $\rho(q)$:

$$\rho(q) = \int f(q,p)dp = D\sqrt{\frac{2\pi}{\beta}}e^{-\beta V(q)} \,. \tag{6.18}$$

A numerical computation of the above function, represented in figure (6.7), shows a great degree of homogeneity and symmetry that is consistent with the finite-size dynamical phases observed in the preceding chapter.

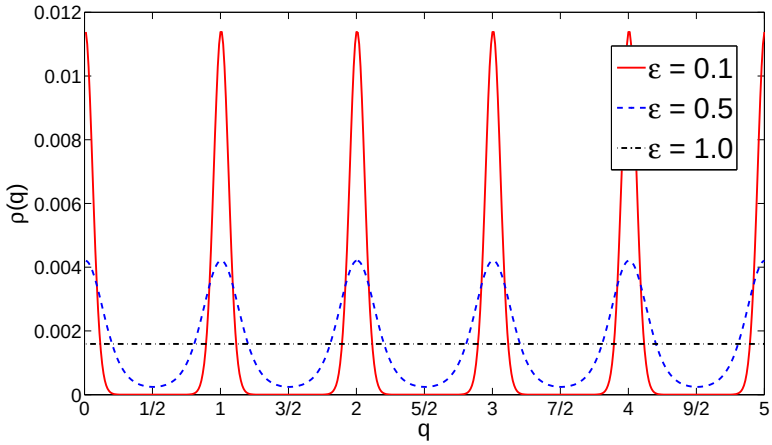

Figure 6.7: Analytically predicted equilibrium distribution densities $\rho(q)$ for different dynamical regimes and $\alpha = 0.5$. Here we plot a small portion of the q axis with 5 periods for a distribution function computed for $l = 100$ periods.

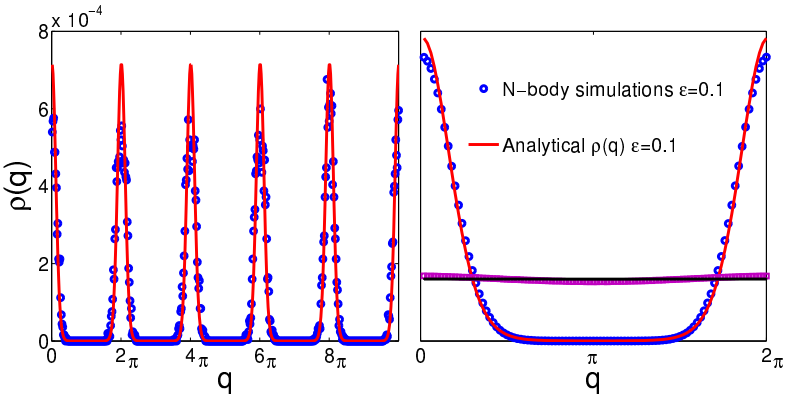

Figure 6.8: Analytical prediction for the density function $\rho(q)$ (straight line) compared to the numerical data coming from N-body simulations performed with $L = 100$, $N = 100$, $\alpha = 0.5$ and different energy densities ϵ. Left: direct comparison between the results showing the first five periods of the lattice. Right: comparison with q coordinates rescaled in the mod(2π) representation. Results correspond to a single point in time.

The comparison between the theoretically predicted $\rho(q)$ and the results of numerical simulations can be easily performed for $\epsilon < \epsilon_c$ (figure 6.8), where particles are fixed in their lattice matrix, and in the case $\epsilon > \epsilon_m$, where they result homogeneously distributed. In both cases we observe a good matching between theory and simulations, even with a low number of particles ($N = 100$) and low density ($\rho_0 = \frac{1}{2\pi}$).

In the intermediate phase the averaging effect due to the particles chang-

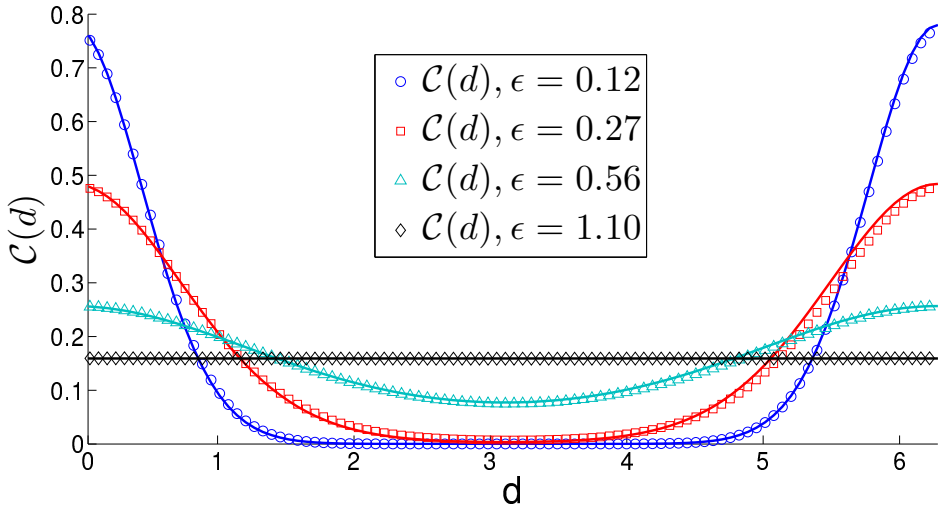

Figure 6.9: Analytical prediction for the distance density function $\mathcal{C}(d)$ (straight line) compared to the numerical data coming from N-body simulations performed with $L = 500$, $N = 500$, $\alpha = 0.5$ and different energy densities ϵ. The results are averaged over a time $\Delta t = 5 \cdot 10^2$ and represented in mod(2π) for the coordinates q.

ing frequently the bunching region makes the direct comparison more difficult, since one have to cope with the numerical artefacts coming from the lack of local translational invariance at finite times. In figure (6.9) we confront the analytical predictions for the distance distribution (6.7). This latter is naturally translational invariant and allows for a straightforward comparison avoiding the above problems. The agreement is almost perfect for all the energy regimes.

Let us note that the analytical results so far obtained are relative to the infinite density thermodynamic limit with L constant. In this context the results shown above are particularly interesting since we are comparing the theoretical limit $\rho_0 \to \infty$ to numerical simulations performed at low densities $\rho_0 = \frac{1}{2\pi}$, meaning that we have on average at least one particle for each period of the cosine term of the potential.
Knowing the distribution function we can compute the two components of the total magnetization vector $\vec{M}$:

$$\begin{aligned} M_x &= \int_\Gamma \rho(q) \cos(q) dq \,, \\ M_y &= \int_\Gamma \rho(q) \sin(q) dq \,, \end{aligned} \tag{6.19}$$

and the modulus $M = \sqrt{M_x^2 + M_y^2}$. The value of M depends only on f.
We can observe how the predicted value for the above quantity obtained from

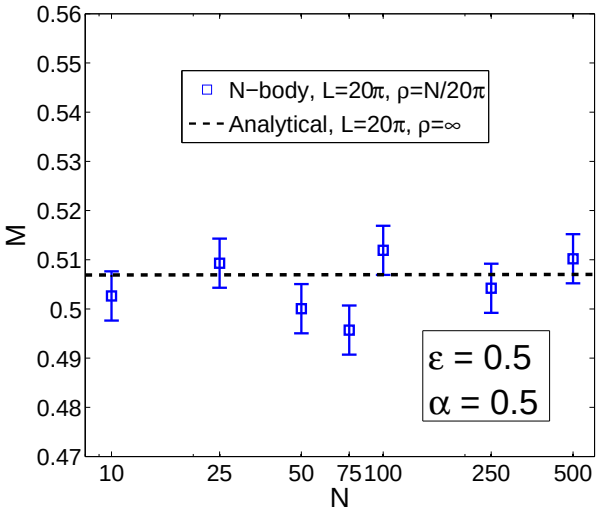

Figure 6.10: Scaling of predicted value for the total magnetization M with respect to the average density ρ_0. Here $\alpha = 0.5$, $l = 10$ and $\epsilon = 0.5$. The dots correspond to the value obtained from N-body simulations, while the dotted line corresponds to the predicted analytical value.

N-body simulations scales with increasing ρ_0, while keeping L fixed, and compare it to the predicted analytical value.
In figure (6.10) we can see that there seems to be almost no dependency of M on ρ_0, and the numerical N-body value is already converged to the analytical one for $\rho_0 = \frac{1}{2\pi}$.

Since the distribution function seems not to depend on ρ_0, we can try to explore the other thermodynamic limit with $L \to \infty$. In figure (6.11) we compare the value of the equilibrium magnetization as obtained from the analytical distribution function with infinite ρ_0 and increasing L, to the one obtained from the simulations with $\rho_0 = \frac{1}{2\pi}$ and same L.
We are quite surprised to observe that the two values converge in the limit of large L. This means that there seems to be a proper $L \to \infty, \rho_0 =$ constant thermodynamic limit and that this shares the same homogeneity and symmetry properties as the infinite density one.

Thanks to the knowledge of the spatial equilibrium distribution $\rho(q)$, we can try to investigate the presence of the previously observed transition between a regular crystal phase and a soft crystal. Numerical simulations gave us an estimate for the energy density threshold of $\epsilon_c \leq 0.2$ for $\alpha = 0.5$. In presence of trapping regions we expect that the distribution $\rho(q)$ will take a small value between the lattice periodicities, approaching zero at the regular crystal

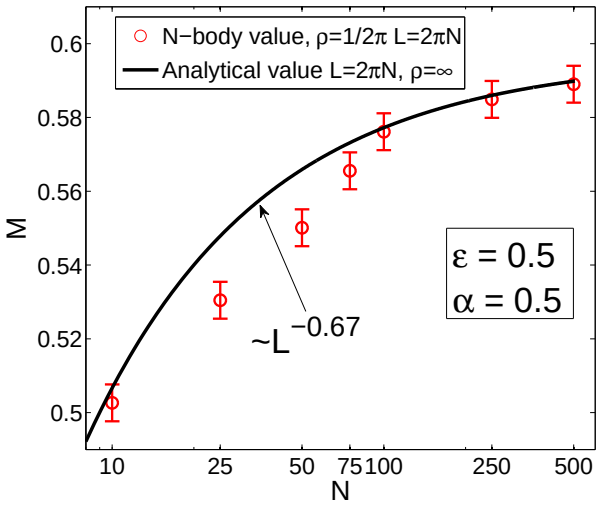

Figure 6.11: Scaling of predicted value for the total magnetization M respect to system length L, $\alpha = 0.5$, $\rho_0 = 1/2\pi$ and $\epsilon = 0.5$. The continuous line corresponds to the value obtained from the analytically predicted distribution function with $\rho_0 \to \infty$, while the dots correspond to the value obtained from N-body simulations with $\rho_0 = \frac{1}{2\pi}$.

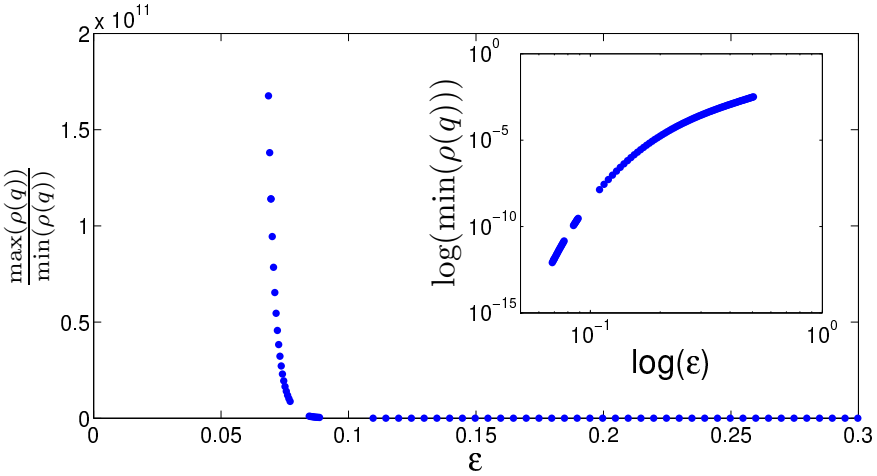

Figure 6.12: Scaling of the ratio $\frac{\max(\rho(q))}{\min(\rho(q))}$ with respect to energy density. The values are computed for $L = 500$ and $\alpha = 0.5$. There seems to be a threshold in energy $\epsilon_C \simeq 0.075$ after which the equilibrium distribution traps the particles in the lattice sites, in agreement with numerical simulations. In the inset, we report the scaling of $\min(\rho(q))$ in loglog scale.

transition threshold.

In figure (6.12) we observe that below an energy density value $\epsilon = 0.075$, the ratio $\max(\rho(q))/\min(\rho(q))$ rapidly diverges, while $\min(\rho(q))$ approaches zero. Since $\rho(q)$ is periodic (figure 6.8), the previous result seems to strengthen the evidences of the transition coming from the N-body simulations, confirming

the substantial difference between the distinct dynamical phases that we have identified.
The difference between the theoretical and numerical estimate, could be due to finite size effects. Below $\epsilon = 0.2$, the value of $\min(\rho(q))$ becomes very small, so we do expect that the mean escape time from the potential well may become quickly greater than our maximum simulation time.

6.4 α-HMF limit

The observed crystal order may be reminiscent of the α-HMF phase structure, even though we must stress that in our case the system self-organizes without the need of imposing a fixed lattice.
To understand better the similarities between the two models we must make some assumptions, based on our theoretical knowledge of the equilibrium distribution function. Let us consider the sum of the type

$$C_i = A(\rho_0, L) \sum_{j \neq i} \frac{\cos(q_j)}{\|q_i - q_j\|^\alpha} , \tag{6.20}$$

which appear in the equation of motion (6.6). Define $q_j = 2\pi h_j + \varepsilon_j$, with $h_j \in \{0, \cdots, n\}$ playing the role of a lattice index and $0 < \epsilon_j < 2\pi$. In the following we will consider the density $\rho_0 = N/L$ as constant. Then we can simplify the previous term as:

$$C_i \sim \frac{1-\alpha}{2^\alpha \rho_0} \sum_{j \neq i} \frac{1}{L} \frac{\cos(\varepsilon_j)}{\left\| \frac{2\pi h_i}{L} - \frac{2\pi h_j}{L} + (\varepsilon_i - \varepsilon_j)/L \right\|^\alpha} . \tag{6.21}$$

If we assume that the equilibrium distribution $\rho(\epsilon, h)$ is not peaked over a few values of the index h, and it is spread enough so to cover the whole length of the system, in the limit $L \to \infty$ we can ignore the contribution to the potential coming from particles which are close and have $h_i = h_j$. In practice, assuming $h_i \neq h_j$, we can avoid the divergence that arises from the following simplifications:

$$\frac{1}{\left\| \frac{2\pi h_i}{L} - \frac{2\pi h_j}{L} + (\varepsilon_i - \varepsilon_j)/L \right\|^\alpha} \approx \frac{1}{\left\| \frac{2\pi h_i}{L} - \frac{2\pi h_j}{L} \right\|^\alpha} - \alpha \frac{(\varepsilon_i - \varepsilon_j)}{L \left\| \frac{2\pi h_i}{L} - \frac{2\pi h_j}{L} \right\|^{\alpha+1}} . \tag{6.22}$$

The second term in expression (6.22) vanishes when performing the sum in the limit $L \to \infty$. Hence, the dependence on ϵ_i in the distance term disappears, while the dependence on the index h_i is not present in the cosine term.

This means that, under the previous assumptions, the numerator and denominator in the expression of C_i become independent, and we fall into a limit which is very close to the α-HMF case.

If we consider $L = \frac{N}{\rho_0}$, we obtain:

$$\tilde{C}_i = \lim_{N\to\infty} C_i \simeq B(\rho_0) \sum_{j=1}^{N} N^{\alpha-1} \frac{\cos(\epsilon_j)}{\|h_i - h_j\|^{\alpha}} , \tag{6.23}$$

where $B(\rho_0) = \frac{1-\alpha}{2^{\alpha}}(2\pi\rho_0)^{-\alpha}$. If we assume that the equilibrium distribution function is homogeneous in the index h and each interval of length 2π, in which we have divided the system, contains the same number of particles, we can reorder the previous term by avoiding to sum over each particle with the same index h_i and we obtain:

$$\tilde{C}_i = (2\pi\rho_0)B(\rho_0) \sum_{j=1}^{n} N^{\alpha-1} \frac{cos(\epsilon(y))}{\|i - j\|^{\alpha}} , \tag{6.24}$$

which, apart for a constant factor, is exactly the same formula that we obtained for the α-HMF. Recall in fact that in equation (5.5) we have:

$$C_i^{\alpha} = \frac{1-\alpha}{2^{\alpha}} \sum_{j=1}^{N} N^{\alpha-1} \frac{cos(\epsilon(y))}{\|i - j\|^{\alpha}} . \tag{6.25}$$

It is easy to show that

$$\begin{aligned} \frac{1}{N}\sum_i \tilde{C}_i &= \frac{1}{N}\sum_{j=1}^{n} \cos(q_j)(2\pi\rho_0)B(\rho_0) \sum_{i=1}^{n} \frac{1}{\|i-j\|} , \\ &= Y(\rho_0)\frac{1}{N}\sum_{i=1}^{n}\cos(q_j) = Y(\rho_0)M_x , \end{aligned} \tag{6.26}$$

where M_x is defined as one of the two components of the magnetization vector $\vec{M}$, and $Y(\rho_0)$ is a constant coming from the sum. Applying similar considerations to the second term in equation (6.6) yields:

$$\tilde{S}_i = (2\pi\rho_0)B(\rho_0) \sum_{j=1}^{n} N^{\alpha-1} \frac{\sin(\epsilon(y))}{\|i - j\|^{\alpha}} , \tag{6.27}$$

and in the end we can recover a simplified mean-field equation of motion which is analogous to the one obtained for HMF and α-HMF (5.3):

$$\frac{\partial p_i}{\partial t} = 2\left(\cos(q_i)\tilde{S}_i - sin(q_i)\tilde{C}_i\right) . \tag{6.28}$$

Of course this equivalence holds under a strict hypothesis of homogeneity and symmetry of the distribution function $f(q,p)$ in the limit $L \to \infty$.

In the previous section we pointed out that the symmetry properties of $\rho(q)$ in the limit $\rho_0 \to \infty, L = \text{cst}$ hold true also in the thermodynamic limit $L \to \infty, \rho_0 = \text{cst}$. Under this assumption we do expect to observe a thermodynamic equivalence between the model (6.2) and the HMF, possibly recovering the same phase transition as described in figure (2.2).

6.5 Equilibrium phase transition

We proceed to compute the curve for the equilibrium magnetization $M(\epsilon)$ for different values of the scaling exponent α and large enough $l = 1000$, which practically sets our computational limit. As depicted in figure (6.13), the analytical and numerical curves are in almost perfect agreement.

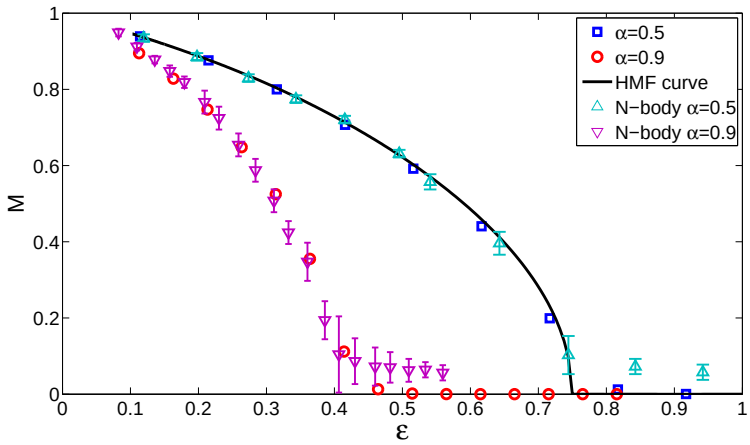

Figure 6.13: Comparison between the magnetization curves obtained from the analytically predicted distribution function, and the data recorded via N-body simulations. Here with $l = 1000$. The N-body data are obtained as the average over a time window $\Delta t = 5000$, and, as expected, are very noisy next to the critical transition energy ϵ_m. The black thick curve represents the HMF equilibrium curve.

As we expected, based on the arguments illustrated in the previous sections, a second order phase transition between ferromagnetic $M > 0$ and paramagnetic $M = 0$ phases occurs for a critical energy density ϵ_m. This latter is the energy which yields to the disappearance of the self organized order. The energy threshold ϵ_c that follows the dynamical study and which respectively separates regular and disordered soft crystal states, does not leave a trace in the magnetization

curves.
As anticipated on pure speculative grounds in section (6.4), we obtain in figure (6.14) the phase transition curve of the HMF with the same critical energy $\epsilon = 0.75$ for a wide range of parameters, with an almost perfect agreement for $\alpha < 0.6$. This result was first numerically observed in [105], for the single case $\alpha = 0.5$.

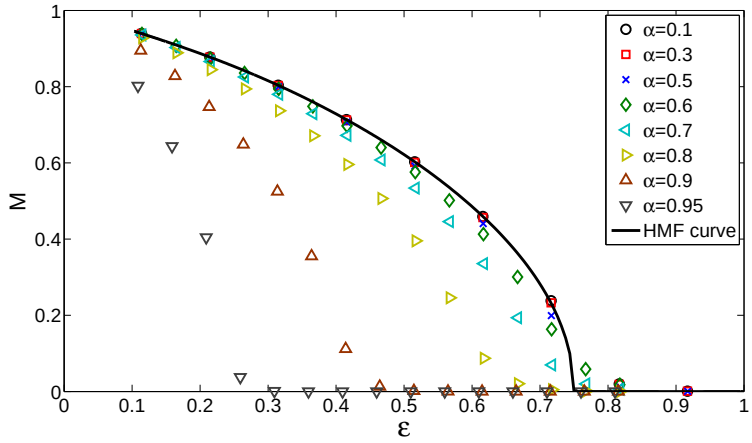

Figure 6.14: In figure we represent the transition curves M versus ϵ for different values of the scaling exponent α. We observe a second order phase transition with a critical exponent $\frac{1}{2}$ that reproduces almost perfectly the HMF curve (thick black) for $\alpha < 0.6$. For increasing values of α the transition moves towards lower energy densities. The values are obtained from the analytical distribution obtained for $l = 1000$.

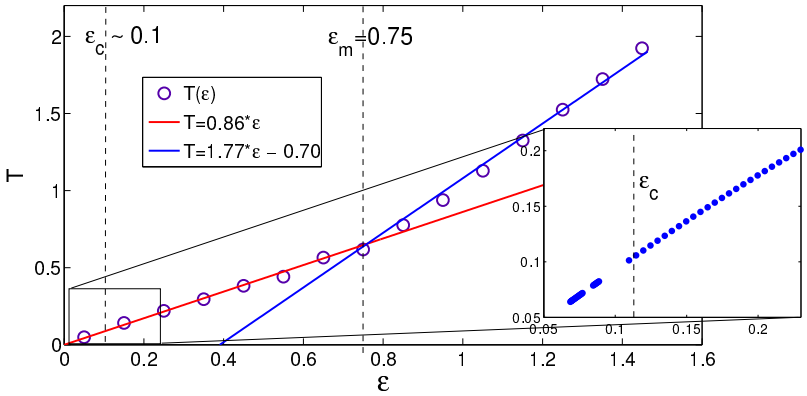

Figure 6.15: Temperature T as a function of the energy density ϵ. The critical energy ϵ_m corresponds to a second order phase transition, while the first energy threshold ϵ_c which separates regular and soft crystal phases seems not associated to a thermodynamic phase transition.

We can observe a signature of the above phase transition also by looking

at the temperature curve $T(\epsilon)$ in figure (6.15). Again the result points to the quantitative analogy with the HMF transition curve [9]. Convergence problems in the numerical algorithm prevented us to completely explore the energy range close to the predicted threshold ϵ_c, between regular and soft crystal. Even if such numerical problems may eventually signal the presence of a phase transition, we were not able to pinpoint any discernible discontinuity in the derivatives of the temperature curve. As now, we cannot make a definitive assessment on the nature of the latter transition.

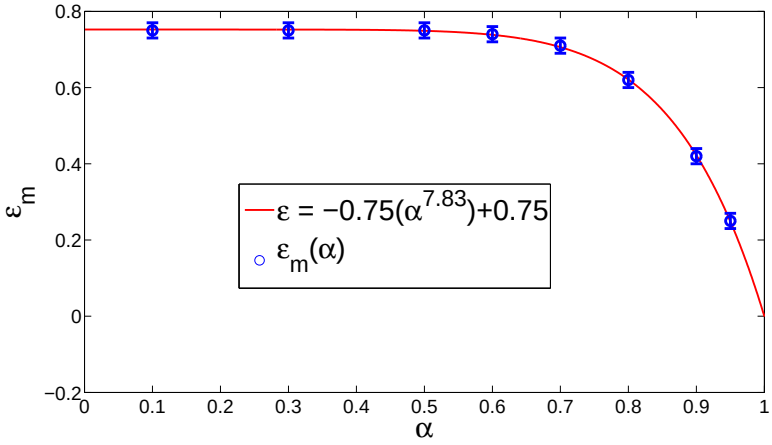

Figure 6.16: Scaling of critical energy ϵ_m with respect to α. ϵ_m is 0.75 (i.e. the HMF transition value) for $\alpha < 0.6$. The data were obtained from the analytical distribution function computed for $l = 1000$. The fit is obtained by adjusting one free parameter, the exponent of α (see legend).

For larger values of α we observe that the critical transition energy ϵ_m gradually moves to zero, as we can easily appreciate in figure (6.16). The phase transition disappears for $\alpha \simeq 1$. This is somehow expected, since for $\alpha \geq 1$ the system is no longer of the long-range type and so it cannot undergo a 1-D phase transition. This is at variance with what we observed in chapter 5.2 in the case of α-HMF, where the "artificial" nature of the distance term in the potential, independent on the actual position of the particles, makes it apparently possible to observe 1-D phase transitions for $\alpha \geq 1$.

All the curves shown in figure (6.14) were obtained for $l = 1000$, which, as previously mentioned, is the maximum value attainable with our computing facilities. To be sure of their convergence to the asymptotic shape in the limit $L \to \infty$, we can observe the scaling of two test curves $\epsilon_m(L)$ reported in figure (6.17), for different values of α. As we can see, the convergence of the critical threshold is slower for larger values of α, and behaves like a power

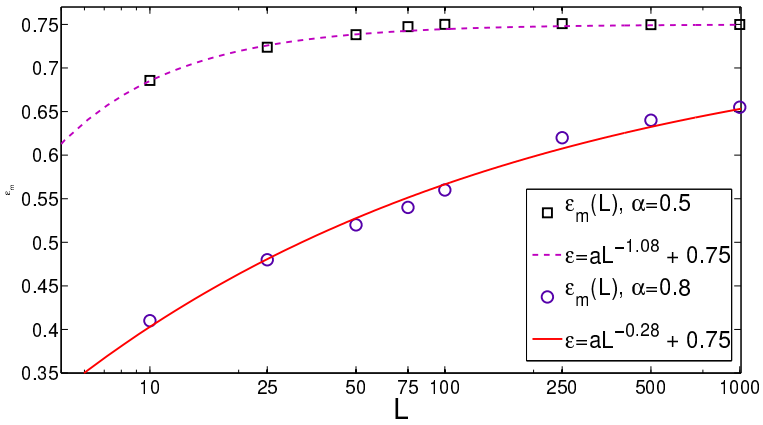

Figure 6.17: Convergence of critical energy ϵ_m with increasing L to an asymptotic value for different values of α. Data obtained from analytically predicted distribution function. The size of the dots corresponds to our precision in identifying the transition, which depends only on the energy resolution of the data.

law $\epsilon_m = aL^{-b} + 0.75$, with parameter b decreasing with α. This suggests that we can be reasonably sure that the curves obtained for $\alpha < 0.6$ are already converged to their asymptotic limit. However, the scaling law for $\epsilon_m(L)$ for $\alpha = 0.8$, that is inferred from a simple fit of the data, indicates that the transition threshold will move also in this case toward the asymptotic value $\epsilon_m = 0.75$. This latter property seems to be true for every value of $\alpha \leq 0.9$ that we analysed. We did not set to study in detail the range $0.9 \leq \alpha < 1$ since there are occasional convergence problems in our numerical algorithm, which require additional computation effort. However, the preliminary data are compatible with the above scaling. If the form of the scaling law that we obtained is confirmed by an analysis performed for larger values of L, then the HMF phase transition could be reproduced for any value of the scaling exponent $\alpha < 1$.

Further studies should focus on the characterization of the newly observed intermediate soft crystal phase, in order to understand if it can be used to model the collective features observed in real long-range systems. Another open question is the possible presence of quasi-stationary out-of-equilibrium states which was non investigated in this work.

Conclusions

Understanding the physics of long-range interacting systems is becoming of central importance in the development of different fields of study, ranging from cosmology to plasma physics, with possible application to the experimental lasers. The work of this thesis was focused on the theoretical and numerical analysis of long-range interactions, and to the characterization of their peculiar dynamical and thermodynamic features.

We initially focused on the study of the out-of-equilibrium quasi-stationary states (QSS), which become proper equilibrium states in the large size limit. An analytical description of the distribution function representing these states is possible thanks to the seminal theory developed by Linden-Bell in the context of galactic dynamics. The technique has been successfully applied to a limited gallery of toy-model systems, the most important being the paradigmatic Hamiltonian Mean Field (HMF) model. However rigorous results have been so far derived only under strict assumptions on the initial condition (one-level water-bag). In this thesis we have taken a step forward by extending the Lynden-Bell solution to the multi-level water-bag, which in principle could be used to approximate any continuous distribution. We have shown that the above generalized theory reproduces the states observed in finite-size numerical simulations with good agreement. The single-level water-bag solution is recovered as a limit case.

When trying to study the interaction of a long-range system with a thermal bath, one encounters several problems, both theoretical and practical, mainly due to the lack of additivity. Using as a case study the HMF model, we have introduced the formal description of QSSs in the canonical ensemble, i.e. for a system at equilibrium with a thermal bath. To this end we recovered the free energy functional from the Legendre-Fenchel transform of the microcanonical entropy. Due to the Fermionic nature of the QSS equilibrium, the system displays *negative kinetic specific heat*. This counter-intuitive evidence ultimately stems from the fact that kinetic and thermodynamic temperatures are different.

Passing heat to the system, we observe a spontaneous self-organization, which yields to a reduction of the kinetic component of the internal energy.
In order to understand the consequences of the previous result, we studied an hypothetical thermal machine, working with an HMF QSS fluid. Despite the fact that formal thermodynamic requirements are respected, we obtain the shocking finding that such machine would violate the second principle of thermodynamics, by performing positive work while passing heat from the cold to the hot reservoir. The latter result is general, and in principle valid for any fluid described by a non-Maxwellian distribution. In order to avoid the paradox, we suggest that Fourier's law for heat exchange could be modified for long-systems. The consequences of these observations are presently challenged via dedicated numerical studies.

The HMF system discussed before is a paradigmatic model of long-range interactions and has been widely studied in past literature. Recently a new model was proposed, called α-HMF, which introduce a decay of the potential with respect to a distance term over a fixed lattice matrix. The scaling is ruled by tunable exponent α, which makes it possible to continuously modify the interaction up to the short-range threshold. In this thesis work, we focused on the description of the QSS of the α-HMF model next and beyond to the classical threshold of long-range interaction, which is assigned on the basis of the dependence of the potential on α. We observed that QSS lifetime still diverges logarithmically around the threshold value $\alpha = 1$, while long-range peculiar features, like the presence of a 1-D phase transition for $\alpha > 1$, are found when in the short-range regime. Consequently, we suggest that a more correct definition of long-range interaction should take into account the scaling of the force, rather than the potential, as already proposed in a recent work by A. Gabrielli et. al. [100]. The latter interpretation seems to be more consistent with the numerical evidences.

Despite the great interest behind long-range phenomenology, the long-range solvable models so far studied in the literature are quite simple, and are defined in a phase space of reduced dimensionality and complexity. To be able to describe complex spatial self-organized structures that emerge in presence of long-range potentials, we have studied, in the last part of the thesis, a novel long-range model first introduced in [105]. By considering a continuous distance term, the latter adds a degree of complexity with respect to the simplified HMF and α-HMF systems, while reproducing the same thermodynamics in the large size limit. In the extended phase space of the above system it is possible to observe a more rich zoology of equilibrium features. Specifically, we were able to obtain three different equilibrium dynamical states, encompassing a regular crystal phase, a

disordered soft crystal phase and a gaseous phase at high energies, which could not be seen in the reduced phase space of previous long-range models. The crystal phases manifest as a generalized self-organized state, in which the local lattice emerge from the collective behaviour of the particles. We were able to analytically obtain a form for the equilibrium distribution function and apply it to describe the system in both the infinitely extended limit and in the infinite density limit. We also shown that assuming the validity of the latter solution, the system can be formally reduced to the HMF in the infinite size limit, thus reproducing the same equilibrium transition between magnetized and homogeneous states. We argue that the newly introduced model could be possibly used to describe more realistic physical systems like self-gravitating models or charged plasmas, so accounting for the collective features observed in presence of long-range interactions.

Bibliography

[1] P. H. Chavanis, International Journal of Modern Physics B **20**, 3113 (2006).

[2] T. Padmanabhan, Physics Reports **188**, 285 (1990).

[3] Y. Elskens, D. Escande, *Microscopic Dynamics of Plasmas and Chaos*, IOP Publishing, Bristol (2002).

[4] J. Miller, Physical Review Letters **65**, 2137 (1990).

[5] R. Robert, Comptes Rendus de l'Académie des Sciences: Série I Maths **311**, 575 (1990).

[6] S. Slama, G. Krenz, S. Bux, C. Zimmermann, P. W. Courteille, Scattering in a High-Q Ring Cavity, *Dynamics and Thermodynamics of systems with long-range interac-tions: Theory and Experiment*, AIP Conference Proceedings **970** (2008).

[7] Ph. Chomaz, F. Gulminelli, Phase transitions in finite systems, *Dynamics and Thermodynamics of Systems with Long-Range Interactions*, Lecture Notes in Physics **602**, Springer (2002).

[8] D. Lynden-Bell, Mon. Not. R. Astron. Soc. **136**, 101 (1967).

[9] A. Campa, T. Dauxois, S. Ruffo, Physics Reports **480**, 57 (2009).

[10] V. A. Antonov, Vest. Leningrad Gros. Univ. **7**, 135 (1962).

[11] D. Lynden-Bell, R. Wood, Monthly Notices of the Royal Astronomical Society **138**, 495 (1968).

[12] P. Hertel, W. Thirring, Annals of Physics **63**, 520 (1971).

[13] K. S. Fine, A. C. Cass, W. G. Flynn, C. F. Driscoll, Physical Review Letters **75**, 3277 (1995).

[14] X.-P. Huang, C. F. Driscoll, Physical Review Letters **72**, 2187 (1994).

[15] M. K. H. Kiessling, T. Neukirch, The Proceedings of the National Academy of Sciences **100**, 1510 (2003).

[16] G. L. Eyink, K. R. Sreenivasan, Rev. Mod. Phys. **78**, 87 (2006).

[17] R. S. Ellis, K. Haven, B. Turkington, Journal of Statistical Physics **101**, 999 (2000).

[18] R. S. Ellis, K. Haven, B. Turkington, Nonlinearity **15**, 239 (2002).

[19] M. Kiessling, J. L. Lebowitz, Letters in Mathematical Physics **42**, 43 (1997).

[20] A. Antoniazzi, D. Fanelli, J. Barré, P. H. Chavanis, T. Dauxois, S. Ruffo, Physical Review E **75**, 011112 (2007).

[21] A. Antoniazzi, F. Califano, D. Fanelli, S. Ruffo, Physical Review Letters **98**, 150602 (2007).

[22] P. H. Chavanis, Eur. Phys. J. B **80**, 3 (2011).

[23] F. Staniscia, A. Turchi, D. Fanelli, P. H. Chavanis, G. De Ninno, Negative specific heat in the canonical statistical ensemble, Physical Review Letters **105**, 10601 (2010).

[24] F. Gobet, B. Farizon, M. Farizon, M. J. Gaillard, J. P. Buchet, M. Carré, T. D. Märk, Physical Review Letters **87**, 203401 (2001).

[25] M. Schmidt, R. Kusche, T. Hippler, J. Donges, W. Kronmüller, B. von Issendorff, H. Haberland, Physical Review Letters **86**, 1191 (2001).

[26] M. Kac, G. E. Uhlenbeck, P. C. Hemmer, Journal of Mathematical Physics **4**, 216 (1963).

[27] P. H. Chavanis, Statistical mechanics of two-dimensional vortices and stellar systems, *Dynamics and Thermodynamics of Systems with Long-Range Interactions*, Lecture Notes in Physics **602**, Springer (2002).

[28] M. K. H. Kiessling, Journal of Statistical Physics, **55**, 203 (1989).

[29] T. Padmanabhan, Physics Reports **188**, 285 (1990).

[30] T. Padmanabhan, Statistical mechanics of gravitating systems in static and expanding backgrounds, *Dynamics and Thermodynamics of Systems with Long-Range Interactions*, Lecture Notes in Physics **602**, Springer (2002).

[31] J. Barré, D. Mukamel, S. Ruffo, Physical Review Letters **87**, 030601 (2001).

[32] W. Thirring, Z. Phys. 235, 339 (1970); P. Hertel and W. Thirring, Ann. Phys. (N.Y.) 63, 520 (1971).

[33] G. De Ninno, D. Fanelli, in press, arXiv:1011.2981 (2011).

[34] A. Campa, S. Ruffo, H. Touchette, Physica A **385**, 233-248 (2007).

[35] D. H. E. Gross, Microcanonical Thermodynamics, World Scientific, Singapore (2001).

[36] R. M. Lynden-Bell, Molecular Physics **86**, 1353 (1995).

[37] R. M. Lynden-Bell, in *Gravitational Dynamics*, Eds. O. Lahav, E. Terlevich, R. J. Terlevich (Cambridge University Presss), Cambridge (1996).

[38] H. Touchette, *The Large Deviations Approach to Statistical Mechanics*, Physics Reports **478** (2009).

[39] A. Antoniazzi, *Non-Equilibrium Dynamics of Mean-Field Models: The Emergence of Quasi Stationary States*, PhD thesis, Università degli Studi di Firenze (2006).

[40] E. Fermi, J. Pasta, S. Ulam, *Los Alamos Reports*, (LA-1940) (1955).

[41] X. Leoncini, A. Verga, S. Ruffo, Physical Review E, **57**, 6377 (1998).

[42] A. Torcini, M. Antoni, Physical Review E, **59**, 2746 (1999).

[43] P. H. Chavanis, G. De Ninno, D. Fanelli, S. Ruffo, in *Chaos, Complexity and Transport*, Eds. C. Chandre, X. Leoncini, G. Zaslavsky (World Scientific), Singapore (2008).

[44] R. Bachelard, C. Chandre, D. Fanelli, X. Leoncini, S. Ruffo, Physical Review Letters **101**, 260603 (2008).

[45] X. Leoncini, T. L. Van den Berg, D. Fanelli, EPL **86**, 20002 (2009).

[46] T. L. Van den Berg, D. Fanelli, X. Leoncini, EPL **89**, 50010 (2010).

[47] T. Dauxois, S. Ruffo, E. Arimondo, M. Wilkens, *Dynamics and Thermodynamics of Systems with Long Range Interactions*, Lect. Not. Phys. **602** (2002).

[48] P. H. Chavanis, Statistical mechanics of two-dimensional vortices and stellar systems, *Dynamics and Thermodynamics of Systems with Long-Range Interactions*, Lecture Notes in Physics **602**, Springer (2002).

[49] D. Lynden-Bell, R. Wood, Monthly Notices of the Royal Astronomical Society **138**, 495 (1968).

[50] E. Caglioti, F. Rousset, Archive for Rational Mechanics and Analysis **190**, 517 (2008).

[51] J. Barré, F. Bouchet, T. Dauxois, S. Ruffo, Y. Y. Yamaguchi, Physica A **365**, 177 (2006).

[52] M. Hauray, P. E. Jabin, Archive for Rational Mechanics and Analysis, **183**, 489 (2007).

[53] A. Campa, R. Khomeriki, D. Mukamel, S. Ruffo, Physical Review B **76**, 064415 (2007).

[54] D. H. Dubin, T. M. O'Neil, Review of Modern Physics **71**, 87 (1999).

[55] A. Antoniazzi, Y. Elskens, D. Fanelli, S. Ruffo, Europ. Phys. J. B **50**, 603 (2006).

[56] A. Antoniazzi, R. S. Johal, D. Fanelli, S. Ruffo, Comm. Nonlin. Sci. Num. Simul. **13**, 2 (2008).

[57] R. Bonifacio, L. De Salvo, Nucl. Instrum. Meth. Phys. Res. A **341**, 360 (1994).

[58] M. Antoni, S. Ruffo, Physical Review E **52**, 2361 (1995).

[59] A. Campa, A. Giansanti, D. Mukamel, S. Ruffo, Physica A **365**, 120 (2006).

[60] J. Barré, F. Bouchet, T. Dauxois, S. Ruffo, Physical Review Letters **89**, 110601 (2002).

[61] T. Konishi, K. Kaneko, J. Phys. A **25**, 6283 (1992).

[62] J. Barré, *Mécanique Statistique et Dynamique Hors Equilibre de Systémes avec Interaction à Longue Portée*, PhD Thesis (2003).

[63] R. Balescu, *Statistical dynamics: matter out of equilibrium*, Imperial College Press, London (1997).

[64] C. Tsallis, A. Rapisarda, A. Pluchino, E. P. Borges, Physica A **381**, 143 (2007).

[65] V. Latora, A. Rapisarda, S. Ruffo, Physical Review Letters **80**, 692 (1998).

[66] Y. Y. Yamaguchi, J. Barré, F. Bouchet, T. Dauxois, S. Ruffo, Physica A **337**, 36-66 (2004).

[67] J. Barré, T. Dauxois, G. De Ninno, D. Fanelli, S. Ruffo, Physical Review E **69**, 045501(R) (2004).

[68] R. Bachelard, A. Antoniazzi, C. Chandre, D. Fanelli, M. Vittot, Comm. Nonlin. Sci. Num. Sim. **13**, 660-665 (2008)

[69] W. Braun, K. Hepp, Communications in Mathematical Physics **56**, 101 (1977).

[70] H. Spohn, *Large Scale Dynamics of Interacting Particles*, Springer (1991).

[71] Yu. L. Klimontovich, *The Statistical Theory of Non-equilibrium Processes in a Plasma*, MIT Press (1967).

[72] D. R. Nicholson, *Introduction to Plasma Theory*, John Wiley (1983).

[73] J. Binney, S. Tremaine, *Galactic Dynamics*, Princeton Series in Astrophysics (1987).

[74] M. Henon, Annales d'Astrophysique **27**, 83 (1964).

[75] I. R. King, Astr. J. **71**, 64 (1966).

[76] J. Binney, S. Tremaine, *Galactic Dynamics*, Princeton Series in Astrophysics (1987).

[77] P. H. Chavanis, J. Sommeria, R. Robert, Astrophys. J. **471**, 385 (1996).

[78] F. Staniscia, P. H. Chavanis, G. De Ninno, Physical Review E, **83**, 051111 (2011).

[79] P. Morel, E. Gravier, N. Besse, R. Klein, A. Ghizzo, P. Bertrand, X. Garbet, P. Ghendrih, V. Grandgirard, Y. Sarazin, Phys. Plasmas **14**, 112109 (2007).

[80] R. I. McLachlan, P. Atela, *The accuracy of symplectic integrators*, Nonlinearity **5**, 541-562 (1992).

[81] F. Baldovin, P. H. Chavanis, E. Orlandini, Physical Review E **79**, 011102 (2009).

[82] F. Baldovin, E. Orlandini, Physical Review Letters **96**, 240602 (2006).

[83] C. Tsallis, F. Baldovin, R. Cerbino, P. Pierobon, Introduction to Nonextensive Statistical Mechanics and Thermodynamics, in *The Physics of Complex Systems: New Advances and Perspectives*, Volume **155**, F. Mallamace and H.E. Stanley (2003).

[84] F. Baldovin, E. Orlandini, Int. Jour. Mod. Phys. B **21**, 4000 (2007).

[85] J. Barré, D. Mukamel, S. Ruffo, Physical Review Letters **87**, 030601 (2001).

[86] P. H. Chavanis, F. Baldovin, E. Orlandini, Physical Review E **83**, 040101 (2011).

[87] K. Huang, *Introduction to Statistical Physics*, Chapman & Hall/CRC (2010).

[88] F. Staniscia, P. H. Chavanis, G. De Ninno, D. Fanelli, Physical Review E **80**, 021138 (2009).

[89] M. W. Zemansky, *Heat and Thermodynamics*, McGraw-Hill, NY (1957).

[90] R. Clausius, *The Mechanical Theory of Heat - with its applications to the Steam Engine and to Physical Properties of Bodies*, London: John van Voorst, (1865).

[91] Kelvin, W. Thomson, *An Account of Carnot's Theory of the Motive Power of Heat - with Numerical Results Deduced from Regnault's Experiments on Steam*, Transactions of the Edinburg Royal Society, XVI, January 2 (1849); Kelvin, W. Thomson, *Mathematical and physical papers*, London: C.J. Clay and son, Cambridge University Press London, (1882).

[92] S. Carnot, *Réflexions sur la puissance motrice du feu et sur les machines propres à développer cette puissance*, Paris: Bachelier (1824).

[93] R. K. Pathria, *Statistical Mechanics*, Elsevier, Oxford (2006).

[94] D. J. Amit, Y. Verbin, *Statistical Physics: an introductory course*, World Scientific, (1999).

[95] P. H. Chavanis, Eur. Phys. J. B **53** 487 (2006).

[96] F. Bonetto, J. L. Lebowitz, L. Rey-Bellet, *Fourier's Law: A Challenge to Theorists*, Mathematical Physics, 128-150, London, Imperial College Press (2000).

[97] R. Bachelard, N. Piovella, private communication.

[98] C. Anteneodo, C. Tsallis, Physical Review Letters **80**, 5313 (1998).

[99] F. Tamarit, C. Anteneodo, Physical Review Letters **84**, 208 (2000).

[100] A. Gabrielli, M. Joyce, B. Marcos, F. Sicard, Journal of Statistical Physics **141**, 970-989 (2010).

[101] H. M. Thomas, G. E. Morfill, Nature **379**, 806 - 809 (1996).

[102] M. H. Thoma, M. Kretschmer, H. Rothermel, H. M. Thomas, G. E. Morfill, Am. J. Phys.**73**, 5 (2005).

[103] A. Bermudex, J. Almeida, F. Schmidt-Kaler, A. Retzker, M. B. Plenio, arXiv:1108.1024v1 (2011).

[104] K. Lakomy, R. Nath, L. Santos, arXiv:1107.3132v1 (2011).

[105] T. L. Van den Berg, *Systèmes avec interaction à longue portée*, Master thesis, director X. Leoncini (2009).

[106] T. Tatekawa, F. Bouchet, T. Dauxois, S. Ruffo, Physical Review E **71**, 056111 (2005).

List of publications

1. F. Staniscia, A. Turchi, D. Fanelli, P. H. Chavanis, G. De Ninno, *Negative specific heat in the canonical statistical ensemble*, Physical Review Letters **105**, 010601 (2010).

2. A. Turchi, D. Fanelli, X. Leoncini, *Existence of quasi-stationary states at the long range threshold*, Communications in Nonlinear Science and Numerical Simulations **16**, 4718-4724 (2011).

3. M. Assllani, D. Fanelli, A. Turchi, T. Carletti, X. Leoncini, *Statistical theory of quasi stationary states beyond the single water-bag case study*, Physical Review E, accepted.

4. D. Fanelli, G. De Ninno, A. Turchi, *Efficency of Cyclic Devices Working with non-Boltzmannian Fluids*, Communications in Nonlinear Science and Numerical Simulation, submitted.

5. A. Turchi, X. Leoncini, D. Fanelli, *Self organization and emergence of crystal ordering in a model of long-range rotators*, in preparation.